THERMAL EXCITATION OF MOLECULAR SPECTRA

by

Robert Peter Arrowsmith, B Sc, ARCS

A Thesis Submitted for the Degree of Doctor of Philosophy in
the University of London

Imperial College of Science and Technology

February 1971

ABSTRACT

A flash pyrolysis apparatus has been used to survey the quartz ultraviolet region in a search for new hydride systems of the transition group elements. A quantitative assessment of the pyrolysis process has been made with particular reference to the formation of excited molecular species. Features in the spectra recorded with copper and scandium in a hydrogen atmosphere were tentatively assigned to new hydride systems.

The spectra of the hydride and deuteride of the copper system were photographed from 3200 to 2200 Å in the second or third order of a 21 ft grating spectrograph. The system was recorded in absorption, using a King furnace to produce the absorbing species. The analysis of this system indicated a $^1\Sigma - {}^1\Sigma$ transition. The structure is similar to the 1a group hydrides, with an open Franck-Condon parabola and a maximum in the B_v' values. An analysis of part of the hydride system has been published by U Ringström (1).

CONTENTS

PART I

CHAPTER 2 - APPARATUS

CHAPTER 3 - SOME QUALITATIVE ASPECTS OF PYROLYSIS

Page

CHAPTER 4 - RADIANT ENERGY AND PRESSURE EFFECTS

CHAPTER 5 - THEORETICAL ANALYSIS

CHAPTER 6 - DISPERSION OF A SPHERICAL GOLD DROPLET IN A HYDROGEN ATMOSPHERE

Page

CHAPTER 7 - EXPERIMENTAL RESULTS FOR GOLD LEAF

CHAPTER 8 - COMPARISON OF PREDICTED AND EXPERIMENTAL RESULTS AND CONCLUSIONS

Page

PART II

CHAPTER 9 - THE ABSORPTION SPECTRA OF CuH AND CuD IN THE 2200 - 3200 Å RANGE

CHAPTER 10 - ANALYSIS OF THE (E-X) SYSTEM IN CuH AND CuD

CHAPTER 11 - ISOTOPE EFFECTS

CHAPTER 12 - THE ELECTRONIC STATE

LIST OF ILLUSTRATIONS

ACKNOWLEDGEMENTS

I would like to thank my supervisor Dr R W B Pearse for the stimulating and sustained support that he has given throughout this work.

I would also like to acknowledge the assistance of the members of the Spectroscopy Department. Especially J E G Wheaton in setting up the pyrolysis apparatus, O Milbank for quartz and glassware and Mrs G Uncles for typing this thesis.

The research work was carried out in the Physics Department of Imperial College with financial support from the Science Research Council.

CHAPTER 1

INTRODUCTION

The basic project suggested for this work was that a flash pyrolysis system should be used to investigate the ultraviolet region of the spectra of thetransition group (3d) hydrides.

The group elements include those metals which have formed the foundations of our modern technical society, and the early investigation of their hydrides may perhaps be traced to this background. However, these hydrides still contain many known but unanalysed systems which have not yet yielded to current computer aided analytic techniques. Notable amongst these are the quintet UV bands of MnH(2) and the very complex CrH systems(3).

The term "Flash Pyrolysis"(4) has been used to describe an apparatus which uses an intense pulse of light to partially or completely evaporate a solid sample. This name follows logically from the term "Pyrolysis" used to describe the evaporating process in Sun or Arc Image furnaces.

The suggested advantage of using a flash pyrolysis system was that since it could produce high densities of atoms(5), in a suitable ambient it might produce equally high densities of the required molecule. The possibilities of producing highly excited states and time resolution(6) of the spectra were additional advantages of this system.

In the present apparatus a fine wire or sheet of material is supported so that there is poor thermal contact with the support. It is placed in a transparent tube surrounded by a high power xenon flash tube. The energy absorbed by the sample during the discharge of the flash tube can be sufficient to vaporise it if one of its dimensions is $\lesssim$ 5 microns. This produces a transient cloud of hot vapour which can react with the surrounding gas. A second flash tube of much shorter pulse width than the heating flash tube is used to record the absorption spectra of the evaporated sample at any pre-selected time. A completely automatic system of this type was first proposed by G Porter(6) for a flash photolysis system. Though the principles of these systems are identical, both the exciting and background flash tubes are now much more powerful and reliable.

The potential advantages of this system compared with photolysis are that the whole spectrum of the flash tube rather than an absorption band can be used, that the initial sample is a solid of high density rather than a gas or liquid and that the final products will be at a high temperature, rather than the low excitation frequently associated with photodissociation.

The flash pyrolysis system was first studied by Kuebler and Nelson(7)(8) and has been used at Imperial College by A Rajaratnam (10) to produce the absorbing column in a Mach-Zehnder interferometer. There has been one report of its use for the study of molecules produced by gas-metal reactions.(9)

During this work, the pyrolysis apparatus was used to observe the spectra of all the 3 d group elements except zinc, in both helium and hydrogen atmospheres. Hitherto unrecorded features were observed in the spectra of Cu and Sc in a hydrogen atmosphere.

The limitations of this system have been carefully examined and put on a quantitative basis. Thus allowing a potential user to determine the suitability of the apparatus for a particular project.

The first section of this work describes how the pyrolysis apparatus was used in the survey for hydrides, and an attempt to reconcile the predicted and experimental parameters for the single case of gold leaf in hydrogen. Since only a single sample is analysed in detail the experimental conditions are carefully examined so that the results can be extrapolated to a wide range of samples. The second section presents the analysis of the (E-X) system, which had been observed using the pyrolysis apparatus in CuH and CuD. The relationships of this system to the 1a group and 1b group hydrides is then discussed.

PART I

CHAPTER 2

APPARATUS

2.1 Introduction

A detailed cross-section of the apparatus is shown in figure (2.1) and a schematic of its operation in figure (2.2). The various units of the apparatus will be considered and then the preparation of suitable samples and operation of the apparatus.

2.2 Optical Bench

The optical bench and its main fittings were designed by J Wheaton and built in the Physics Department workshop. The parallel rod optical bench chosen, though quite sturdy, requires special fitting and is less easy to adjust than the 'lathe bed' type of bench. As shown in figure (2.1) there is a sliding seal to allow rapid replacement of the sample tube for the cleaning required between firings.

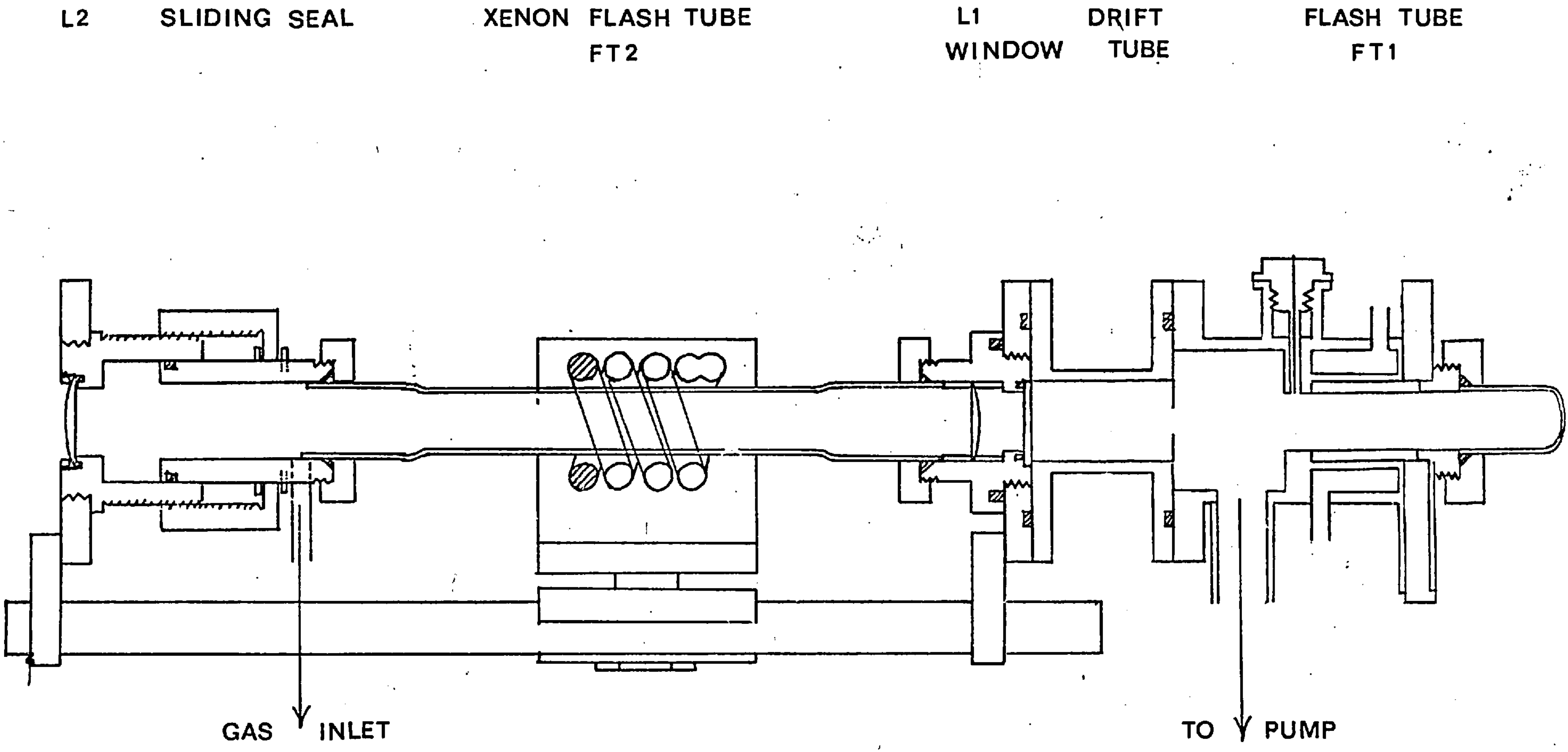
L2
SLIDING SEAL
XENON FLASH TUBE FT2
L1 WINDOW
DRIFT TUBE
FLASH TUBE FT1
GAS INLET
TO PUMP

FIGURE 2.1

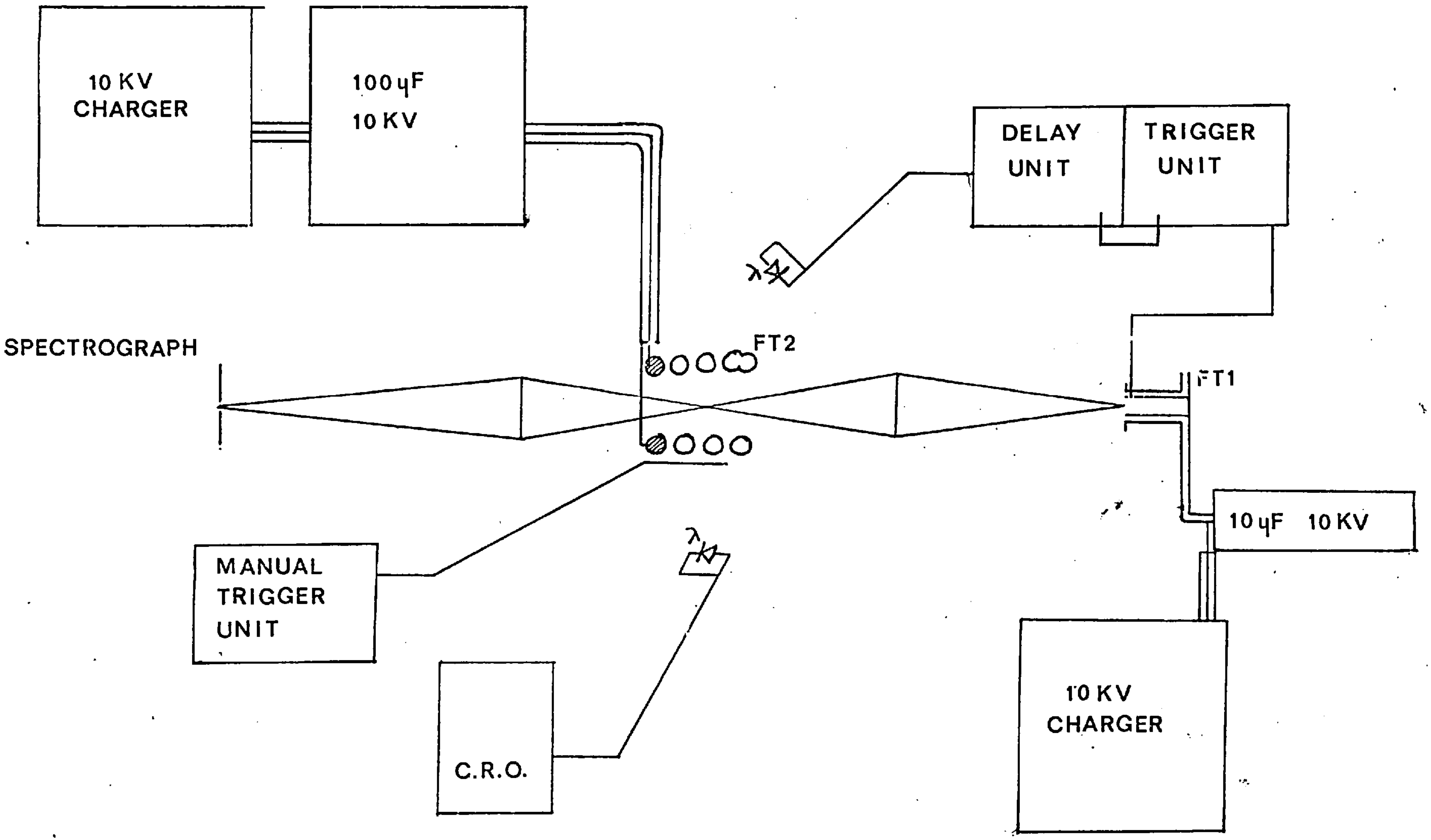
10 KV CHARGER
100 μF 10 KV
DELAY UNIT
TRIGGER UNIT
SPECTROGRAPH
FT2
FT1
MANUAL TRIGGER UNIT
C.R.O.
10 μF 10 KV
10 KV CHARGER

FIGURE 2.2

2.3 Spectroscopic Flashtube

FT1, the spectroscopic flashtube, its charger-trigger unit and the delay unit were supplied by Chelsea Instruments Ltd. This flashtube(11)(12) is of the Lyman type, using a cylinder of ceramic to contain the hot plasma which is the light source. When coupled to a 10 μ F, 10kV low inductance capacitor and fired at 8kV, the pulse width is 3-5 μ secs, and about 0.5 joules of light energy is produced. A fast diffusion pump was used to obtain the required operating vacuum ($\sim 10^{-3}$ torr), though this can be replaced with a rotary pump and cold trap. An initial difficulty with this flashtube was that the quartz window isolating the flashtube from the pyrolysis chamber required regrinding and polishing after only a few discharges so severe was the surface ablation. However the addition of a single baffle and a 5" drift tube allowed the window to be used for more than 10 shots after which light polishing restored the far UV transmission.

2.4 Xenon Flashtube

FT2 was a re-entrant spiral xenon flashtube with a maximum rating of 5k joules/discharge. Two of these flashtubes were given to the Department by the Argonne National Laboratory, but these were later modified and a slightly larger flashtube was assembled. The flashtubes were filled and sealed in the Department following the method described by Porter(6).

The flashtube was joined to a clean high vacuum system and subjected to strong heating with continuous pumping. This process is essential to desorb traces of oxygen and nitrogen from the walls which later make triggering of the flashtube increasingly difficult. After this treatment the flashtube was filled with specpure xenon through a solid CO_2 cold trap, and closed off from the pumping system. It was connected to a 100 μ F capacitor bank and fired a few times at full power before reopening to the vacuum system, rebaking, and filling. The filling pressure was adjusted from a nominal 100 torr until the flashtube 'held off' 9kV and triggered easily up to 8kV. The flashtube was then sealed off and removed from the system.

The triggering of the flashtube became more difficult with use and the static breakdown voltage fell to about 6.5kV.

One of the flashtubes used a small tungsten block cathode and the other a much larger one of molybdenum. Neither was as satisfactory as a polished disk electrode in preventing spluttering from the electrode.

As well as the darkening due to the deposits from the cathode, all the flashtubes formed a white deposit especially along the outer wall of the spiral. However, the reduction in transmitted power due to this deposit was compensated by the increased reflection from the outer face. Thus the performance of the flashtube was stable for several hundred firings.

2.5 Capacitor Bank

The capacitor bank for the xenon flashtube consisted of 5, 20 μ F rapid discharge capacitors, connected in parallel using 30kV co-ax. cable. The wiring inductance was not critical since even with a re-entrant spiral structure, the flashtube inductance will normally predominate. A separate unregulated 12kV half wave charger powered this capacitor bank. The flashtube was fired manually by applying a pulse of about 50kV to the surface of the flashtube.

2.6 Gas Supply

Gas supplies for the system were fed through a needle valve and a zeolite and two empty cold traps. The traps were cooled with liquid nitrogen or oxygen. High pressures were measured with a mercury manometer, low pressures with a pirani gauge. The deuterium used was supplied by the Atomic Energy Authority.

2.7 Preliminary Experiments

The assembled apparatus was tested using 0.1 μ thick gold leaf samples, the spectra being recorded with a Hilger medium quartz spectrograph. A problem that arose at this stage was that the triggering of FT1 was unreliable. This was later traced to a slightly low HT triggering pulse and after correcting this the system reliability approached 100%. However, as a complete check every shot was recorded by using a photodiode and oscilloscope.

It was soon apparent that the resolution of the medium quartz spectrograph was inadequate for any useful molecular work and all later spectra were recorded using the Hilger automatic large quartz-glass spectrograph. This is a large aperture and hence fast spectrograph. Scattered light from the xenon flashtube limited the operating region to below 3500 Å with a pyrex sample tube and below 3000 Å with one of quartz. Fortunately this is also the region where this spectrograph has sufficient dispersion hence it was well suited to the apparatus. It will be shown that there is only a small difference between the total transmitted energy of quartz and pyrex sample tubes hence pyrex tubes were used for all the quantitative measurements.

2.8 Preparation of Samples

The final requirement before the project could be commenced was a source of suitable samples of the 3d group elements. Gold leaf was known to be satisfactory but there was no source of the 3d group elements with a similar geometry. Etching of 1 thou strip down to $\lesssim$ 10 μ could not be controlled and the use of gold leaf contaminated in a solution of the metal salt chosen was unuseable since the AuH systems are so strong in this region. The basic parts of an evaporation plant were available and this could be used to make thin films of the 3d group metals. It will be shown that generally wire will be a more suitable sample, but its production is considerably more difficult. Figure (2.3) shows the vacuum evaporation system. The LT supply was a 20vt, 60 Amp transformer which will supply sufficient power to enable use of carbon boat elements. The HT transformer was a large 2kV unit so that resistive damping was required to limit the maximum ion current to $\sim$ 100 m Amps.

EVAPORATION PLANT

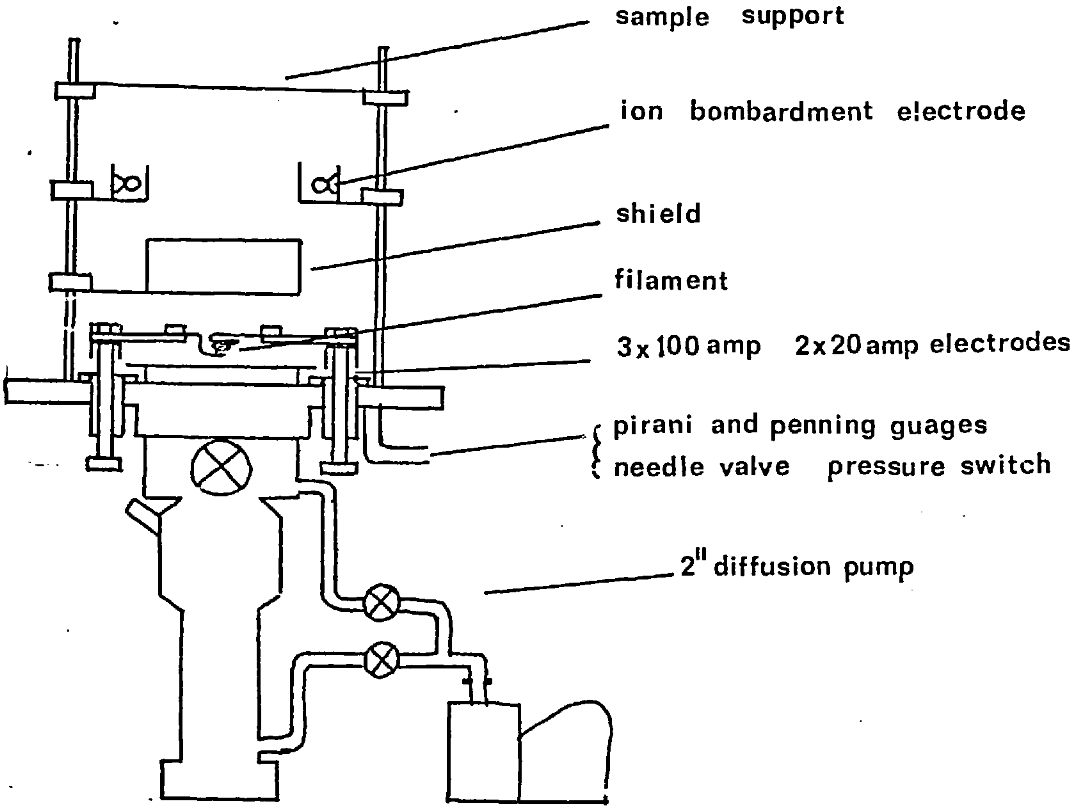

POWER SUPPLY

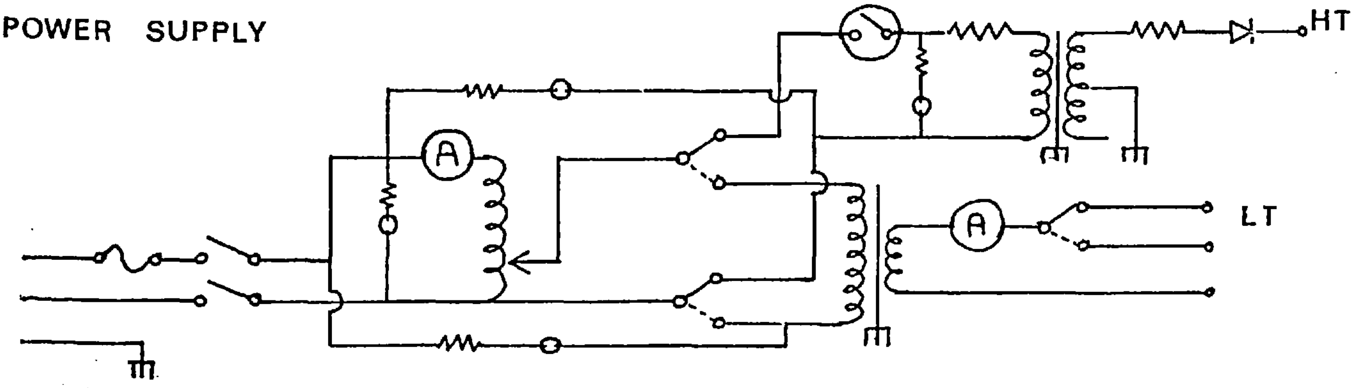

FIGURE 2,3

The thin film samples were prepared on a glass slide. This was first thoroughly cleaned and degreased then mounted in the vacuum vessel about 12" from the element. The system was then pumped down to $< 10^{-4}$ torr and held at this pressure for about 5 minutes. The diffusion pump was throttled back and the leak adjusted to give a suitable pressure for ion bombardment. After 20 minutes of ion bombardment the system was again pumped down to $< 10^{-4}$ torr. A thin film of KCl was evaporated on to the slide from a molybdenum boat element. The LT current was then switched to the filament holding the required metal. (Details for the evaporation of the 3 d group metals were taken from Holland(14)). The coated slide was then allowed to cool and removed from the vacuum vessel.

The metal film was floated off by slowly dipping the slide into distilled water (a slight trace of detergent eases this process but increases potential contamination and should be avoided). The individual samples were picked up on wire frames from the film which floats on the water.

All the 3d group elements except zinc were prepared using this technique. The elements Ti, Co, Ni and Fe could only be produced as very thin films (100-300 Å). However, these films were less subject to strain than thicker films and gave a higher yield of free standing samples. Thick films of Cr are especially liable to break up on removing the slide from the vacuum vessel. The evaporation of zinc from a carbon crucible was attempted but it did not deposit on the KCl substrate. To avoid the possibility of contaminating the whole pumping system no further attempts were made to obtain zinc films.

CHAPTER 3

SOME QUALITATIVE ASPECTS OF PYROLYSIS

3.1 Samples

The geometry of the sample is a critical restriction of the flash pyrolysis sytem. Thus the first aim was to determine what constituted a suitable sample. The materials examined were powders (down to a few microns), wire (to $12\frac{1}{2}\mu$) and sheet (to $\lesssim .03\mu$). For samples with no dimension $< 12\frac{1}{2}\mu$ only loose debri on the surface was removed. Near $12\frac{1}{2}\mu$ the results were more dramatic but the spectra showed that only a very small amount of material was evaporated. For example, a $12\frac{1}{2}\mu$ Cu wire grid could be completely destroyed but left a deep brown suspension in the sample chamber. This consisted of the drops formed at the intersections of the grid when the Cu was melted.

As the sample dimension decreased below $12\frac{1}{2}\mu$ the amount of evaporated material gradually increased. Powder samples nominally with dimensions of 5-10μ could produce usable densities of absorbers. But they are unsatisfactory since they must be intimately supported and are initially out of the light path. This leads to only partial evaporation of the material and since the process is inhomogeneous precludes

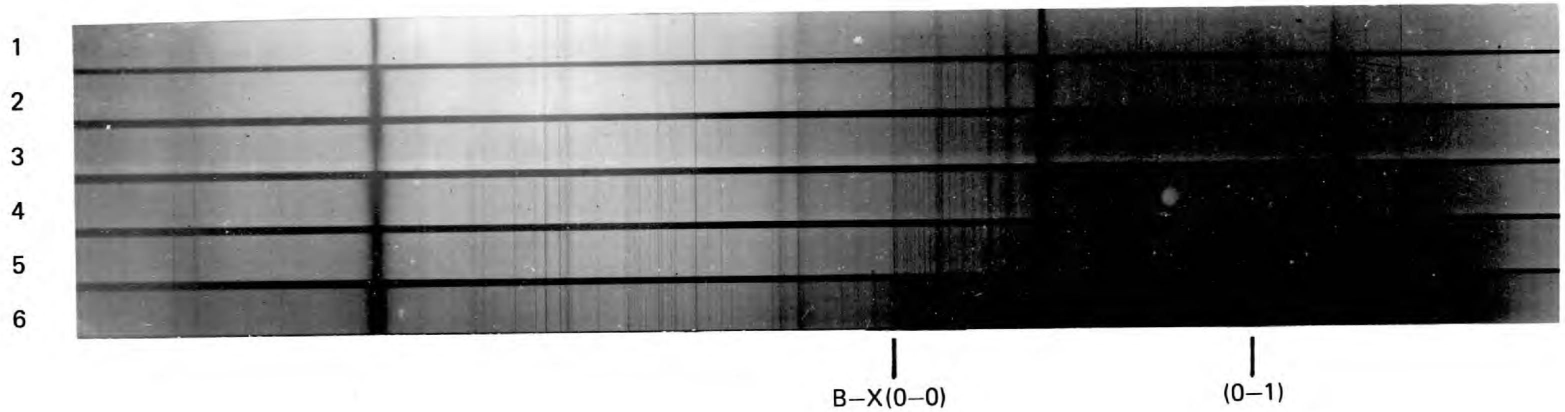

PYROLYSIS OF GOLD LEAF IN HYDROGEN (1 atmos)

	DELAY	T_{rot}	T_{vib}
1	50	3500	
2	75	3300	
3	100	5200	
4	150	4350	4600
5	250	2500	3300
6	500	3400	3500

PLATE 3 - 1

the full use of the time resolving facility except at long delay times. For sheet samples the apparent density of absorbers continued to increase as the thickness fell except for a few completely transparent V samples estimated to be < .03μ thick.

3.2 Conditions

The required sample geometry having been defined and produced, some known molecular systems were examined to determine the optimum time delay at which to record the spectra and the required ambient gas pressure. Part of a time resolved sequence using Au leaf in 1 atmosphere of H_2 is shown in plate (3.1). There is no apparent absorption before about 50μ secs then between 50 and 100μ secs the atomic absorption density rises rapidly. The density of hydride formed by a gas-metal reaction peaked between 500 and 700μ secs, though any excited states tended to depopulate rapidly after about 500μ secs. The apparent density of absorbers appeared to be fairly insensitive to pressure in the range 0.5 to 1.5 atmospheres.

Naturally the first spectra examined were some known hydride bands of the 3d group. The strong 2200 Å CuH band and the 3600 Å and 3200 Å groups of bands in CrH were readily produced, but the near UV bands of Mn, Co and NiH could not be observed.(15) This is due to the rise in scattered light and falling dispersion which effectively limits this apparatus to wavelengths $\lesssim 3500$ Å. (The use of a timed shutter can extend this range(6)). Outside the 3 d group the UV systems of AuH could be easily produced, but those of AlH only weakly and BiH not at all. It was now apparent that only fairly strong systems would be observed and that higher dispersion would be needed for any detailed analysis.

3.3 Results

Some representative spectra are shown in plate (3.2) and some details from the spectra of Cu and Sc in plate (3.3). The two potential hydride systems in Cu and Sc were observed in He, H_2 and D_2 atmospheres to try and verify the carrier of the bands. This process was unsuccessful since both Cu and Sc are rapidly attacked by exposure in moist air. The sample then contains its own supply of hydrogen, so that the observed spectra always contain the hydride. The two spectra of the 2200 Å band of CuH in vacuo and ½ atmosphere of D_2 clearly illustrate this effect.

Cu 0.5 atmos H_2 0.5 msecs

Sc 1atmos H_2 0.5 msecs

Ti 1atmos H_2 0.3 msecs

Mn 1atmos H_2 0.3 msecs

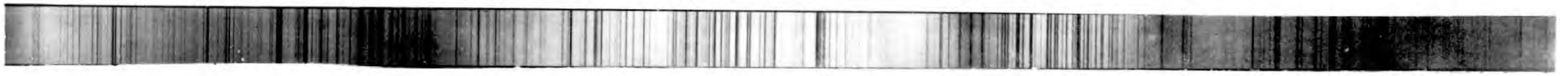

V 0.2atmos H_2 0.3 msecs

PLATE 3 - 2

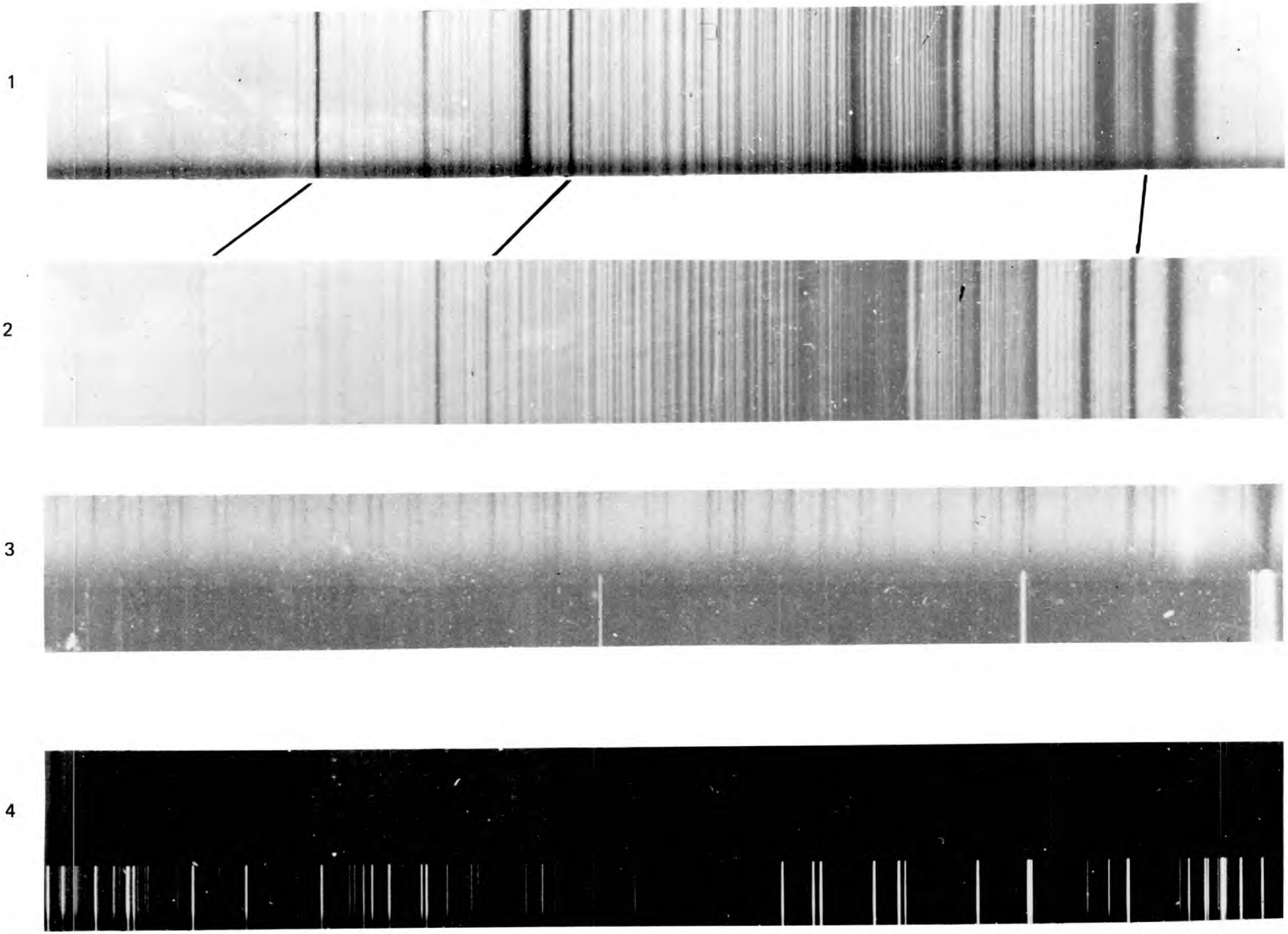

1 Cu 10^{-3} torr 0.3 msecs   2 Cu 0.2atmos D_2 0.5 msecs   3 Cu 1atmos H_2 0.7 msecs   4 Sc 1atmos H_2 0.5 msecs

PLATE 3 - 3

The remaining members of the 3d group were observed in He and H_2 from 3500 - 2200 Å but did not yield any further potential hydride systems.

The spectra in plates (3.2) and (3.3) illustrate some of the potential difficulties that arise using this system. It was stated earlier in this Chapter that the density of absorbers was greatest for very thin samples. Thus for good sample geometry the surface to mass factor is very high, and since contamination is essentially a surface problem, the percentage of any contamination is also high. The method chosen for making the samples brings them into contact with KCl, water and air. For samples $\gtrsim 10\,\mu$ thick it is possible to remove most of any surface impurities by subjecting the mounted sample to a low energy level light pulse before the full power discharge. However, for thinner samples this cannot be controlled. The extensive OH system is the principal contaminant system observed, plate (3.2). The interesting aspect of this impurity is that though it is known to be chemically present in the Cu, Sc, Mn and Ti samples, the OH system is only observed with Sc and Ti. This can be partially explained if the proposed Mn OH systems, plate (3.1) are indeed Mn OH, since then there are known stable Cu and Mn OH systems, but none known for Sc and Ti. These observations also assist in demonstrating that there is poor mixing of the sample and the surrounding gas. The production of AuH clearly shows that metal-gas products can be obtained, but the lack of any significant OH in Cu and Mn shows that the reactants in the sample do not significantly disperse. The process cannot be interpreted quite so simply in this respect since the oxidized surface is removed prior to the evaporation of the bulk of the sample and will therefore have a different space, time and thermal distribution. Nevertheless the thermal energy of this oxide will be as high or higher than the bulk of the sample.

Metal chloride bands are the only other significant impurity (plate (3.2)) but these are weak compared with the OH derived systems. The bands in Cu are not known to be recorded, but the ΔG values fit quite well if it is assumed that CuCl is the carrier.

Variable time delay made possible the suppression of some of the impurities. In the pyrolysis of Mn, by choosing delays between 50 and 150 μ secs most of the region can be freed from Mn OH and similarly the Bi spectrum could be freed from Bi_2 in this period. It could also be used for sorting out the excited and ground states in atomic and molecular systems. Even for a complex spectrum such as V, the rapid decay of the excited state transitions and the rising intensity of those from the ground states enables rapid differentiation. However for the hydride systems studied, the application of time resolution is limited since the excited molecular states decay more slowly than those from atoms and also the impurity bands are normally strong before the hydride systems are observed.

3.4 Discussion

Though the experiment was essentially successful in producing a system for detailed analysis, it was not possible to operate the apparatus with a spectrograph of sufficiently high resolution to do the rotational analysis. To obtain sufficient density using a 10 ft grating spectrograph(16) required at least three exposures. Since the sample is destroyed at each exposure this procedure is not practical. A further disadvantage is that a large excess of atomic material is required to produce an acceptable density of hydride and the band lines are hence much broader than can be obtained using a furnace. Thus the analysis of the CuH system was continued in a King furnace.

This Chapter has tended to show the defects of the pyrolysis apparatus in this application but its unique advantages cannot be overlooked. For less than a mgm of sample it is possible to obtain spectra over a large range of temperature and pressure. The former by varying the time delay and the latter the starting pressure. The system is indifferent to the boiling point of the sample. Thus, the full range of elements can be investigated. Containment and wall contamination present no difficulties. This permits the rapid investigation of a wide range of samples restricted only by the availability of suitable samples. The analytic sensitivity is naturally very high but this again assumes that the material geometry conforms to the apparatus requirement. In consideration of these special advantages and the qualitative observations recorded, the need for a quantitative assessment of the apparatus became apparent. Though the flash pyrolysis system has been studied by several authors(7)(8)(13) there is no report of such a detailed analysis relevant to molecular species. If the detailed analysis could be associated with a simple model then the evaluation of the apparatus for any other reaction would be aided. The development and testing of a model for the pyrolysis of gold leaf in H_2 is the subject of the remainder of this section.

CHAPTER 4

RADIANT ENERGY AND PRESSURE EFFECTS

4.1 Radiant Energy and Irradiance

The radiant energy and irradiance functions of the xenon flashtubes are essential to the development of any quantitative model. The total radiant energy incident on the sample is determined by measuring the heat absorbed during a discharge by a small cylinder of graphite held in the normal sample position. The reflectivity, area, mass and specific heat of the cylinder are required. A knowledge of the time history of the discharge can then be used to find the irradiance. This method has been used by Kuebler and Nelson(17) in characterising some similar flashtubes.

A graphite cylinder (Ringsdorf RWO) 19.5 mm long and 6.15 mm in diameter was held symmetrically in the pyrolysis tube supported by a thin bright copper wire frame. A copper-constantan thermocouple inserted in a small hole in the cylinder was used to determine its temperature. The thermocouple EMF was recorded on a Leeds and Northrup pen recorder whose linearity had been previously checked . The reflectance and thermal capacity of the graphite were taken from the above reference(17).

A calibrated silicon photo diode * was used to determine the time distribution of the radiant energy. The peak sensitivity for this type of detector is in the near IR, but it should still show the approximate distribution of total radiant energy with time.

The heat absorbed by the cylinder

$$H = m\int_{\theta_o}^{\theta_m} C_p dt$$

where m is the mass of the cylinder, $C_p = 2.673 + 2.617 \cdot 10^{-3}\,\theta - 116,900\ \theta^{-2}$ cals/°K and θ_o and θ_m are the temperatures recorded immediately before and after the discharge. θ_m is corrected for the finite response time of the measuring system. The contribution from the supports is small and can be approximated by

$$S = m\,(\text{support}) \times 0.1 \times (\theta_m - \theta_o)\ .\ \text{cals}$$

Then the radiant energy incident on the cylinder

$$E = J(100/(100 - R))\ (H + S)\ /\ A \ \text{joules/sq cm}$$

where J is the mechanical equivalent of heat. R is the percentage reflectance and A the area of the cylinder. This varied from 57 to 140 joules/sq cm for bank voltages from 5kV (without reflector) to 6kV (with reflector).

The voltage trace from the photodiode was recorded for each discharge. The area of this trace

$$A_T = \int_{o}^{t_f} V(t)\,dt$$

where t_f is an arbitrary time beyond which the radiant energy is negligible.

---

* EG & G type SGD-100A.

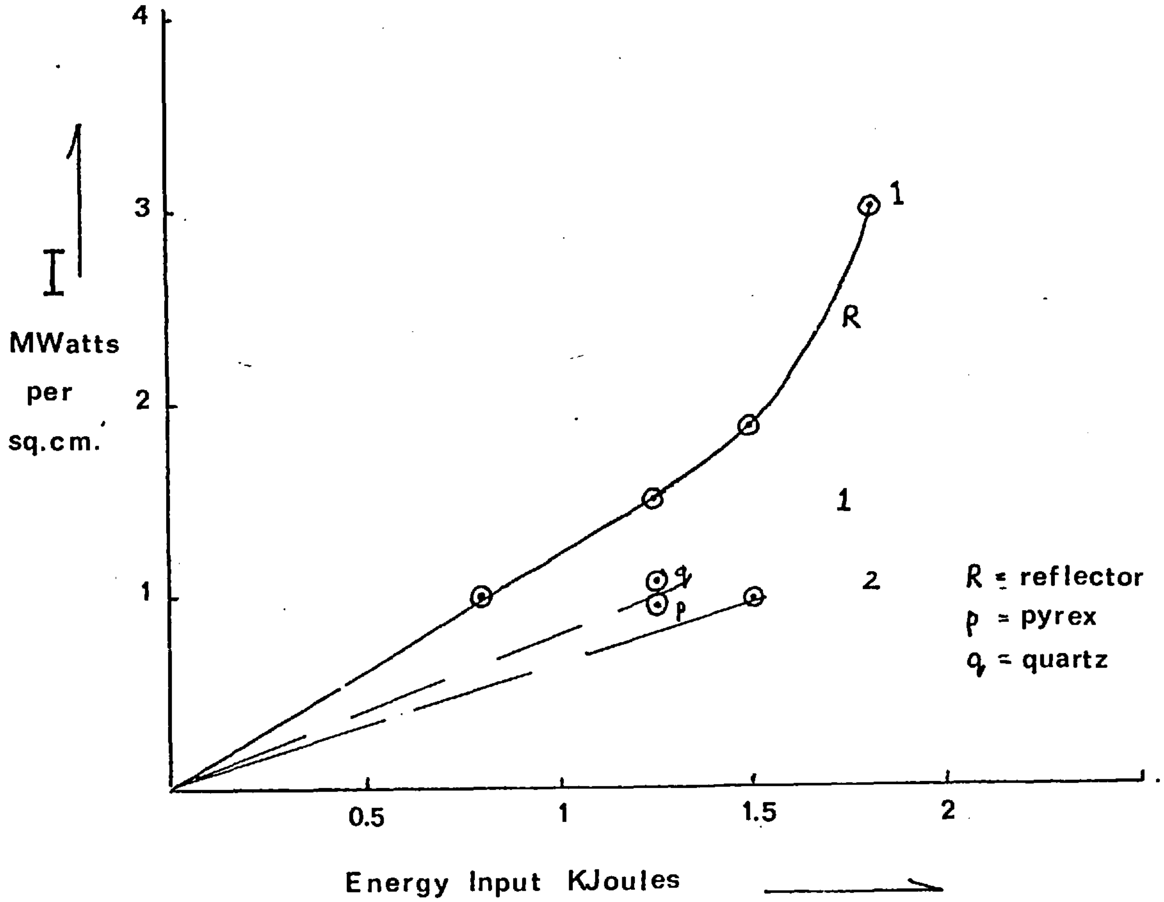
4
3
2
1
I
MWatts per sq.cm.
0.5
1
1.5
2
Energy Input KJoules
1
R
1
2
q
p
R = reflector
p = pyrex
q = quartz

FIGURE 4 , 1

Then the irradiance at time t is

$$R(t) = E \times V(t)/A(t),$$

V(t) need only be defined to the extent that it is a parameter directly proportional to the radiant energy produced by the flashtube at time t. Figure (4.1) is a graph of some peak irradiance measurements for the two flashtubes used. The values obtained with a reflector are significantly higher than without, however the reflector also acted as an aerial for the triggering pulse which caused premature firing of the background flashtube. The xenon flashtubes were thus always used without a reflector. Both quartz and pyrex sample tubes were tested showing only a few per cent difference in transmitted energy. The pyrex tubes are however subject to surface crazing and required replacing after about a hundred discharges.

To complete this section a summary of physical details of the flashtubes used will be given.

ZFT1

Length 5.5 cm; ID 2.5 cm; OD 4.5 cm; number of turns 2.5; material - fused quartz; filling specpure xenon plus trace of Hg. This flashtube had been shortened and refilled as previously described.

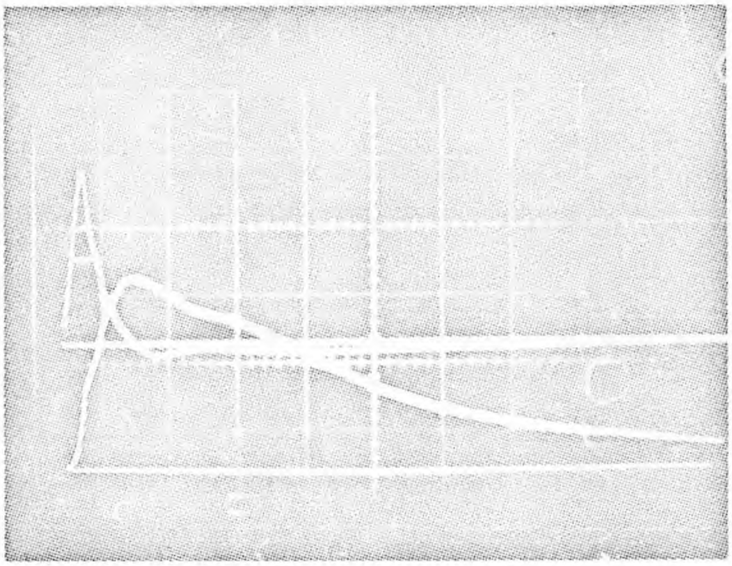

FLASHTUBE 2 dI/dt and Erad

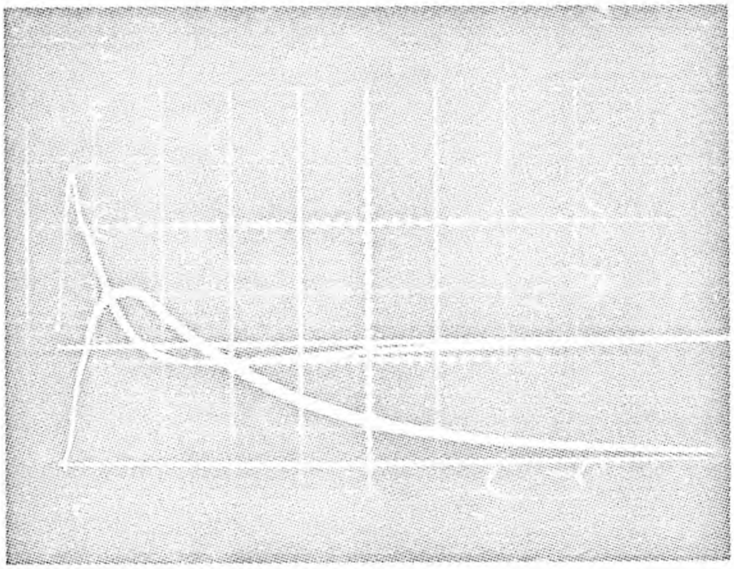

FLASHTUBE 1 dI/dt and Erad

FIGURE 4.2

ZFT2

Length 7.5 cm; ID 2.5 cm; OD 4.5 cm; number of turns 3; material - spectrosil; filling specpure xenon.

The current through the flashtubes was deduced from measurements using a Rogowski coil round the power lead. A typical record of each flashtube is shown in figure (4.2). The accompanying traces of the light pulse are only approximate since the measuring circuit was assembled with a long time constant. The traces show that the radiant energy output closely follows the current which has a maximum value of about 5 k Amps in both flashtubes.

4.2 Discussion

The physically smaller flashtube ZFT1 produced the higher irradiance for the same firing voltage and appeared to match the discharge circuit nearer to the critically damped condition. ZFT2 overdamps the discharge and this could not be efficiently corrected by adding external inductance. The measured efficiency for the conversion of stored energy to radiant energy was between 60 and 70% for all the measured points. This is in agreement with the measurements of Kuebler and Nelson(17). However the irradiances are approximately forty times higher than those measured by these authors. This is principally due to the re-entrant structure of the flashtubes which enables them to produce pulse widths 1/10 of those with a single coil helix. Under the normal operating conditions the peak irradiances and total radiant energies are

77.3 joules/sq cm 1.2 M Watts/sq cm ZFT1)
) V = 5.6kV no reflector
73.4 joules/sq cm 1.0 M Watts/sq cm ZFT2)

4.3 Pressure Probe Measurements

The measurements with the pressure probe were undertaken to show that there were no significant excess pressures developed during flash pyrolysis. This would then limit the maximum thermal temperature of the evaporated sample to its boiling point. Whether the sample is volatilised or passes through a liquid phase, the critical period for the absorption of energy occurs when the sample attains its boiling point. If the rate of energy absorption is then sufficiently high a transient high pressure will be produced and superheating can occur. This effect certainly does occur for extremely high irradiances as occur in laser pulses(18) but for the lower irradiances used here it is shown not to occur.

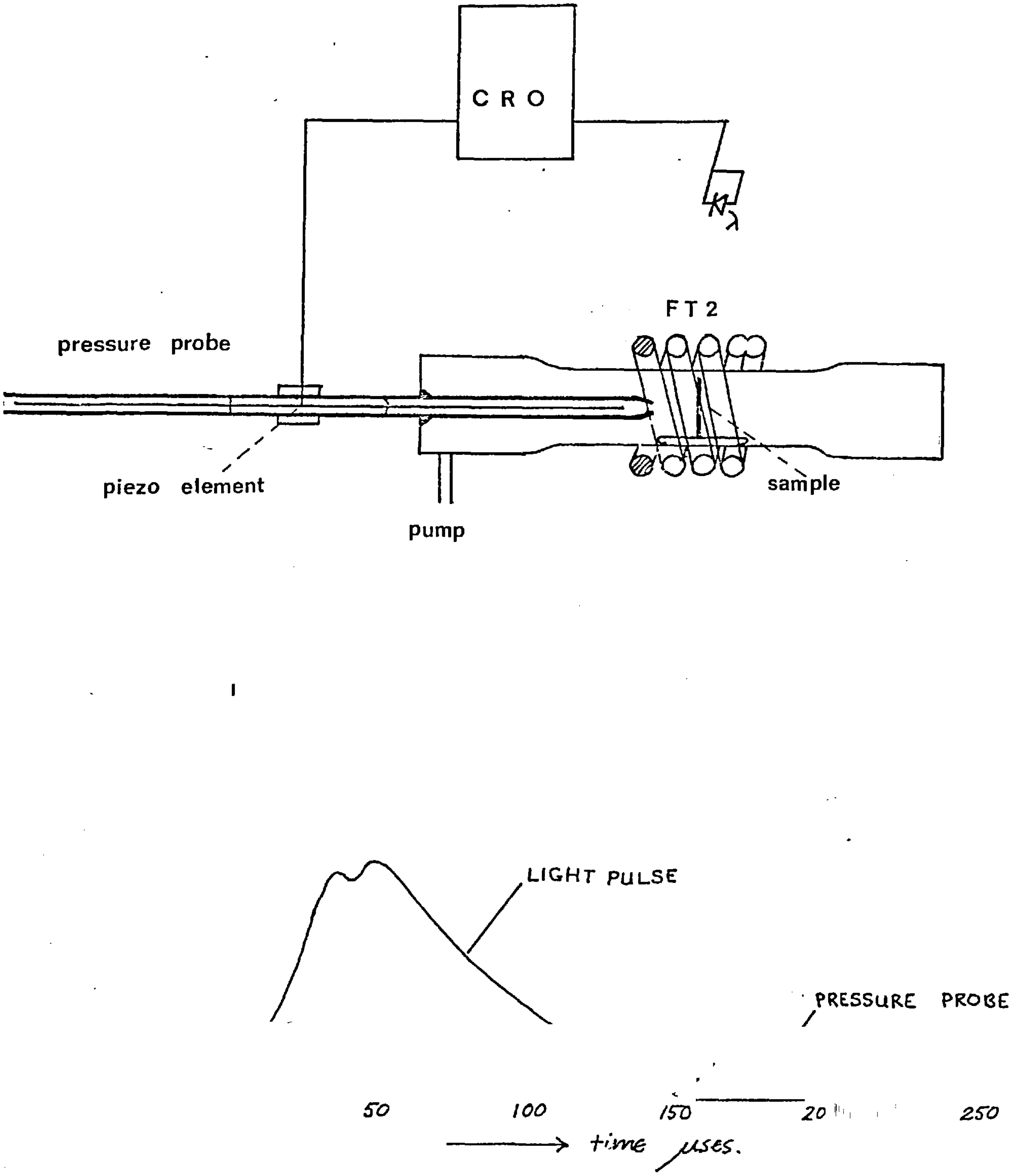
C R O
F T 2
pressure probe
piezo element
pump
sample
LIGHT PULSE
PRESSURE PROBE
50
100
150
20
250
time µses.

FIGURE 4 . 3

A fast sensitive pressure probe(19) was used as shown in figure (4.3.1) to detect any transient pressure effects. The probe was made by R Measures and is described in his thesis(19). The falling ball method which he describes was used to check the sensitivity and this agreed with his calibration within 5%.

The quartz rod near the sample transmits any pressure pulse to the shielded piezo transducer which is connected to an oscilloscope. There is a delay of 150 μsec while the pulse is transmitted down this rod and then an open period of 150μ sec before reflections from the open end of the matching rod appear. To avoid direct heating of the piezo crystal by light funnelling down the quartz, the tip of the probe was coated with platinum black. This was shown to be completely satisfactory since the instantaneous effect of direct heating is easily distinguished from the delayed pressure effect. To check that a heat pulse generated at the tip would not be recorded a thin metal diaphragm was placed over the end of the probe. This showed that there were no heat effects in the open period of the probe.

Figure (4.3.2) shows a typical tracing of the probe output produced in this case by a Bi sample in ½ atmosphere of He, the flashtube being fired at 6kV. There is an initial pulse of small magnitude (less than

0.01 atmospheres) which lasts for about 50μ secs. This corresponds to the time during which the sample is evaporating. The complex trace after about 300 μ sec is due to the reflected pulses and heat pulse effects. Since there is no recorded pressure excess greater than 0.01 atmospheres during the whole of the discharge there can be no significant super heating of the sample and hence the maximum thermal temperature attainable is limited to the boiling point of the material, at the ambient pressure selected.

One can also deduce from this result that the sample is not evaporated as a lamina since then the evaporation would be so rapid that a pulse must occur. In the case of gold leaf consider the sample to be completely liquid and at the boiling point but still a lamina.

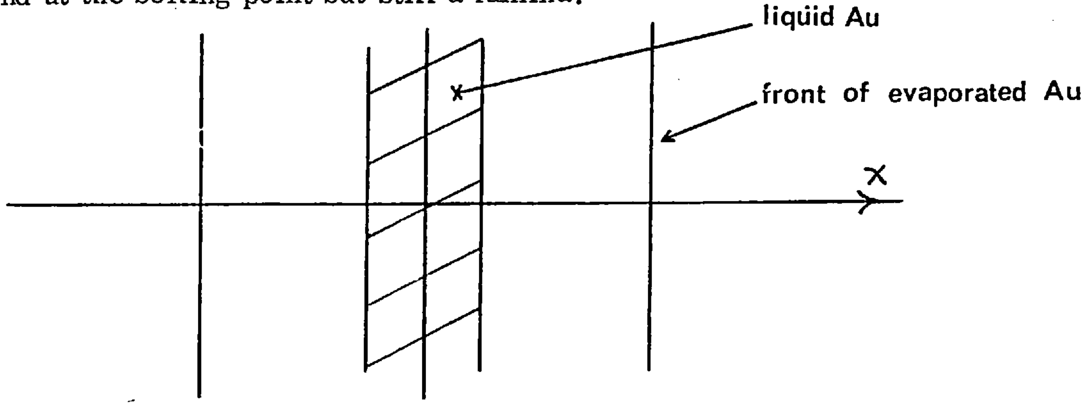

The rate of loss of mass/unit area of the sample $dm/dt = RdE/dt/L_b$, where RdE is the energy absorbed by the sample in dt and L_b is the latent heat of boiling. Then $dx/dt \approx (dm/dt/M_{Au}) \frac{kT}{p} \approx 1.5_{10}5$ cm/sec, for a sample of gold leaf in one atmosphere of H_2. The velocity of sound under these conditions is less than $3_{10}4$ cm/sec, which is very much smaller than the rate at which the evaporated gold front moves. Thus since no pressure pulse is recorded the sample cannot evaporate as a lamina.

CHAPTER 5

THEORETICAL ANALYSIS

5.1 Introduction

A complete solution for the flash pyrolysis of a sample would require the simultaneous solution of the particle and heat diffusion equations. This would be a formidable task even if the boundary conditions and diffusion constants could be defined. The alternative approach adopted here was to use the experimental observations to try and pick out the dominant processes involved. A simplified model was then produced which could be checked by further experiment.

The sample chosen for the analysis was commercial gold leaf. This is an ideal sample since it is readily available in consistent quality and the AuH bands are a strong system in the quartz UV region. Additionally the sample is virtually free from atmospheric contamination (especially OH) and thus the hydride is formed by a gas-metal reaction. Gold also has a high boiling point, potentially leading to higher populations in excited states.

5.2 Constants

In the experiments the gold leaf was supported vertically and perpendicular to the axis of the flashtube on a thin bright copper wire frame. A single sample 1 cm x 0.75 cm, positioned at the centre of the flashtube was used. The xenon flashtube was fired at 5.6kV which gives ~ 1 M Watt/sq cm peak irradiance. The irradiance function can be approximated as

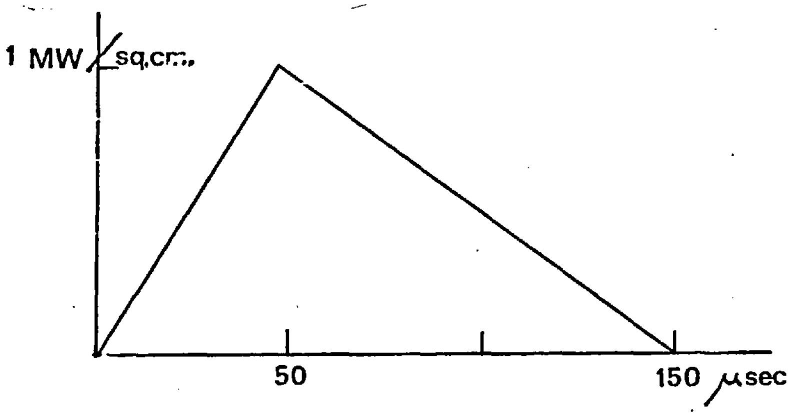

$$
\begin{array}{lll}
I & = 1/50 \times 10^{12} t \text{ Watts/sq cm} & t < 50 \mu \text{ sec} \\
 & = 1.5 \times 10^{6} (1 - 10^{6}/150 \times t) & 150 > t > 50 \mu\text{sec} \\
 & = 0 & t > 150 \mu \text{ sec}
\end{array}
$$

where t is in μ secs from the start of the pulse.

Some constants for the gold leaf and the definition of the symbols are collected below.

d	thickness 0.1 μ
χ	mass/unit area 0.2 mgm/sq cm
ρ	density 19.33 gms/ml (This is the bulk density at 0°C, the sample density will be about 5% lower)
k	thermal conductivity 0.7
R	reflectivity 84% at .6 mμ, 34% at .4 mμ, 18% at .2 mμ(29)
T_m	melting point 1063°C
T_G	boiling point 2966°C
S	specific heat 0.03 at 0°C to 0.033 at 1100°C
L_f	latent heat of fusion 15.8 cals/gm
L_b	latent heat of boiling [415 cals/gm]
S_T	surface tension 1100 cgs (580 to 1100)
M_{Au}	atomic weight 197

The constants are taken from the Rubber Handbook(20), L_b is from E Sargent & Co. and is consistent with Trouton's rule.(21)

5.3 Heat Diffusion Depth

It is desirable to show that the heat diffusion depth is greater than the sample thickness since then the heating effects can be considered to act uniformly on the sample.

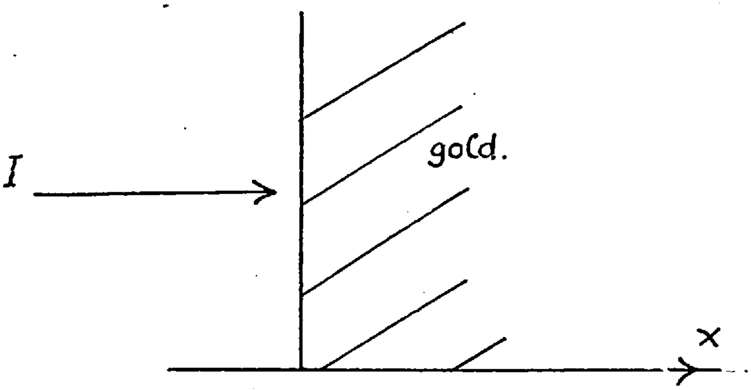

The heat diffusion equation is $kd^2\theta/dx^2 = \rho C_p d\theta/dt$. The boundary condition for an infinite slab adjacent to a vacuum with the slab initially at $\theta = 0$ are $\theta = 0$ $t \leq 0$ and $\theta = 0$, $x < 0$. With $K = k/(\rho C_p)$ then $K d^2\theta/dx^2 = d\theta/dt$ and the Laplace transformed equation is $K d^2\Theta/dx^2 = p\,\Theta - p\,\theta(x,0)$. Then applying the boundary condition $\theta(x,0) = 0$ the solution is

$$\Theta = A\,\frac{e^{-\sqrt{\frac{p}{K}}x}}{p} + B\,\frac{e^{\sqrt{\frac{p}{K}}x}}{p}$$

and since $\Theta(x = \infty) = \theta(x = 0)$ then $B = 0$ and

This can be inverted by Cauchy's method

$$\theta = \int_{Br} \exp(zt)/z \quad A\,e^{-\sqrt{z/K}\,x} \;/z\,dz$$

where Br is a Bromich path, then

$$\theta = Ae^{-x^2/4Kt} \Big/ \sqrt{Kt} \qquad (5.1)$$

This is singular at $t = 0$, $x = 0$ and represents the dispersion of a heat pulse of magnitude $\int \theta\,dx$ incident at $x = 0$, $t = 0$. For a unit pulse

$A = 2/\sqrt{\pi}$. The second boundary condition is fulfilled if equation (5.1) holds for $x > 0$ only, and $\Theta = 0$ for $x < 0$. The diffusion depth is the value of x when Θ / Θ_{max} has fallen to 1/e.

For $t = 1/100\,\mu$ sec the diffusion depth

$$2\sqrt{Kt} = 2\sqrt{kC_p t/\rho}$$

$$\simeq 2\,\mu$$

Hence if the incident radiation can be considered as a series of $1/100\,\mu$ sec pulses, then the sample thickness is very much smaller than the diffusion depth. $1/100\,\mu$ sec is a reasonable unit of division since the maximum energy available in $1/100\,\mu$ sec is $2\,I_{max}(1 - R)t \approx 0.003$ joules/sq cm, which can evaporate from the sample

$$0.003/(J(S\,.\,T + L_b + L_f))\text{ gms/sq cm}$$

$$\simeq .15 \times 10^{-5}\text{ gms/sq cm.}$$

This is about .7% of the sample and is hence negligible. The sample can now be treated as uniformly heated by the incident radiation.

5.4 Conservation of Energy

Experimentally it is observed that there is only a small amount of vaporisation before $50\,\mu$ secs. If the sample remained as a lamina for this period then the energy absorbed is $2(1 - R)\int_0^{50} I\,dt$

$$\simeq 7.5\text{ joules/sq cm}$$

and the energy required to vaporise the sample is $(S\, T_b + L_b + L_f)\, J\chi$

$\simeq 0.4$ joules/sq cm.

Hence if the sample did remain as a lamina the incident energy is 10x more than sufficient to completely evaporate it.

Since the sample is only starting to evaporate after $50\,\mu$ secs it either assumes a shape such that the surface area is minimised or most of the absorbed energy is lost from the sample. The only mechanisms by which the sample can lose energy are re-radiation, diffusion of heat into the surrounding gas and loss to the support.

For a lamina the radiation loss would be $< 2\,\epsilon\sigma\, T_{max}^4$, which, in the case T_{max} always less than T_{boil} gives 1000 Watts/sq cm. Then in $50\,\mu$ secs the heat lost by re-radiation is $\lesssim 0.1$ joules/sq cm. Hence radiation loss accounts for $< 5\%$ of the absorbed energy.

Diffusion of heat into the surrounding gas cannot be a significant effect since there is no apparent difference in the time delay before absorption appears whether the sample is in a high pressure or in a vacuum.

Since the diffusion length of heat is of the order of microns there can only be a small area of the sample close to the support which will be significantly affected by the support.

5.5 Surface Effects

Thus since it has been shown that the sample can be treated as uniformly heated it must pass through a stage where it is completely liquid. In this state the dominant force on the sample is surface tension. Though it is not possible to calculate exactly how the liquid sheet will break up under the influence of surface tension a rough estimate of the effect can be made.

Assume that a circle of radius A in the sheet forms into a drop of radius a. The mass is $\pi A^2 d\rho$. If surface tension is the only significant force acting to form the drop then the initial force is $2\pi A S_T$ and the initial acceleration $2\pi A S_T/(\pi A^2 d\rho) = 2 S_T/(A d\rho)$. If it can also be assumed that to form a drop from the sheet, half the mass of the final drop has to be transported a distance A then $A = \frac{1}{2}\, 2 S_T t^2/(A d\rho)$.

Then $t = \sqrt{\frac{A^2 \rho d}{S_T}} = A\sqrt{\frac{\rho d}{S_T}}$

For $t = 10\,\mu$ secs, $A = 20 \times 10^{-3}$ cm and $a = 15\,\mu$. If a drop of this radius is formed at about 45 to 50 μ sec after the initiation of the light pulse and is at T_b then the energy required to evaporate the drop = $4\pi a^3 \rho L_b/3$ and the energy absorbed is $(1 - R) \int I\,dt\, 4\pi a^2$. Equating these to find t_{min} for the drop to completely evaporate

$$t_{min} \simeq 100\,\mu \text{ sec},$$

though this is obtained only when the first part of the irradiance function is used. When the true irradiance function is used t_{min} cannot be reached and the drop is never evaporated. Effects not considered in this estimate are the energy absorbed while a drop is forming and the decreasing surface area to mass factor as the drop evaporates. Even so this does indicate that drop formation is a suitable mechanism to explain the lack of vaporization before 50 µ secs.

The experimental verification of the formation of drops in the pyrolysis of gold leaf is indirect but Kuebler and Nelson(5) in photographing tungsten strips during pyrolysis clearly showed that it occured in these thicker samples and occasionally with thicker samples small drops of metal were found in the sample tube. With gold leaf or samples of equal thickness there is insufficient material to leave visible drops. The only evidence that droplets are still formed is the observation of fern leaf type patterns on the walls of the sample tube when lower energies and larger samples are used. This suggests that molten balls of the gold are evaporating while moving along the surface.

Though there is no doubt that the sample assumes a shape of minimum surface energy, the size of drops formed (if they are formed in this case) is doubtful. From the observation that there is little absorption before

50 μ secs and keeping the previous assumption regarding the formation of drops then $a \propto t^{\frac{2}{3}}$ then for $t = 50\,\mu$ sec, $a = 30\,\mu$. An alternative method of deriving the probable radius which is independent of the mechanism requires only the definition of a characteristic time τ for the formation of the drop. The sample will be a liquid at about 20 μ sec and would be completely evaporated by about 25 μ secs if it remained as a lamina. Hence a value of τ about 1 μ sec would be reasonable. Then a characteristic length would be $V \tau$ where V is the velocity of sound in the medium which is about 1000 mtrs/sec. The drop radius thus formed would be about 40 μ, as compared with 30 and 15 μ derived previously. The maximum size that a droplet could be is 150 μ when there is only one drop formed.

To try and determine the final distribution of the dispersed sample it is necessary to consider all the forces on the sample in the liquid state. Gravity, with an acceleration of 10^3 cm sec^{-2} is negligible compared with surface tension with an acceleration of $\sim 10^8$ cm sec^{-2}. Capillary waves are only significant if their velocity υ is comparable to the velocity of sound. But since $\upsilon = \sqrt{\frac{2\pi S_T}{\lambda \rho}} \simeq 17/\sqrt{\lambda}$ cm sec^{-1}

$\lambda \sim 1$ A for $\upsilon \sim$ 1000 mtrs/sec and this is a negligible perturbation.

The presence of a differential pressure across the sample would be a significant effect. From the pressure probe experiment, the upper limit on such a differential pressure is 0.01 atmospheres or 10^4 dynes/sq cm and this gives an initial acceleration of $5_{10}7$ cm/sec^2 which is the same order of magnitude as the surface tension effect. A differential pressure could arise due to the different static volumes on each side of the sample, the effect would be to bell or break the sample. The effects of a differential pressure becomes negligible as soon as the sample is broken into drops.

The possibility of large scale defects in the sample introduces a variable which cannot be evaluated. These would be particularly effective if a differential pressure exists since then the sample would be easily fragmented leading to an entirely different evaporated density on the optical axis. The gold leaf was examined before each firing, but this does not ensure that the samples were free from weak areas. The use of gold leaf does exclude one effect recorded by Kuebler and Nelson(5) on tungsten strips, in that the mechanical strength is sufficiently low so that distortion of the sample by differential energy absorption will have only a small effect near the support.

5.6 Discussion

The results of these 'order of magnitude' calculations have shown that the gross features of the pyrolysis experiment can be explained if the sample is uniformly heated until it is completely liquid and then rapidly breaks up into an array of droplets. This explains the lack of observed vapour before $\sim$ 50 μ secs and the improved performance obtained as the film thickness is decreased. The lower limit of the thickness will occur when all the sample is evaporated even after it has formed into drops. There does not appear to be any lower limit after which drop formation does not occur since in all cases the absorption density increased from 50 - 100 μ secs thus evaporation must be occurring in this period. The superiority of wire over sheet samples is also apparent since the maximum drop size available in a wire is much smaller than in a sheet of the same thickness. This allows the use of much thicker wires $\sim$ 5 to 10 μ which have a comparable performance as regards percentage evaporated with sheet samples of .5 to 1 μ.

Having predicted that an array of droplets will form it is now necessary to look more closely at the evaporation of a single droplet to obtain values of N, the total number of absorbers, and n the density. The variation of N and n with time and ambient pressure would also be desirable. The more general objectives are to try and find a set of conditions where the sample will form a uniform absorbing column on the optical axis. This would be useful for any work on f-values or interferometry. Though at this stage the most probable size and distribution of the droplets has not been clearly defined it was felt that later comparison with the experimental results would be more profitable than trying to make a more detailed calculation.

CHAPTER 6

DISPERSION OF A SPHERICAL GOLD DROPLET IN A HYDROGEN ATMOSPHERE

6.1 First Order Calculation

It will be assumed that the droplet is at T_b at $t = 50\,\mu$ sec (after the initiation of the discharge). Then the radiant energy formulae applicable are:

$$I = 3 \times 10^6/2\ (1 - 10^6 t/150) \text{ Watts/sq cm}$$

for $50 < t < 150\,\mu$ secs and $I = 0$ for $t > 150\,\mu$ sec.

A dropsize of $30\,\mu$ will be assumed though this probably represents a lower limit on the radius. The effects of larger drop sizes will be evaluated by extrapolation from the results for the $30\,\mu$ drop.

The general solution of this restricted problem is still very difficult so that it is necessary to consider evaporation and thermal and particle diffusion separately.

The energy absorbed by the drop at time t in dt $t > 50\,\mu$sec dE

$$= (1 - R)\, I\, 4\pi\, a^{*2}\, dt - \epsilon\sigma (T^4 - T_0^4)\, 4\pi\, a^{*2}\, dt - \bar{E}dt$$

Where the first term is the energy absorbed from the flash, the second the re-radiated energy and the third the energy lost by thermal diffusion into the surroundings. As previously the re-radiated energy can be removed since this factor is $< \sigma T^4 \sim 500$ Watts/sq cm, whereas $R \cdot I \sim 70000$ Watts/sq cm.

Though it is known that $\bar{E}dt$ cannot be a large effect since the sample behaves similarly in an initial high ambient pressure and in vacuo, the magnitude of the term can be estimated. By using equation (5.1), the diffusion depth is $2\sqrt{D^1 t^1}$ where t^1 is measured from 50μ sec and $D^1 = k^1/(\rho^1 C_p^1)$, the constants being applied to a hydrogen gas.

$$2\sqrt{\frac{k^1 t^1}{\rho^1 C_p^1}} \simeq 23\sqrt{t^1}\,\mu \qquad \text{with } t^1 \text{ in } \mu \text{ sec.}$$

Thus if the droplet uniformly heated the surrounding gas to this depth for 100μ sec (the time beyond which there is no evaporation) then the total heat required would be

$$4 \pi (230)^2 \times 10^{-8} \; \rho^1 C_p^1 \, . \, J = 7.6 \times 10^{-6} \text{ joules}$$

This is very small compared with the total heat absorbed by the sphere hence the small effect observed in the evaporation in a high pressure and vacuo.

Thus it is a good approximation to use $dE = (1 - R)\, I\, 4\pi a^2 dt$ during the period of the evaporation. As I falls to zero the loss mechanisms will dominate and this period will be treated in the next section.

Since the droplet is assumed to be at T_b then only L_b need be supplied to produce evaporation, thus the mass lost at time t in dt is dm where

$$dm = dE/(4.18\ L_b) \text{ and } dm/dt = (1 - R)\ I\ 4\pi a^2/(4.18\ L_b)$$

Then $da/dt = (1 - R)\ I/(\rho L_b 4.18)$ and therefore

$$\Delta a = -\int_{50}^{150} (1 - R)\ I/(\rho L_b\ 4.18)\ dt$$
$$= 6\mu$$

This result is independent of the initial diameter of the drop and includes the effect of the reduction in radius while the drop is evaporating. For $a \approx 30\mu$ this will correspond to a fraction not evaporated $\approx \frac{1}{2}$, but for a drop of 60μ this becomes $\approx \frac{3}{4}$ and 120μ to $\sim .86$. This shows that the fraction evaporated will decrease rapidly as a increases and that it will be reasonable to expect that the droplet size can be deduced from experimental data on the total number of absorbers.

For a droplet radius of 30μ, the total number of absorbers after 200μ sec delay would be $\simeq \frac{1}{2}\ X/M_{Au} \approx 2.5_{10}\ 17$ atoms/sq cm. The experimental results will be for the impurities in the gold leaf so that Cu which is a 1.22% impurity yields $N_{Cu} \simeq 3_{10}\ 15$ atoms/sq cm. These values can only be achieved after sufficient time has elapsed to allow a uniform distribution of the absorbers.

The variation of N in the period to 150 μ secs can also be evaluated. It is assumed that there is no evaporation before 50 μ secs.

t = 70 μsec	$\Delta a = 2.2\,\mu$	N(t) = $1.1\,{}_{10}{}^{15}$ Cu atoms
90	3.8	$1.9\,{}_{10}{}^{15}$
110	5.0	$2.5\,{}_{10}{}^{15}$
130	5.8	$2.9\,{}_{10}{}^{15}$
150	6.0	$3\,{}_{10}{}^{15}$

The value of N only changes by a factor of 3 after the first 20 μ secs and thus when comparing intensities on a photographic plate there will be only a small visual variation over the period of the evaporation.

6.2 Particle Diffusion

To obtain the values of n, the density of absorbers it will be necessary to consider the diffusion of the evaporated gold away from the droplet. It will be assumed that until evaporation is complete n is fixed at the density which will balance the ambient pressure. Thus in the period 50 - 150 μ sec delay the measured value of n is expected to be approximately constant. To simplify the problem it will be necessary to neglect any thermal diffusion and turbulence.

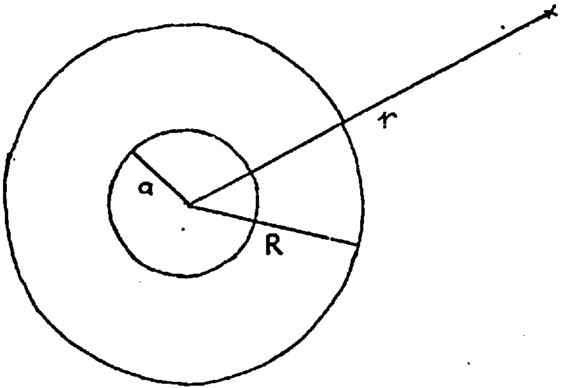

The initial conditions are

$$n = n_o \quad a < r < R$$

and $$n = 0 \quad r > R$$

a is the radius of the gold droplet at 150μ sec and R is the radius of the sphere of gold vapour around the droplet. The diffusion equation can be reduced to the spherically symmetric form since turbulence is being neglected.

$$\frac{\partial^2 n}{\partial r^2} + \frac{1}{r}\frac{\partial n}{\partial r} = \frac{1}{D}\frac{\partial n}{\partial t}$$

The solutions required need only be valid for $t > 0$ and $r > a$ and satisfy the boundary condition $n \to 0$ as $t \to \infty$.

Let $y = nr$ then $\frac{\partial^2 y}{\partial r^2} = \frac{1}{D}\frac{\partial y}{\partial t}$

By reference to the solution equation (5.1) which is also a particular solution of the above equation for a pulse distribution of particles at $t = 0$, $r = 0$.

Then

$$y = Ae^{-(r^2/4Dt)} / \sqrt{Dt}$$

And for an initial distribution y(r,0)

$$y(r,t) = \int_{-\infty}^{\infty} \frac{Ay(z,0)e^{-(z-r)^2/4Dt}}{\sqrt{Dt}} dz$$

Then for $y(r,0) = n_o y$

$$y(r,t) = 2An_o \int_a^{\infty} \frac{z}{\sqrt{Dt}} e^{-(z-r)^2/4Dt} dz$$

where $\int_{-\infty}^{\infty}$ has been replaced by $2\int_a^{\infty}$ since the function y(r,0) is symmetric and the region $-a < r < a$ is being avoided.

Then

$$y(r,t) = 2An_o \int_a^R \frac{ze^{-(z-r)^2/4Dt}}{\sqrt{Dt}} dz$$

$$= \frac{2An_o r}{\sqrt{\pi}} \left(\operatorname{erf}\left(\frac{R-r}{2\sqrt{Dt}}\right) - \operatorname{erf}\left(\frac{a-r}{2\sqrt{Dt}}\right)\right)$$

$$+ \frac{A\sqrt{Dt}}{4r\sqrt{\pi}} \left(e^{-(r-a)^2/4Dt} - e^{-(r-R)^2/4Dt} \right)$$

This is the solution if free diffusion back into the region $-a < r < a$ is allowed, and though this is not possible it will produce only a small discrepancy if $R \gg a$, and that this is so will be shown later.

For $t = 0$ and $a < r < R$ $n = n_o$, therefore $A = \frac{1}{2}$ and $n(r,t) =$

$$\frac{n_o}{\sqrt{\pi}} \left(\operatorname{erf}\left(\frac{R-r}{2\sqrt{Dt}}\right) - \operatorname{erf}\left(\frac{a-r}{2\sqrt{Dt}}\right)\right) + \frac{\sqrt{Dt}\, n_o}{8\sqrt{\pi}\, r} \times$$

$$\left(e^{-(r-a)^2/4Dt} - e^{-(r-R)^2/4Dt}\right) \qquad (6.1)$$

For $t \rightarrow 0$ and $r > 0$, $n \rightarrow 0$, therfore the above solution satisifies this boundary condition.

Before going on to consider when the above solution can be reduced to the simple erf form it is necessary to obtain values for R and a particular to the gold droplet. For $\Delta a = 6\mu$ which was previously derived and $a = 30\mu$, then the mass of drop evaporated

$$\Delta m = 4/3\ \pi\ \rho\ \ (30^3 - 24^3)\ 10^{-12} \text{gms}$$

And

$$N = \Delta m / M_{Au} \quad \text{atoms}$$
$$= 3.24\ .\ 10^{15} \quad \text{atoms}$$

If $p = nkT$ is used with $p = 10^6$ dynes/sq cm and $T = 3240^{\circ}K$ then $n = 10^6/(1.38 \times 3240 \times 10^{-16})$ atoms/cc. Then the radius of initially evaporated gold R is given in $4/3\ \pi\ R^3 = N/n \doteq 1.4.10^{-4}$ cc assuming $R \gg a$. This gives $R \sim 600\mu$ which makes the previous assumptions that $R \gg a$ valid in this case. The above argument will also be true up to the maximum size that the droplet can be ($\sim 150\mu$) since then $R/a \; a > 30\mu$ will be much greater than $R/a \; a = 30\mu$.

In evaluating equation (6.1) there were two objectives: to try and determine n(t) (the average density of absorbers) and to derive the conditions for which the absorbing column could be assumed to be uniform. The second condition is most important since the measurement of the number density will only be an integrated value unless there is a significant uniform region.

By equating the mass of the droplet to a square in the sample, the interdrop spacing can be estimated. For a 30 μ drop this will be approximately 700 μ. Clearly in this case a drop size of 30 μ yielding a 600 μ radius cloud of gold vapour will be unifrom from about 200 μ secs delay without any need to consider equation (6.1). For a larger drop of radius 80 μ, under the same conditions, the interdrop spacing is $\sim$ 0.45 cm and the value of R is $\sim$ 0.15 cm. In this case there is a large spacing between the expanding spheres of gold vapour and hence the absorbing column will be totally non-uniform. The value of r between two drops would be 0.225 cm so that the terms in (a - r) would be insignificant. A reasonable value for D would be 0.5 $\text{cm}^2 \text{ sec}^{-1}$ (22) and for uniformity the value of the diffusion length in the erf term can be used to obtain an approximate value of t. This gives a time of nearly 1.2 m secs before this criterion can be reached, and the effect of the exponential term which represents less than 5% of the erf term will tend to increase this time.

The criteria for uniformity can be relaxed slightly but this will not bring t to a value below 500μ sec.

6.3 Discussion

Thus for a droplet radius $\lesssim 30\mu$ the absorbing column can be approximately uniform, but for greater radii, the column is never uniform before there is signficant cooling and diffusion away from the light path. This also implies that the measured values of n will only be meaningful if the droplet radius is $\lesssim 30\mu$ otherwise it would be necessary to know the variation in n along the light path in order to obtain the values of n.

Values of N, N(t) and n have been deduced and an upper limit on the kinetic temperature defined. The next steps would be to introduce thermal diffusion and vapour-gas mixing. However this would be largely academic since constants for this system are not known and the experimental accuracy could not check any results. However the model and experimental results can now be compared and any further anomalies tested by extending the model.

CHAPTER 7

EXPERIMENTAL RESULTS FOR GOLD LEAF

7.1 Calibration

Commercial gold leaf was used throughout these experiments. The gold samples 1 x 0.75 cm, supported on a wire frame were pyrolysed by the light pulse from the xenon flashtube fired at 5.6 kV. The delay before firing of the background flashtube was measured from the commencement of significant light output from the xenon flashtube. A pyrex sample tube was used to reduce the effects of scattered light at high wavelengths.

Visual estimates of the density of absorbers on photographic plates had shown that the shot to shot repeatability would not be sufficiently uniform to allow the use of a photomultiplier. A pre-condition of performing the measurements using photographic plates is a relative calibration of each plate. It is desirable to avoid time response effects and use the same source for calibrating the plates and for making the exposure. A step wedge could not be used since the background flash could not be made sufficiently uniform over the slit consistent with a reasonable working exposure. Thus calibrations used a set of partially transparent aluminium films deposited on standard quartz windows. These filters were calibrated from 2500 to 3500 Å using the lines from a mercury lamp. The calibration set-up used an approximately collimated beam of parallel light passed through a filter holder and the focused to the slit of a small Hilger and Watts monochromator. An IP28 photomultiplier measured the ratio of the light transmitted with and without the filter which gives the percentage transmission. The transmission curves for the filters were smooth in the measured region but did not all vary uniformly. Since a large area of the filters is utilised, the development of pinholes has a negligible influence and a re-calibration after 3 months use showed no significant change in transmissions.

The background flashtube must be reproducible to better than 5% for at least 3 shots if separate filters are to be used for the plate calibration. The inclusion of the baffle and drift tube allowed this to be achieved except for the region below about 2300 Å. Trying to avoid a set of filters by using a single filter with multiple exposures fails since this requires up to 20 shots and the flashtube intensity cannot be retained accurately for this number of shots. Thus the full set of filters was normally used for the seven calibration levels beginning and ending with no filter as a check on the reproducibility. The plate densities were measured using a Jarrol Ash microdensitometer, a standard curve being drawn for each region of the plate used.

7.2 Rotational Temperature

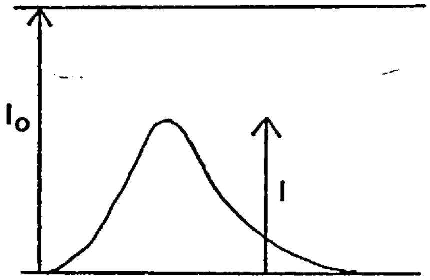

For an absorption line of peak height I in the continuum I_o, Lambert's law gives

$$I = I_o(1 - e^{-\alpha_\nu N})$$

where α_ν is the atomic absorption coefficient and N is the total number of absorbers in the light path. When α_ν N is small then

$$I = I_o \, \alpha_\nu \, N$$

For a ${}^1\Sigma - {}^1\Sigma$ transition(23)

$$I = C(J' + J'' + 1) \, e^{- hc B_v'' (J'' + 1) J''/kT_{rot}}$$

This assumes that the energy levels are filled according to a Boltzman distribution. C contains the rotational transition probability and assuming that this is constant throughout the band

$$\log_{10} (k'I/(J' + J'' + 1))/\log_{10} (e) = B_v'' J'' (J'' + 1) \times 1.23_{10}^{-4} / kT_{rot}$$

with kT_{rot} in eV and $k'I$ being the relative peak intensities of the band lines.

It is reasonable to assume that C is constant through a strong (0,0) band$^{(24)}$ and should be approximately constant through the (0,1) band. The fit of the experimental results to a straight line tests for a Boltzmann distribution. Though a_v is large, N is sufficiently small for the approximation $\exp(-a_v N) = 1 - a_v N$ to be valid. The use of I_{peak} rather than $\int I d\nu$ is a poorer approximation since the line width is of the same order as the instrument width. This means that any broadening of the lines at higher J values will have a fairly large effect on I_{peak}.

Plate (3.1) shows a typical set of exposures for the determination of T_{rot} ν time and the results obtained. A set of representative graphs of $\log_{10}(k'I/(J' + J'' + 1))$ ν $B_v'' J'' (J'' + 1)$ show that for the majority of the results a straight line can be drawn through the experimental points except for the very low J values. These graphs are very similar to ones published by Penner$^{(25)}$ and Learner$^{(24)}$ for strong (0,0) bands, also showing the lower members lying well above the extrapolated straight line graph. The best straight line fit was determined by eye since then account could be taken of the partially overlapped lines which were systematically displaced.

The results appear to show that the rotational temperature is a good parameter for the bands. During the light pulse T_{rot} rises to nearly 6000°C which is also the approximate colour temperature of the flashtube. T_{rot} then falls to a value near the boiling point of gold, and then there is the fall in temperature as the reactants diffuse into the cold buffer gas. The results do not vary smoothly nor does a plot of the integrated intensity of the (0,0) band. The intensity however does gradually rise up to 500μ sec and then begins to decay and it is reasonable to extrapolate from these measurements and say that for any single experiment the intensity rises smoothly to 500μ sec and that T_{rot} after rising rapidly to about 5,500°C falls to $\sim T_{boil}$ and then gradually decreases.

As a check on T_{rot} measured for the (0,0) band a similar procedure was used to obtain T_{rot} for the (0,1) band. This could only be satisfactorily measured for the longest delay and gave $T_{rot} = 1600°C$. This is very much lower than T_{rot} for the (0,0) band which was measured on the same plate. Since the plot for T_{rot} is an acceptable straight line, the energy distribution in the band appears to be still following a Boltzmann distribution, unfortunately with a different value for T_{rot}. This was an isolated measurement and as a further check on the molecular temperature the vibrational temperature was measured.

7.3 Vibrational Temperature

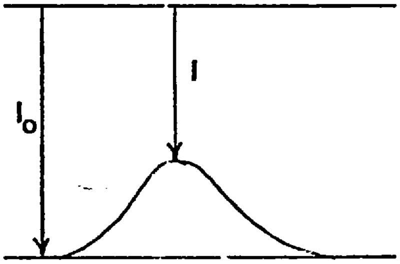

It is more convenient here to use $I = I_o \exp(-\alpha_\upsilon \int n\,dx)$ as the form of Lambert's law with $\int n\,dx = N$, the total number of absorbers in the light path.

$$\text{Then}\qquad \ln(I/I_o)\,\Delta\upsilon = (-\alpha_\upsilon \int n\,dx)\,\Delta\upsilon$$
$$= \pi \quad gf \int n\,dx$$

where $\alpha_\upsilon \Delta\upsilon \simeq \int \alpha_\nu\, d\nu$ and gf is the statistical weight x the f-value of the transition. Then for the P(i) line in the (0,1) and (0,0) bands.

$$\frac{\ln(I/I_o)_{P(i)\ (0,1)}}{\ln(I/I_o)_{P(i)\ (0,0)}} = f_i\, n_{i1} / f_o\, n_{io}$$

Peak intensities only are used so that this assumes the line widths will be nearly constant. If the vibrational levels are filled following a Boltzmann distribution then

$$n_{i1}/n_{io} = \frac{n_{o1}\ e^{-B1\ i(i+1)/kT}}{n_{oo}\ e^{-B2\ i(i+1)/kT}}$$
$$\simeq e^{-\Delta_1 G/kT_{vib}}$$

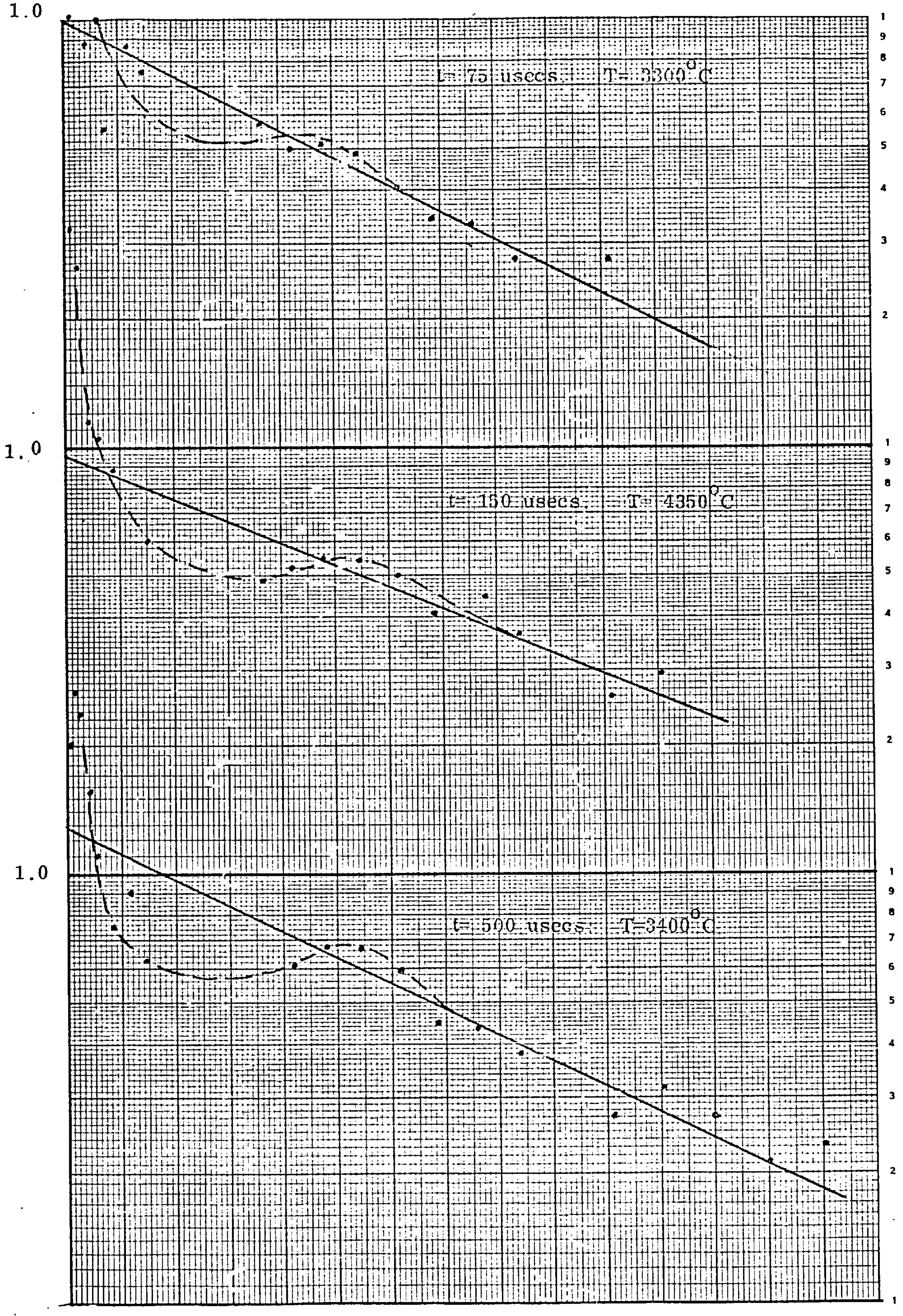

GRAPHS OF LOG_{10} (RELATIVE INTENSITY/$(J' + J'' + 1)$) v $J''(J''+1)$

This is nearly always valid since $\Delta_1 G$ is usually very much larger than $(B_2 - B_1)$. Summing over any equivalent sets of lines in the two P and R branches gives

$$\sum_{i}^{m} \log_{10}\left(\frac{f_o}{f_1} \times \frac{\log_{10} (I_{i1}/I_o)}{\log_{10} (I_{io}/I_o)}\right) = -m.\Delta_1 G \ \log_{10}(e)/kT_{vib}$$

In this expression the I_{i1} and I_{io}'s can be measured and $\Delta_1 G = 2305 \text{ cm}^{-1}$(23) but f_o/f_1 has not been measured experimentally. A theoretical value is given by U Ringström(26) but this is based on a fairly crude approximation for the potential function. A program written by R Learner(24) was used to obtain a set of relative dipole moments based on a Morse-Peckeris potential function. Both this set and those published by Ringström are in general agreement with observed relative intensity measurements.(26)

v' \ v"	0	1	2
0	1.0	1.31	0.54
1	1.07	0.18	0.34
2	0.87	0.003	0.54

The values of I_{i1} and I_{io} were substituted in the above expression for at least six pairs of well resolved lines in the P and R branches, with

$f/f_o = 1.31$ giving the following values for T_{vib}.

T_{vib}(°C)	Time delay (μsec)
4600	150
3300	250
3500	500

These results are in fairly good agreement with T_{rot} for the (0,0) band and tend to show that T_{rot} for the (0,1) band is an isolated anomaly. However the results are strongly dependent on f_1/f_o and this is the weakest point in the derivation of T_{vib}. It is also assumed that the f-value varies in the same way for the (0,0) and (0,1) transitions and can be represented by a single value f_1/f_o for the whole band.

7.4 Rotational Temperature Versus Pressure

These measurements were obtained by keeping the delay fixed at 200 μsec and varying the ambient pressure of hydrogen. A 200 μsec delay was chosen because this corresponds to the end of the xenon flash-tube light pulse. This is the period where the energy in the vapour will be a maximum without any photolytic effects from the light pulse.

T_{rot}(°C)	P (atmospheres)
3500	1.0
3500	0.75
3200	0.5
3600	0.25
2300	0.125
2900	0,1

T_{rot} at 1 atmosphere is in good agreement with the values previously obtained for delays of 150 and 250 μ secs. For pressures less than 0.1 atmospheres, the bands were too weak to give acceptable plots.

The first observation drawn from these results is that T_{rot} falls significantly for pressures $\lesssim$ 0.25 atmospheres. This is expected since at low pressures the gold vapour will diffuse more rapidly out into the cold buffer gas and there is no possibility of obtaining a region of vapour in thermal equilibrium at T_{boil}.

7.5 Atomic Excitation Temperature

Reviewing all the data at this stage, it appears that for the period 200 - 500 μsecs and pressures above 0.25 atmospheres, $T_{rot} \simeq T_{vib} \simeq T_{boil}$.

It would be misleading however to suppose that this implies a limited range of thermal equilibrium. If there is thermal equilibrium then T_{ex}, the atomic excitation temperature, should also be $\simeq T_{boil}$. The relative total intensities of lines from the ground states of Fe were used to try and obtain T_{ex}. Assuming these are filled according to a Boltzmann distribution then

$$T_{ex} = (E_1 - E_2) \log_{10} e / (k \log_{10}(n_1/n_2))$$

$$= (E_1 - E_2) \log_{10} e / (k \log_{10} (f_2 I_1/f_1 I_2))$$

Where $(E_1 - E_2)$ is the energy separation of two of the ground states and f_1 and f_2 are their f-values. The values of T_{ex} derived from this formula ranged from + 1100°C to - 50°C in the same plate. Though it is true that the criterion for thermal equilibrium between levels in the ground state is very much stricter than for excited levels(27), it is surprising that T_{ex} should be such a poor parameter whereas T_{vib} and T_{rot} are quite reasonable. A marked follow up to this experiment would be to obtain T_{ex} from relative populations of more highly excited states which have allowed direct transitions. However there are no available elements which have such states with any measurable population of the excited state at this temperature. Close levels above the ground state given equally random values for T_{ex} as those measured in the Fe ground state.

7.6 Discussion

The object of these extensive measurements of the excitation temperatures was first to verify that T_{boil} was the maximum temperature attained and second to delineate a region, if it existed, where T_{boil} could be substituted for the excitation temperatures. That T_{rot} exceeds T_{boil} during the light pulse indicates that energy can still be absorbed by the evaporated material provided there is a system of closely spaced levels to absorb the light energy. Thus T_{boil} is not the maximum temperature that a molecular product can reach. However at the end of the light pulse T_{rot} and T_{vib} are approximately equal to T_{boil} for a period of about 300 μ sec. But for this case there is no region where all the excitation temperatures can be replaced by T_{boil}. The poor agreement of T_{ex} also casts doubt on the application of $T_{rot} = T_{vib} = T_{boil}$ to other molecular systems.

Regarding the accuracy of the measurements since plate densities were used and the temperature is in the exponent part an error of between 10 and 20% can be anticipated. The values of T_{rot} and T_{vib} are based on a fairly large number of data points so that the error should be nearer the lower limit. Accepting an error of 10% puts too many of the measurements outside the limits of error if it is assumed that the values should be smoothly varying. However, the droplet model would yield a non-uniform distribution of vapour and though the average of a large number of experiments would yield a smooth variation of the excitation temperatures, individual experiments can have a large random variation. Hence the lower experimental error is consistent with the experimental results.

7.7 Total Number of Absorbers and Number Density

The total number of absorbers was measured from a set of calibrated plates containing either copper or silver resonance lines. These were broad enough to neglect spectrographic broadening but not sufficiently strong to go through the continuum like the Au resonance lines.

Following the same pattern as for T_{vib} from $I = I_o e^{-a_\nu \int n\,dx}$ then

$$\ln (I_o/I) = a_\nu \int n \, dx$$

and $\int_{line} \ln (I_o/I) \, dv = \int n \, dx \quad \int_{line} a_\nu \, dv = \pi e^2/mc^2 f \int n \, dx$

Hence

$$\int n \, dx = mc^2/\pi e^2 \int_{line} \log_{10} (I_o/I) \, dv / \log_{10} e / f$$

I/I_o was determined for several values of ν across a line profile and then plotted on logarithmic graph paper. The points were joined with a smooth curve and $\int_{\text{line}} \log_{10}(I_o/I)\, dv$, evaluated either using a planimeter or counting squares.

Since the gold resonance lines could not be used it was necessary to obtain an analysis of the gold leaf to determine the ratio of Cu and Ag in the gold. The percentages of silver and copper in the gold leaf were determined by the Analytic Laboratory at Imperial College as 5.55% and 1.22%. Other impurities were not checked so the gold content will be only approximately 93.24%. Iron, irridium and Ca were the only other impurities detected and they were relatively very much less abundant than copper or silver.

With $N = \int n dx$ and assuming that there is negligible re-emission or scattered light then tables of N versus pressure and delay could be formed.

Table 1

N Versus Delay Time

Pressure = 1 atmosphere H_2

Delay sec	N (per sq cm)		N(Au)
75	$3.38_{10}14$	(Ag)	$.69_{10}16$
100	1.01	Cu	.83
150	1.13	Cu	.93
250	1.38	Cu	1.13
500	0.76	Cu	.62

Table 2

N Versus Starting Pressure

Delay = 200 μ sec

Pressure (atmospheres)	N (per sq cm)	N (Au)
1.0	$0.58_{10}{}^{14}$	$0.48_{10}{}^{16}$
0.5	0.73	0.60
0.13	0.59	0.49
0.066	0.24	0.20
10 mm Hg	0.09	0.069
5 mm Hg	0.10	0.078
1 mm Hg	0.047	0.036

These values for N(Au) can be compared with the predicted values for a 30μ drop array of N(Au) $\simeq$ $2.5_{10}{}^{17}$/sq cm and $1.2_{10}{}^{17}$/sq cm for a 60μ array. The experimental results are an order of magnitude below either of these values. Thus the calculated value is in the correct direction but does not go far enough to explain these results.

So far only $\int$ ndx has been determined. To obtain n (or at least an average value for n), it is necessary to determine the line widths. The broadening mechanism will be predominantly resonance broadening so that the relation between the half width $2\Delta\lambda$ and n is given by[27]

$$2\ \Delta\lambda = 5.2\ f\ (g_1/g_2)^{\frac{1}{2}}\ (n/10^{19})\ \text{Å}$$

$$(2\ \Delta\lambda = 3.62\ f\ (n/10^{19})\ \text{Å}\ )^{(28)}$$

Use of the above formula with a small compensation for the slit width contribution gives a value for n along the light path. Resonance broadening will result in a gaussian profile. However, the measured profiles were not gaussian and the values of n derived are not satisfactory, though the variation of n with p and t seemed to be reasonable.

Table 1

$2\Delta\lambda$ v Time Delay

Delay (μsec)	$2\ \Delta\lambda$ *1(Å)	$2\ \Delta\lambda$ *2(Å)
75	2.74	3.83 Ag
100	1.99	1.47 Cu
150	2.09	1.68 Cu
250	2.36	1.70 Cu
500	2.15	1.75 Cu

*1 The half widths are determined from the curve log(I) v λ rather than I v λ .

*2 Half widths determined from the curve I v λ .

TABLE 2

2 Δλ v Pressure

Pressure (atmospheres)	2 Δλ ^{*1} (Å)	
1.0	1.83	Cu
0.5	1.78	Cu
0.13	1.62	Cu
0.066	1.08	Cu
10 mm Hg	1.07	Ag
5 mm Hg	1.09	Ag
1 mm Hg	1.02	Ag

Substituting these half widths into the above formula give values of n very much higher than atmospheric pressure. This result not only brings into doubt the validity of the profiles for determining n but also indicates that N will be underestimated. If 2 Δλ is too large because of defocussing then N will be correct, but if this is due to scattered light or emission, then N will be low due to the centre of the line being depressed. A check was therefore made to determine the scattered light level by taking exposures with the normal sample but with no background. These showed that the scattered light is negligible in the region of the line so that N is valid.

Since these resonance lines did not produce useful values for n an attempt was made to measure n_{Au} more directly from the pressure broadening of a weaker impurity magnesium. The Mg 2852 Å line though much weaker than the resonance lines of Cu and Ag, appeared to have a less distorted profile. Plots of intensity versus wavelength were obtained for the line and compared with voigt profiles. This could be done by obtaining the ratios of the width to the half width at 0.1 (times the total intensity) steps and comparing with a table of voigt profiles. The profiles could not be fitted exactly to a voigt profile going smoothly from case A to case B as shown below.

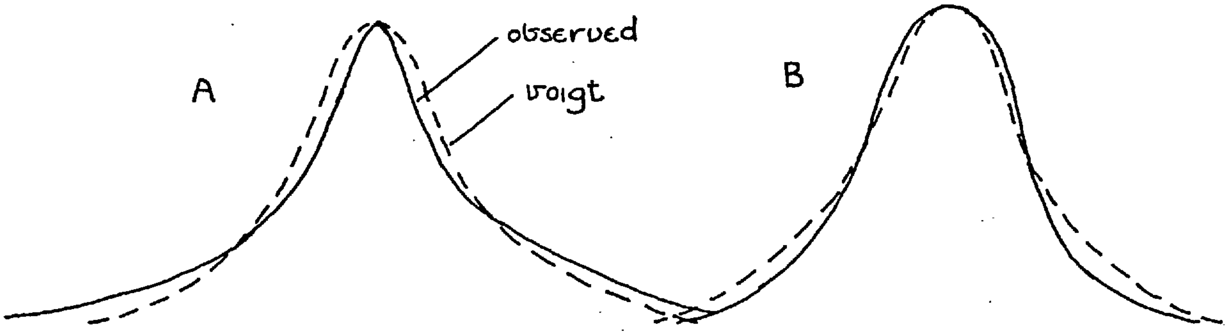

The line profile followed case A at short delays going through the voigt profile between 100 and 150 μ sec. However a fairly consistent value of the ratio of Doppler to Gaussian broadening could be obtained and the results will show that n is not very sensitive to this parameter for this line width.

The Doppler to Gaussian ratio d/g is defined in the respective formulae $A/(1 + x^2/d^2)$ and $A \exp(-x^2/g^2)$. of the component profiles.

The profile is determined by the convolutions of all the broadening functions. Of these processes natural broadening is negligible. The contribution from resonance broadening is also small. The transition is a $^1S_0 - {}^1P_1$ with gf = 1.6 and for this transition $gf = f_{abs}$ and substituting into the formula for resonance broadening gives

$$2\,\Delta\lambda = 3.62 \times 1.6 \times n^1/10^{19}\ \text{Å}$$

For $n \simeq 3_{10}19$/cc and therefore $n^1 \simeq 3_{10}14$/cc then

$$2\,\Delta\lambda = 0.00018\ \text{Å}$$

This will be shown to be very small compared with pressure broadening. n^1 is obtained from the relative total absorptions of the Mg and Cu lines.

Since there is no significant ionization the only other mechanisms are doppler broadening and pressure broadening. Doppler broadening can certainly be neglected since even at a temperature of 6000°C this would be insignificant. For pressure broadening the formula

$$\omega_a = \pi n\,(9\pi\,\hbar^5\,\overline{R}_a^2 / 16\, m^3 E p^2)^{2/5} \times \bar{v}^{3/5}$$

with $\overline{R}_a^2 = \frac{1}{2} E_H/(E_\infty - E_a) \times (5z^2 E_H/(E_\infty - E_a) + 1 - 3 \times \ell_a(\ell_a + 1))$

given by H Griem(27) can be used. The notation is the same as in this reference.

Using $E_{H_\gamma} = 13.6$ eV, $E_\infty = 7.64$ eV, $z = 1$, $\ell a = 1$, $E_a = 2852$ Å ~ 4.31 eV then $k_a = 31.4$ (a_0^2 units).

Also from $\frac{1}{2} m v^2 = 3/2\, kT$, then

$$\bar{v} \simeq \sqrt{3\, k/m} \times T^{\frac{1}{2}}$$

$$\therefore \quad \bar{v}^{3/5} \simeq 67.7\, T^{3/10} \; (\text{cm/sec})^{3/5}$$

Then $2\pi c \dfrac{\Delta\lambda}{\lambda^2} = \pi n \,.\, 1.08_{10}{-12} \,.\, 67.7 \;\, T^{3/10}$

And $2\Delta\lambda = 0.00105\, (n/10^{19})\, T^{3/10}$ Å

For $T \simeq 4000^\circ$C and $n \simeq 3_{10}19$

$$2\Delta\lambda \simeq 0.076 \text{ Å}$$

This is the dominant source broadening by at least an order of magnitude. However, it is necessary for this narrow line to account for the spectrograph broadening.

Since the source broadening is predominantly pressure broadening with a solely Lorentz component, it is convenient to use the slit approximation which gives Lorentz and Gaussian half widths. The Lorentz components can then be added and convoluted with the gaussian to give a voigt profile. The experimental profile gives the average d/g value for the profile and hence the source Lorentz component can be found. Only the effects of slit width and finite resolving power will be considered for the spectrograph broadening. These were not measured directly but obtained from the data supplied by Hilger and Watts for this instrument in good focus. From Astrophysical Quantities$^{(29)}$ the formulae relating resolution to d and g, for a resolving distance ℓ, are $d = 0.14\,\ell$ and $g = 0.43\,\ell$, and relating slit width, for a slit width s, are $d = 0$ and $g = 0.41$ s.

At 2850 Å the resolving power is 39000 therefore $\ell = 0.071$ Å, hence $d_r = 0.01$ and $g_r = 0.03$ Å.

The slit width was 25 μ and therefore $g = 0.10$ Å.

The Lorentz component from the spectrograph is very small so that as a first approximation if d/g is obtained, the d value can be assumed to be contributed totally by the source.

Various methods of fitting d/g are tabulated to show that the d/g value is not too critical. The results most in accord with the theory are obtained by forcing a fit to the spectrograph data given above.

TABLE 1

Delay(μsec)	N tot Mg (per cc)	Whole half width Å	n^{+}_{Au}(T=3500^{o}C) per cc
50	0.34_{10}^{14}	0.128	1.7_{10}^{19}
75	0.47	.129	1.7
100	0.50	.120	1.6
150	0.86	.176	2.4
250	1.00	.191	2.6
500	1.72	.253	3.4

† With d/g taken as the average value through the profiles of 0.5 and assuming all the Lorentz component is due to the source.

TABLE 2

Delay	d/g*	n	d/g**	n	g
(μ sec)		/cc		/cc	Å
50	.4	$1.5_{10}{}^{19}$	.37	$1.36_{10}{}^{19}$	.09
75	.2	0.85	.37	$1.36_{10}{}^{19}$	
100	.5	1.6	.37	$1.36_{10}{}^{19}$	
150	.8	3.2	.48	2.34	
250	.1		.52	2.67	
500	.6	3.8	.64	3.98	

* With d/g found for each profile used separately, but the d/g value being derived only from data below the half width.

** With d/g assumed to be constant up to 100 μ sec by averaging and g constant throughout.

These tables give values of n_{Au} in good agreement with the theory except for the value at 500 μ sec. These results were all obtained at 1 atmosphere hence only for the 500 μ sec delay would there be any significant diffusion of the Au vapour, and the theory is not applicable to non-uniform columns of vapour. This is confirmed by the profile being distorted near the centre of the line for the longer delay times.

The inconsistency of the results is due to the variable nature of the absorbing column rather than experimental error, and the density measurements at 150 and 250 μ sec which should correspond to the most uniform period of the dispersion also give the closest approach to the filling pressure density. The values are consistent with the pressure probe measurement in that there is no very high pressure reached and that the pressure rises rapidly when the droplets start to evaporate near 50 μ secs.

7.8 Discussion

The total number of absorbers in the light path N, and the number density n, of the gold vapour were measured to obtain comparative values to check the results from the model. But whereas n has been shown to yield a consistent value, N is too low by a large amount. The variations of N with delay and pressure are in good agreement with the predictions so that it is natural to try and find an error in the determination of N. Though a factor of 10 cannot be explained it is likely that N is underestimated by as much as a factor of 2. The distortion of the profile and any scattered or emitted light will all contribute to decreasing N. The measurement random errors are obviously considerably smaller than such a systematic error since the results are self-consistent within 15%.

CHAPTER 8

COMPARISON OF PREDICTED AND EXPERIMENTAL RESULTS AND CONCLUSIONS

8.1 The Discrepancy in the Total Number of Absorbers

In the brief discussions following the measurements of each group of experimental parameters, the deviations from the model have been considered in terms of experimental accuracy. The overall disagreements must now be considered and alternative models proposed.

The parameter which is most basic to the model is the total number of absorbers. This parameter is also in greatest disagreement with the droplet model. Not unnaturally the experimental deviation of this parameter was carefully reassessed. However, a few order of magnitude calculations show that there is no experimental error of the required magnitude. Typically, the lines are about 1 to 2 Å wide corresponding to $\sim 25\ \text{cm}^{-1}$ and they were chosen so that the peak absorption was less than half of the background intensity. This leads to a value of $\log_{10}(I_0/I) < 1$ and also means that the approximation $e^{-\alpha_v N} \approx 1 - \alpha_v N$ will not be greatly in error. Thus any defocussing of the spectrograph will only have a marginal effect on the accuracy. With the values given above, the total number of absorbers is $\sim 1_{10}14/\mathrm{cm}^2$ for copper and $\sim 0.5_{10}16/\mathrm{cm}^2$ for gold.

8.2 Reassessment of the Model

Since the experimental errors cannot explain the disagreement it is necessary to reconsider the model in the light of these results. If the droplet model is retained then the total number of absorbers N in the light path will depend on the time at which the droplets start to evaporate, the rate of, and total energy absorbed after this time, and the radius of the droplets. Additional factors such as errors in L_b and the reflection coefficient will not influence the value of N by more than a few per cent. The time at which the droplets start to evaporate must coincide with the appearance of significant numbers of absorbers, so that there is no doubt that this is close to 50 μ sec as was assumed. However the radiant energy function used was only a crude approximation to the observed function. At 50 μ sec the intensity has fallen well below the peak value and is also tailing off exponentially rather than linearly. This leads to a large difference in the energy absorbed compared with the idealised radiant energy function used. This accounts for a factor of four in the observed value of N, bringing much closer agreement with the droplet model. The remaining variable is the droplet size. Assuming that this was of the order of 80μ and allowing for the above correction, then there would be complete agreement with this model on the basis of N only. However if the droplet radius is $\simeq 80\mu$ then the interdrop spacing would be large and a larger random variation in the measured values of N would be expected. Therefore, the droplet radius is restricted to $\lesssim 70\mu$ and the observed value of N is approximately a factor of 2 lower than the model would predict. This is not a sufficiently large discrepancy to reject the model since it has been shown that all the systematic errors in measuring N would tend to produce low values of N.

The remaining parameters fit very well with the droplet model. The variation of N with time is close to the expected values for a droplet of about 70μ and as predicted the observed value of N continues to rise after the evaporation is complete. This again agrees well with a radius of $\sim 70\mu$ since the observed value of N will only reach its maximum value when the absorbing column is sensibly uniform. And for a 70μ radius this would not occur until at least 200μsecs after end of the evaporation. The variation of N with pressure is only a measure of the pressure at which the diffusion length of the vapour becomes comparable with the dimensions of the apparatus. Until this pressure is reached N will be approximately constant, then fall rapidly until the diffusion length is much greater than the diameter of the pyrolysis tube, after which the value of N will only fall slowly. The measurement of the number density is in poorer agreement with the model since it was assumed that n would correspond nearly to the filling pressure until 150 μ secs and then slowly decrease. The deviation from this ideal form is due to the measurement yielding an average value for n rather than the peak value. Since the light from the background is only roughly focussed through the sample a large area of the sample is averaged. Thus the measured region includes a large region of lower density as well as the high density regions. This explains the deviation of the profiles from the voigt form and the rise in n beyond 150 μ secs. However the smoothness of the increase in both N and n with delay is not easily explained by the simple model. This smooth increase in N and n can be explained by assuming that there will be some gradation in the droplet size which will lead to smoother values of these parameters, but it also points to an alternative model for the process.

8.3 An Alternative Model

In this alternative description of the destruction of the sample, it is assumed that the sample is liquified but the effect of surface tension is sufficiently high for the bulk of the sample to reach the support without evaporating. In this case all the observations are made in a region where there is initially only a small amount of evaporated material, and the vapour reaches this region only by diffusion from the support. Evaporation still only occurs after about 50 μsec, since this observation was measured independently of this particular sample. For this case then, the value of N is much smaller since only the largest drop size is going to form on the support. But the value of N should rise at the centre only fairly slowly and would be strongly dependent on the pressure. This is counter to the experimental results which show a very rapid initial rise in N, and N versus pressure does not vary rapidly. Thus in this case the only parameters that fit well are N and n. n is in better agreement since this parameter rises smoothly with delay as would be expected as more material diffuses into the absorbing column.

Since the experimental results cannot be fitted very well to either model it is necessary to consider an intermediate state. In this case it will be assumed that most of the sample reaches the support but that a significant fraction forms into droplets and remains nearer the centre of the light path. But this model can be immediately questioned since it does not give a smooth variation in N. Therefore it is necessary to extend this case and say that the fraction not reaching the support forms into drops of varying sizes. Now all the number parameters can be made to fit.

This is a very unsatisfactory result since the object of this section was to produce a simple model. However, it has been shown that the simple droplet model will give a valid result within a factor of about 2, though it is likely that a rather more complicated model could give improved agreement.

8.4 The Excitation Temperatures

The excitation parameters have not been considered so far, since once it is deduced that the sample breaks up into drops these will not be affected by the model chosen. The most interesting aspect of these measurements is that T_{rot} and T_{vib} both appear to be good parameters and both have values much higher than T_{boil} during the period of the discharge.

In the previous discussion it was suggested that this was due to the closely spaced energy levels in the bands coming into equilibrium with the light pulse from the flashtube. However, though this explanation gives a good fit, it can be argued that the excitation of the molecule must be higher than the surrounding thermal temperature. Since $D_o^o(H_2) =$ 4.476 eV, and it is necessary to form atomic hydrogen in order that AuH can be formed, then the AuH that is produced will be at a high excitation. The possibility of photodissociation can be rejected since the lowest wavelength transmitted by the pyrex tube would be insufficient to cause dissociation. Photodissociation by cascading through the absorbing of several lower energy photons however may contribute slightly to the production of AuH . Thus, the minimum excitation of the AuH formed will be $\sim$ 2 eV which is not very much below the dissociation energy of the ground state 3.1 eV. The molecule thus formed will be highly excited, and the measurements of T_{rot} and T_{vib} will reflect this energy rather than the thermal temperature if the system as a whole is not in thermal equilibrium. That T_{ex} does not agree with T_{rot} and T_{vib} confirms this latter supposition, and therefore this process would be equally capable of explaining the high values of T_{rot} and T_{vib}. It is a preferable explanation in that it would give high values of T_{rot} and T_{vib} but would allow large variations in T_{rot} between bands which would justify the anomalous value of T_{rot} for the (0,1) band. If the excitation is in equilibrium with the radiation then T_{rot} in all bands would be equal but T_{vib} would only equal T_{rot} if the vibrational spacing was sufficiently small so that it was below the peak of the radiant energy distribution. This would be valid for the (0,1) band hence T_{vib} would equal T_{rot}. Therefore it is not clear from the experimental results which process causes the high values of T_{rot} and T_{vib} measured during the discharge.

The more satisfactory aspect of the excitation measurements is that $T_{rot} = T_{vib} = T_{boil}$ for about 250 μ secs after the end of the light pulse. This is one of the regions that was sought since in principle this will extrapolate to other gas metal combinations. However at no time does $T_{ex} \simeq T_{boil}$ and this was not expected since the vapour is remote from thermodynamic equilibrium by collisions(27).

8.5 Conclusions

It is thus a reasonable conclusion to say that the simple model developed can with caution be extended to consider other similar systems. The close agreement sought was not achieved and possible causes of this disagreement have been discussed both in terms of the detailed experiments and the qualitative results.

8.6 Summary

It has been shown that pyrolysis can be a useful method of producing molecular spectra. The spectra of the 3d group elements have been photographed at moderate dispersion and two possible hydride systems observed. The limitations of this particular system have been considered and a simple model developed and tested to try and show these limits in a quantitative manner. Among the objectives that were not achieved was the use of the apparatus with a spectrograph of high dispersion and a method of obtaining an improved yield of hydride.

Because of the low yields that are attained it will be only for the more refractory compounds that pyrolysis will be an important tool in the production of molecules. Certainly for work in absorption the low yields and inhomogenous absorbing column will be more than offset by the controlled comparatively low temperature vapour that can be produced. Since the comparable sources for refractories will be arc and spark sources the pyrolysis system will normally be a low excitation source. However the severe geometrical limitation on the sample inherent in the present system are a crucial barrier to its widespread use and this is reflected in the sparse number of works published in this field.

PART II

CHAPTER 9

THE ABSORPTION SPECTRA OF CuH AND CuD IN THE 2200 - 3200 Å RANGE

9.1 Introduction

The spectrum of CuH was first analysed by R Frerichs(30) and E Bengtsson(31) in 1923. They observed the spectrum in emission and correctly assigned the ground state. The spectrum has been extensively investigated since then, notably in absorption by E Hulthen & R Zumstein(32) and B Grundström(33), and in emission by A Heimer and T Heimer(34). Both hydride and deuteride have been observed for all the major transitions and the $Cu_{63}H$, $Cu_{65}H$ isotope effect has been previously analysed by Jeppesen(35) and Heimer(34).

During the preliminary work on the production of the spectra, U Ringström(36) published a detailed account of the lower states of CuH and CuD, clearing up much of the uncertainty remaining about these states and producing an accurate list of second differences. Much of the following analysis depends on this work. More recently U Ringström(1) has published an analysis of part of the state covered in this analysis and where these overlap any differences have been carefully checked. Also, the opportunity has been taken to include some graphical data that could not be covered in a paper. The close agreement between the detailed analyses provided some reassurance on the assignment of a few doubtful lines.

The analysis of this transition was of interest since besides being an opportunity to fill in the levels between the 2200 Å band and the known lower states, it would allow a more complete comparison between the Li, Na, KH series and the Cu, Ag, AuH subgroup. The spectra of group 1a typically involve transitions between the states derived from the "intersection" of an ionic and a covalent state. Both are $^1\Sigma$ states, but whereas the ground state has a normal potential curve near equilibrium, the upper state has a very wide potential curve. This results in a wide Franck-Condon parabola and a maximum in B_v' and w_v'. Due to the higher ionisation potentials in the 1b group there are no simple equivalent systems. The strongly perturbed A state in AgH though superficially similar has been assigned to the interaction of two atomic states.(24)

CuH is not a typical transition metal group hydride in that it does not have a high multiplicity ground state. But, though the initial aim of this project was to study high multiplicity states, the survey work done using the pyrolysis apparatus had positively shown that a new hydride system occurred in this region in CuH. Thus an attempt was made to analyse this system rather than the complex CrH or MnH violet systems. Two preliminary plates of scandium in hydrogen were taken near 3000 A using the residue of the ampoule used for making pyrolysis samples. However, careful examination of the pyrolysis spectra had shown no significant structure and it was decide to devote all the time to the copper spectrum.

9.2 Apparatus

A large King furnace$^{(38)}$ was available and it was decided to use this in conjunction with the 21 ft eagle spectrograph. The long absorbing column allows weak transitions to be observed and the dispersion of the spectrograph (2.7 Å/cm in the third order) gives ample resolution.

Since the availability of the furnace was limited it was necessary to take the complete set of plates for the hydride and deuteride before the analysis could be commenced. Due to the $Cu_{63}H$, $Cu_{65}H$ isotope splitting one could assuredly assign the spectrum observed to the CuH molecule. However, the open nature of the spectrum and the lack of definition of the heads meant that an initial survey at low resolution would give little assistance. Therefore, this step was omitted and the pyrolysis spectra were

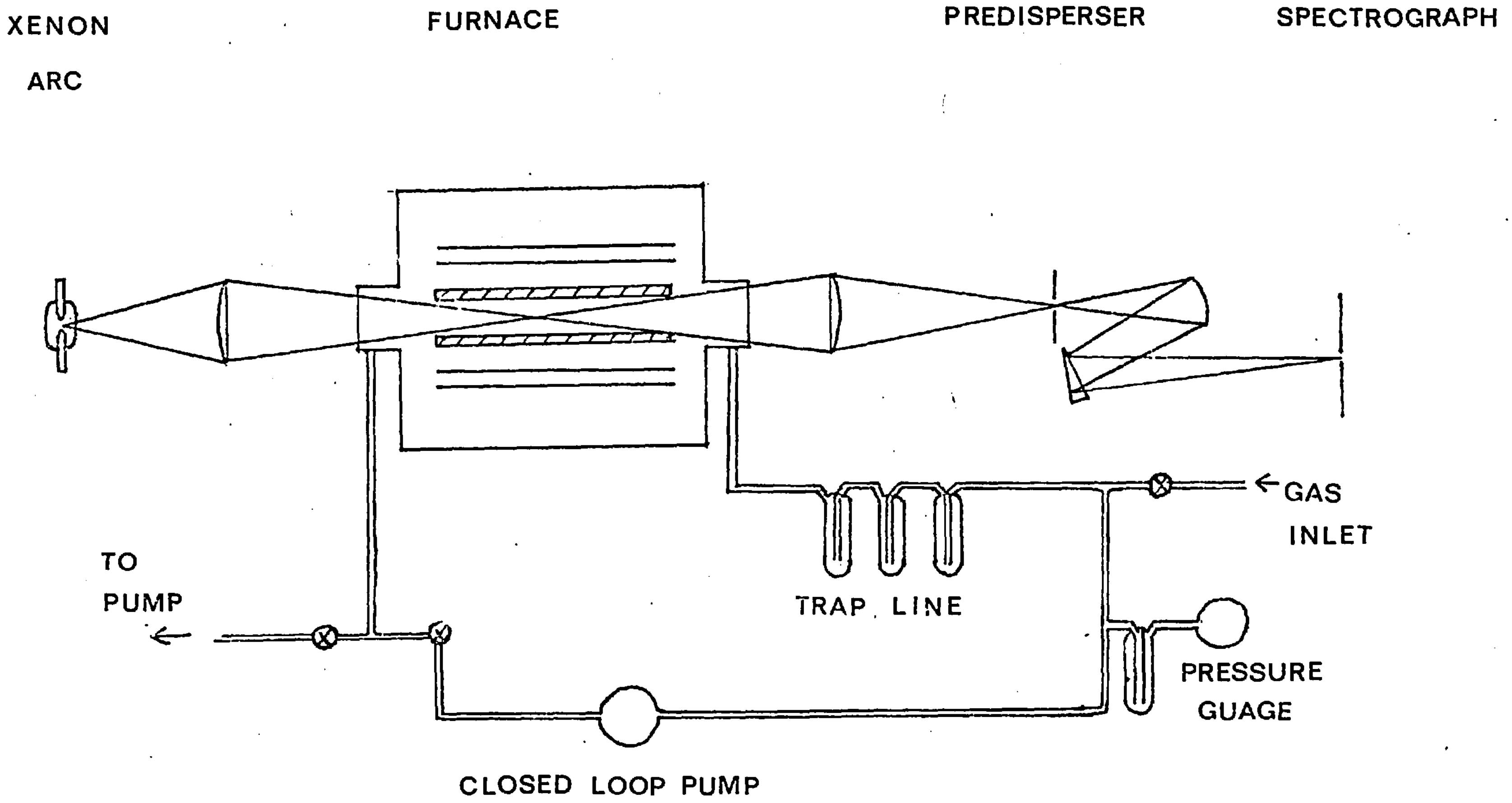
XENON
ARC
FURNACE
PREDISPERSER
SPECTROGRAPH
GAS
INLET
TO
PUMP
TRAP LINE
PRESSURE
GUAGE
CLOSED LOOP PUMP

figure 9.1

used as the low resolution guide. Also, since the analysis could not be started until the experimental work was completed, some regions of the spectrum were optimised to give a reasonable density of lines on a plate rather than to resolve a particular feature. Thus the low J value lines, which are relatively weak at high temperatures tend to be too weak to resolve in some bands.

A general outline of the apparatus used is shown in figure (9.1). Crossed optics are the obvious choice since the furnace tubes are not necessarily straight and this method allows a slightly larger degree of bending before the aperture is limited.

9.3 Background Light Source

The background light source was required to cover the range 3200 Å to less than 2200 Å . The high pressure xenon arc is ideal above about 2500 Å , but its intensity falls rapidly below this region. Two alternative sources for the lower wavelength region were tested, a 1.1 Amp hydrogen tube(39) and a Lyman flash tube which was the same type as that used as the background source for pyrolysis. A strict comparison is not obtained since the flashtube aperture was limited by extra baffles and a drift tube to allow for the large number of shots required. Without these modifications the flashtube window becomes opaque before a satisfactory density can be obtained on the plate. The hydrogen tube was found to require exposures an order of magnitude smaller than the flashtube fired at one shot per minute

Exposures varied from 10 minutes using the 500 Watt xenon arc at 3200 Å in the second order, to over 5 hours with the hydrogen tube in the third order at 2200 Å. The very long exposures required and the lack of a specific objective at the time, precluded the photographing of the region below 2200 Å, though a preliminary plate shows the (n – 0) progression is still present below the 2200 Å band.

9.4 Furnace

The King furnace was rated at 27 k watts and used a directly heated 18 inch graphite or carbon tube as the element. Each tube was carefully abraded until it fitted smoothly into the carbon plugs which held the element into the water cooled copper electrodes. A burn-in period of about 1 hour at 2200°C in vacuum removed most of the impurities from the element. The major impurities detected were Fe, Mn and Mg (only the resonance line). To avoid atmospheric contamination, the furnace was always brought to atmospheric pressure by leaking in hydrogen before opening it and inserting the copper charge. The number of exposures before the carbon element failed decreased at high temperatures and pressures, with three exposures of 20 minutes at 2000°C in 1/2 atmosphere of H_2 being typical.

9.5 Gas Supplies

When using hydrogen a continuous stream of gas was leaked through the system. This was fed from a cylinder through a liquid nitrogen cooled trap line, and pumped out to atmosphere by a rotary pump. Throttling valves could be adjusted to retain a steady pressure in the furnace.

With deuterium a closed loop system was used. The deuterium was fed in to the required pressure and then pumped through the trap line and furnace using a small recipricositor pump. The pumping rate could be adjusted with a variac in the supply to the pump motor. There did not appear to be any significant increase in contamination using this system. The pressure in the system was measured with a mercury manometer isolated by a liquid nitrogen cooled trap.

9.6 Predisperser and Spectrograph

Order sorting for the 21 ft spectrograph was obtained using a small LiF prism spectrometer(40) between the furnace and spectrograph slit.

This could be set up by using an iron arc to give a band of about 150 Å, and this more than covers each plate in the third order of the 21 ft in this region. Adjustments for the predisperser and spectrograph had already been recorded, thus only alignment and fine focussing were required. A laser was used to obtain the final alignment and an iron arc running in air provided a satisfactory source for focussing. The dispersion of the spectrograph is ~2.7 Å/cm and this was very useful in the deuteride and lower hydride bands. But since the band lines are significantly broadened in the furnace the full resolution of this instrument is not realised.

9.7 Plates

Ilford Q2 and Zenith plates were used initially but then either HP3 or Fast Blue sensitive type XK plates. The latter plates were finer grained and were used for the final plates in the region above 2500 Å. However the former plates though much coarser were faster in the lowest region of the spectrum. Since the exposures in this region were of the order of 3 - 5 hours the faster plates were essential. Standard developing solutions were used but without close temperature control.

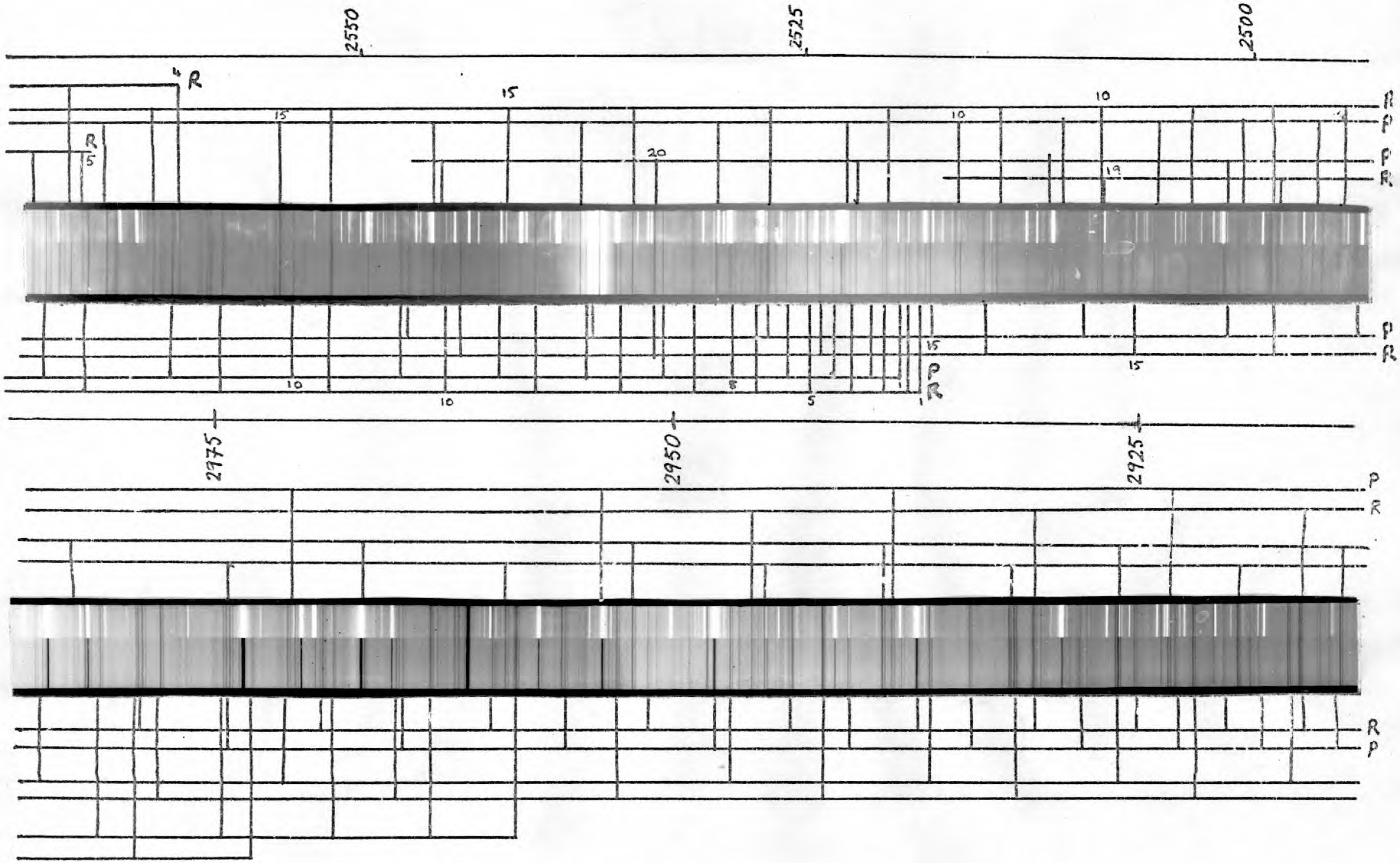

Part of the spectrum of CuH

PLATE 9.1

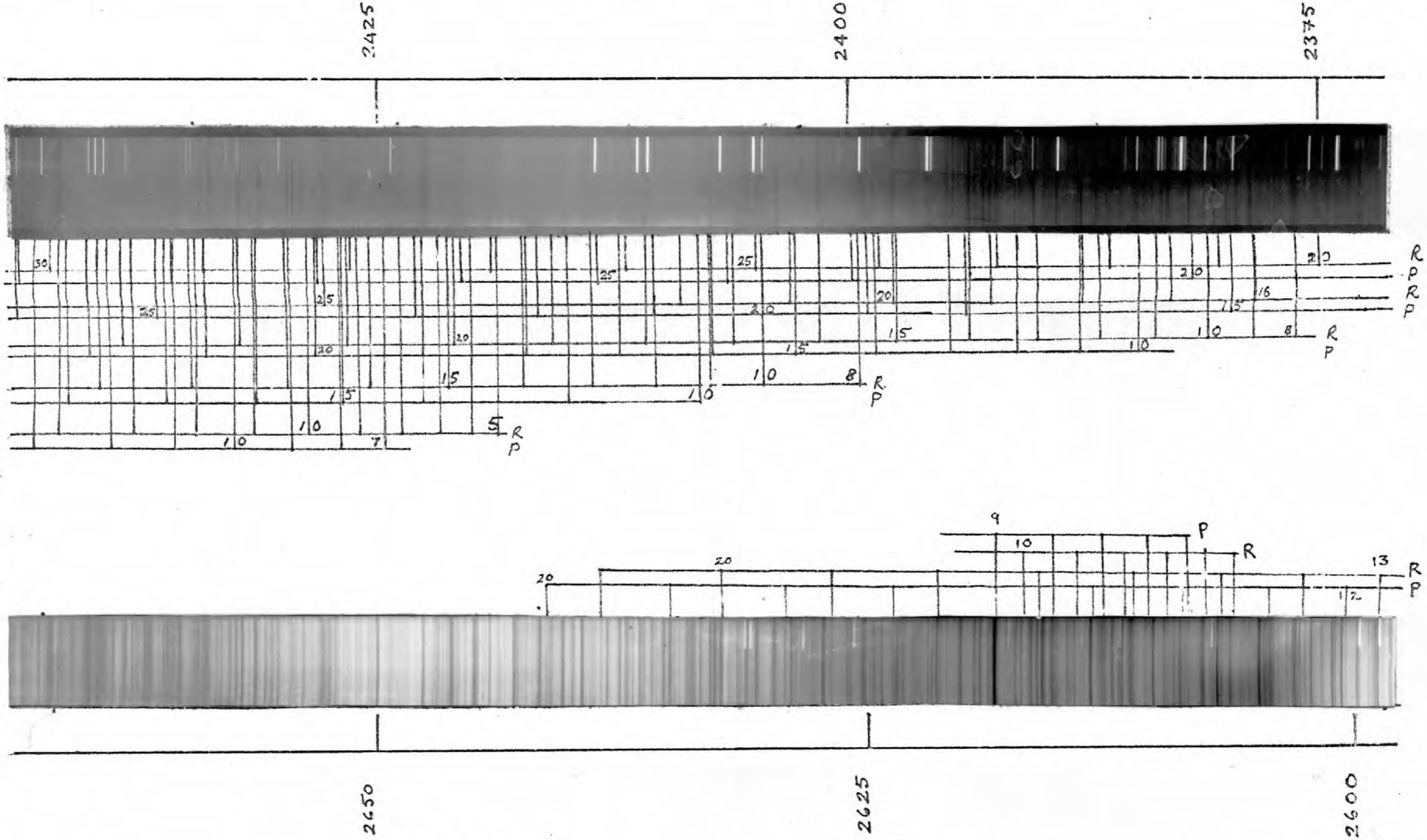

Part of the spectrum of CuD.

PLATE 9.2

9.8 Spectra

A section of the hydride spectrum is shown in plate (9.1) and of the deuteride in plate (9.2). The conditions for obtaining the spectrum were obtained by first observing the hydride bands in the region above 3200 Å that had been observed by Ringström(36). These bands appeared strongest for high temperatures and pressures but it was necessary to reduce both of these parameters in moving down to the 2200 Å band. For the hydride the pressure varied from $\frac{3}{4}$ atmosphere for the 3200 Å region to $^1/_{10}$ atmosphere at 2200 Å, while the temperature was lowered from 2300°C to ~1750°C. With the deuteride slightly lower values were used throughout this range. The high temperature used for the high wavelength plates severely limited the exposure time due to loss of the copper charge, but probably accounts for the absence of the Cu_2 bands which appeared in Ringström's spectra. Since the evaporation was not controlled the observed intensity of the bands does not give a meaningful guide to the relative transition probabilities and thus only a record of the peak eye intensity is recorded for each band with an approximate correction for the temperature.

Though plates were taken of the deuteride spectrum over the whole region, it was not possible to obtain a density of lines suitable for measurement over wide ranges of the spectrum. Plate (9.2) shows a sample of the extremely dense spectrum which cannot be improved significantly by altering temperature or pressure. In retrospect this observation is not unexpected since the deuteride will have approximately twice as many lines in each band and twice as many bands as the hydride, also the excitation in the lower state is higher resulting in more available strong transitions. Lowering the furnace temperature does not resolve this problem since then the Cu_2 bands and an unidentified intensity modulation in the 2500 - 2200 Å region limit the resolving of the band lines.

9.9 Measurement

All the plates of the hydride spectrum and the four lower plates of the deuteride spectrum were measured using a Zeiss-Abbe comparator. Each plate was measured in three sections and each line was measured at least three separate times. An iron arc, running in air, was used to provide standard lines. As far as possible only the Fe I lines given to 4 decimal places by H Crosswhite(41) were used for the plates above 2700 Å. Below

2700 Å insufficient Fe I lines are available and Fe I absorption lines, Fe II and Fe I arc lines, and Cu(42) arc lines were then used as standards. Normally only the $Cu_{65}H$ lines were measured, though the splitting was not resolved below 2550 Å.

Using a least squares curve fitting program(43) on an Elliot 803 computer, a dispersion equation was formed for each third of a plate. The standards were accepted when a third order polynomial gave a fit to them with a standard deviation of less than 0.002 Å. The series of plates and measured sections all overlap and a fit in these regions was also required before the standards were accepted.

The measured accuracy of the lines is estimated to be from 0.06 cm^{-1} in the long wavelength region to 0.1 cm^{-1} near 2200 Å. The accuracy is limited not by the spectrograph, but by the width of the lines, due to pressure broadening, and in the lower wavelength region to lack of resolution of the Cu_{63}, Cu_{65} splitting, which effectively results in an asymmetric broadening of the lines.

CHAPTER 10

ANALYSIS OF THE (E-X) SYSTEM IN CuH AND CuD

10.1 Preliminary Analysis

Examination of prints of the complete set of plates of the hydride system revealed no obvious band heads or long sequences. This suggested that further analysis would be greatly aided if the wavenumbers of all the lines were obtained. This would then allow accurate checking of test series and hence rapid rejection of incorrect sequences. The test sequences are obtained by assuming a constant second difference between members of a band, then, if a reasonable guess can be made for this difference, a visual search of the prints can pick out test sequences. The presence of the $Cu_{63} - Cu_{65}$ isotope splitting and the wide extent of the system with the absence of distinct heads, had already shown that this region certainly contained a new system, but it also gave a guide to the value to choose for the second difference. Since the spectrum occurred in absorption at moderate temperatures it was likely to involve the ground state and to obtain the widely spaced system must have a B_v' very different from that of the ground state. Since a similarity with the 1a group hydrides occurs with this state, assuming a B_v' value of half the B_v' for the ground state gave a reasonable starting point.

The first region examined in detail using this method contained the (n-3) and (n-4) bands, whose second differences are not given by ref 36. Thus only slow progress was achieved until the search was moved to the 2500 Å region. Even here the first results were a set of apparently unconnected series. They did not form a pattern consistent with a multiplet transition and therefore it was assumed that perturbations were breaking the sequences. The bands were completely resolved only by going through all the pairs of lines in the region of the missing numbers. As soon as this region was completed the analysis of the whole system followed rapidly, however each new perturbed region required a separate search for the missing lines.

An alternative approach to the analysis of many lined spectra of this type has been suggested(44). This requires that all the wavenumbers are fed into a program which then proceeds to try and find test series based on the constant second difference. It seems possible that this system would have been ideal for this method since the lines are well resolved, and the perturbed regions require a similar search technique in any case. However, in the deuteride, the spectrum is so dense that spurious equal second differences are common and the perturbation has a relatively larger effect. This prevented the finding of many of the perturbed lines even after all lines in the region were tested.

10.2 Identification of the Transition

Only a single band was found for each upper state to one of the ground states and each band had a single P and R branch with always at least one missing member and no Q branch. This strongly suggests that the state is a $^1\Sigma$ state, but since the ground state is also a singlet it is possible that the side bands of a multiplet could be suppresed. However, a search of a region where all the lines on the plate were identified showed no traces of a further weak system. Thus it is concluded that the upper state is a $^1\Sigma$.

The perturbations present throughout the system are clearly due to the "intersection" of this state with a triplet state. The perturbation is heterogeneous and increases as J increases. These observations are in accord with the $^3\Pi$ state suggested by ref 1. Since this also gives agreement with the perturbation in the deuteride this assumption is further confirmed. A further lower state in the hydride was found below those shown by ref 1 and this is also unperturbed. This would tend to confirm that the first observed perturbation is the $v = 0$ level, however this does not fit with the deuteride spectrum.

10.3 Results

The wavenumbers of the analysed hydride and deuteride lines are given in Table 10.1.

Table 10.2 gives the derived energy levels and Table 10.4 and graph 10.1 the B_v, D_v and H_v values for all the bands. All the bands have been included even where they overlap with reference 1, and where this occurs all the values have been compared with those in reference 1.

The accuracy of the wavenumbers can be checked by comparing the second differences derived for the ground and upper state and the absolute wavenumbers with reference 1. There is a small but significant systematic deviation in the absolute wavenumbers but the second differences do not show any such systematic discrepancy. The random error appears to be in agreement with the estimated random error of 0.06 cm^{-1} but a systematic absolute error larger than this appears to be present. Though this will not affect the constants for the bands, it is surprising that such an error can occur when both of the spectra used free running iron arcs to produce the standard lines.

In the reduction of the data the values of $\Delta G(v)$ and w_v are taken from ref 36 where they are then more accurate. For the transitions to the higher vibrational levels of the ground state an average of the constants

TABLE 10.5

Comparison of Second Differences and Measured Wavenumbers

Band 4-1 Table 1			Table 2	
*	†		†	*
39 696.06			.09	- .06
693.54	693.74	+ .20	.01	- .22
82.23	82.45	+ .22	.28	- .08
62.03	62.28	+ .25	- .12	- .12
33.03	33.14	+ .11	.06	.07
595.24	595.31	+ .07	.10	.11
48.67	48.79	+ .22	.02	.02
493.33	493.58	+ .25	- .14	- .03
29.79	29.85	+ .06	- .07	- .22
355.27	355.49	+ .22	.00	- .13
277.10	277.21	+ .11	- .03	- .23
178.90	179.11	+ .21	.12	.04
085.58	085.70	+ .12	- .03	.11
38 971.12	971.17	+ .05	- .13	.14
856.92	856.86	- .06	- .11	.00
732.57	732.69	+ .12		

TABLE 10.5 (contd)

Comparison of Second Differences and Measured Wavenumbers

Band 4-1 Table 1			Table 2	
*	⌿		⌿	*
599.52	599.55	+ .03		
457.90#	457.48#			
308.13	308.20	+ .07		
149.90	150.30	+ .40		
984.27	984.57	+ .30		

* from U Ringström ⌿ as measured in this work

Table 1 compares the absolute wavenumbers of the (4-1) band.

Table 2 compares the residues of the derived second differences by subtraction from those given by ref 36 for the ground state.

derived in this analysis and those of references 34 and 35 are used. There is significantly poorer agreement between the ground state second differences derived in this analysis as compared with references 34 and 35 and those compared with reference 36.

10.4 The Constants for the Bands

Graphs (10.2) are for $\Delta_2 F - 4\overline{B}_v (J + \frac{1}{2})$ v J for the hydride and deuteride bands. They clearly show the form of the perturbation through the system and the comparatively poor resolution of this perturbation in the deuteride system. Values of B'_v can be derived from the graphs but they were not sufficiently accurate and two alternative equations were used.(23)

$$F(J) = B'_v J(J+1) - D'_v J^2 (J+1)^2 + H_v J^3 (J+1)^3 \tag{10.1}$$

$$R(J-1) + P(J) = 2\nu'_o + 2((B'_v - B''_v) - (D'_v - D''_v)) J^2 - 2(D'_v - D''_v) J^4 \tag{10.2}$$

A non linear least square parameter estimate program(45) run on the IBM 7094 at Imperial College was used to find the constants.

For equation 10.1, both H_v set to zero and H_v allowed to be non zero, were examined. For the v' = 1 and 2 levels in the hydride the three term formula gave a significantly improved fit to the data than only retaining two terms. The bands are not unusually long so that it is not expected that

H_v would be required unless there is a further overall vibrational perturbation of the system. Further evidence for such a perturbation is given in Chapter 11 but the strongest reason is that a $^1\Sigma$ will not be significantly perturbed by a $^3\Pi$ unless it is further perturbed by a third state. In this case the perturbation extends to the lowest J values of the bands and thus a vibrational perturbation would be expected. In the v' = 3-9 and deuteride bands there is not a sufficiently long unperturbed set of points to differentiate between the two and three term formulae.

The table 10.4.1 gives the values derived using equation 10.1 and table 10.4.2 using equation 10.2. There is a large difference between the B'_v and D'_v 's in these tables and also between these results and those of ref 1. Since the constants derived in ref 1 use a two term formula they should agree with table 10.4.2, that they do not does not mean that there is any further discrepancy in the accuracy of the wavenumbers, it only reveals the very slow variation in the B'_v values which requires very high accuracy to obtain the form of the variation of B'_v. Since the variation in B'_v is of the order of 0.02 cm^{-1} then the accuracy of B'_v must be much less than 0.02 cm^{-1} but this would require more than the 20 - 40 unperturbed lines to be available in any band. Many of the bands do not contain sufficient lines to ensure that this accuracy can be achieved so that the values of B_e, α_e and γ_e are not necessarily very accurate. However, the signs of α_e and γ_e are much more certain. Random error brackets are not given for the B_e values since the above discussion suggests that systematic errors will be dominant.

The variation in Δ_2G is also slow and depends strongly on the band lines near J = 0. Since these are weak and frequently missing the accuracy of the v_o' s used to derive Δ_2G is not high. Also discrepancies occur in the hydride, deuteride isotope systems in fitting the hydride v_o' s to those of the deuteride which suggests a significant perturbation. If only w_e and w_ex_e are used to fit the Δ_2G's then w_ex_e becomes negative. This obviously makes the significance of w_ex_e very dubious and only allows w_e to be determined to $\pm$ 15 cm^{-1}.

The Constants for the $E^1\Sigma^+$ state of CuH.

v_{oo} = 38895.0 (38883.3)* B_e = 3.043 (3.033)**

w_e = 591.4 (601.6) α_e = - 0.0613 (- 0.0709)

w_ex_e = - 0.696 (1.65) γ_e = - 0.00796 (- 0.00965)

w_ey_e = - 0.157

* numbers in brackets are for $w_ey_e = 0$

** numbers in brackets are for equation 10.2.2 others are for equation 10.2.1.

The values of all the constants are outside the generous errors given by ref 1 and it is likely that the above values will again be varied when the $v' = 0$ level is analysed. A similar process occurred in the analysis of the NaH system, where the constants were changed as bands closer to the $v' = 0$ band were analysed. However, since the above analysis includes the $v' = 1$ band which is unperturbed and has a B'_v value past the maximum the derived constants B_e, α_e and γ_e should be at least fully representative. This is not true for w_e, w_ex_e and w_ey_e, where in comparison with the group 1 hydrides, a maximum in Δ_2G should be expected for v' greater than 2.5 where the maximum in B'_v occurs. The data is not sufficiently ordered to show such a maximum even if it does exist.

The constants for the CuD band are not derived since the important bands near $v' = 0$ were not observed. It is more accurate in this case to calculate the constants for the CuD system from the CuH data. Adding a correction for the differences in the derived and observed v_{00}'s then gives good agreement with the observed deuteride levels.

The foregoing analysis has assumed that $v' = 1$ is the first observed hydride state. The derivation of this and the detailed effects of the isotope effect are considered in the next chapter. They do not help to resolve any of the doubts expressed concerning the derived constants since all of the forms of the constants give an equally accurate representation of the deuteride derived from the hydride data.

TABLE 10.1

Wavenumbers for the (E-X) Band of CuH

	1 - 2		1 - 3		1 - 4	
J	R(J)	P(J)	R(J)	P(J)	R(J)	P(J)
0						
1			34410.07	34391.46	32765.495	32747.75
2			400.35	369.23	756.97	
3			383.18	339.40	741.033	
4			357.53	301.70	717.35	661.85
5			324.19	256.18	686.77	618.65
6			282.35	202.87	648.45	568.24
7			234.01	141.77	602.93	507.84
8			177.01	72.88	549.89	445.85
9			112.30	33996.31	489.56	373.54
10			39.44	912.68	421.90	294.30
11			33959.34	820.23	347.01	207.85
12	35550.90		871.24	720.80		114.27
13			775.41		175.28	13.72
14		35165.90	671.99	499.56		
15		36.77		377.96	31975.34	31792.39
16		34899.93	442.18	248.99		
17			316.72	112.77		543.07
18			183.39	969.36		
19			42.72	819.11		
20				661.85		

TABLE 10.1 (contd)

Wavenumbers for the (E-X) Bands of CuH

	2 - 2		2 - 3		2 - 4	
J	R(J)	P(J)	R(J)	P(J)	R(J)	P(J)
0						
1						
2			34994.19			
3	36693.68		978.52		33336.48	
4	666.91	36610.69	953.50	34897.13	313.368	33256.89
5	631.60	563.08	920.71	851.86	282.87	214.11
6	588.14	506.60	880.07	798.85	245.35	164.09
7	535.66	442.57	831.59	738.15	200.30	107.00
8	475.54	370.27	775.34	669.85	148.15	42.72
9	407.26		711.26	593.78	88.44	32971.17
10			639.71	510.13	21.57	892.34
11		104.47	559.79	419.12	32947.39	806.80
12	152.037	35999.97	472.53	320.53	865.98	714.134
13	50.74	887.04	377.60	214.52	777.61	614.46
14	35941.497		275.145	100.92	682.00	507.84
15	824.85	638.94	165.09	33980.426	579.32	394.49

TABLE 10.1 (contd)

Wavenumbers for the (E-X) Bands of CuH

	2 - 2		2 - 3		2 - 4	
J	R(J)	P(J)	R(J)	P(J)	R(J)	P(J)
16		502.77		852.12	469.66	274.09
17		359.40	33922.58	716.88	353.07	147.35
18			790.23	574.34	229.30	13.86
19			650.67	424.91	99.14	31873.80
20			503.81	268.59	31962.27	727.00
21			350.08	105.45	818.79	574.08
22			189.54	935.40	668.51	415.08
23			21.57	759.03	512.42	250.31
24					349.783	

TABLE 10.1 (contd)

Wavenumbers for the (E-X) Bands of CuH

	2-5		3-0		3-1	
J	R(J)	P(J)	R(J)	P(J)	R(J)	P(J)
0						
1						
2						
3						
4					39048.43	
5						
6					38956.60	38882.81
7			40755.65		903.15	
8		31490.90		40579.71	839.78	731.23
9		421.28		491.92	767.10	648.45
10	31476.83	347.76	40524.49	394.37	685.81	555.74
11	408.51	267.57	428.56	287.45	595.807	454.28
12	332.82	181.22	323.96			344.25
13	250.26	87.36	210.25	46.30	389.46	225.84
14	160.68				273.76	
15					148.77	37963.047
16					15.96	819.59
17						667.29

TABLE 10.1 (contd)

Wavenumbers for the (E-X) Bands of CuH

	3-2		3-3		3-4	
J	R(J)	P(J)	R(J)	P(J)	R(J)	P(J)
0						
1						
2						
3						
4	37261.09					
5						
6	174.31	37101.03	35466.32			
7	124.73	26.80	420.35	35323.34		
8	65.52	36957.29	364.85	255.79	33737.67	
9	36997.24	878.52	301.31	182.49	678.53	33559.824
10	921.00	790.85	229.78	99.54	612.08	482.09
11	836.19	694.42*	150.53	9.32	538.29	396.99
12		590.72	63.74	34911.16	457.30	304.65
13	624.39	478.54	34969.15	911.15	369.19	205.28
14	533.80		867.06	805.31	273.85	99.00
15	416.26	230.48	757.24	692.33	171.54	32985.98
16		94.67	639.71	443.82	62.21	865.98
17	157.59	35951.67	515.39	308.88	32947.39	741.00
18			383.23	166.80	822.63	606.20
19		642.32	242.73	17.73		469.66
20			97.62	33861.74		
21				697.44		
22				529.24		

TABLE 10.1 (contd)

Wavenumbers for the (E-X) Bands of CuH

	4-0		4-1		4-2	
J	R(J)	P(J)	R(J)	P(J)	R(J)	P(J)
0						
1			39693.74	39676.85*	37902.07	37883.24
2			682.45	650.88	891.90	860.38
3			662.28	618.08	873.08	829.09
4		41437.36	633.14	576.71	846.06	789.78
5	41453.53	384.36	595.31	526.22	810.80	741.88
6	403.92	322.93	548.79	467.50	767.17	685.79
7	344.14	251.17	493.58	399.74	715.36	621.60
8	277.07	171.17	429.85	323.56	655.75	549.52
9	198.37	81.63	355.49	238.95	585.64	469.45
10	115.41		277.21	146.14	512.63	381.51
11	11.95	40876.22	179.11	42.63	420.07	283.21
12	40913.67	762.73	85.70	38935.54	332.28	182.36
13	791.93	629.56	38971.17	808.95	224.21	62.00
14	670.41	501.10	856.86	687.30	116.84	36947.22
15	538.67	350.92	732.69	545.02	36999.96	812.24
16	397.92		599.55	403.26	874.75	678.59
17			457.48	251.93	741.44	535.66
18			308.20	91.54	600.92	384.52
19			150.30	37924.05	452.40	225.97
20			37984.57	748.31	296.35	59.81
21				564.50	131.26	35887.04
22				374.14	35960.09	706.58

TABLE 10.1 (contd)

Wavenumbers for the (E-X) Bands of CuH

	4-0		4-1		4-2	
J	R(J)	P(J)	R(J)	P(J)	R(J)	P(J)
23				174.31		518.49
24						323.34

TABLE 10.1 (contd)

Wavenumbers for the (E-X) Bands of CuH

	4-3		5-0		5-1	
J	R(J)	P(J)	R(J)	P(J)	R(J)	P(J)
0						
1					40278.12	40257.44
2					266.69	235.32
3			42109.17		246.23	202.11
4	36131.26			42021.85	216.99	160.97
5	99.42		37.41	41969.08	178.75	110.63
6	59.81	35977.62	41987.31	907.16	131.68	51.47
7	10.61	917.29	928.14	835.57	76.21	39983.54
8	35955.20	849.46	858.85	754.38	11.52	906.85
9	887.04	771.39		664.42	39938.02	821.48
10	822.21	689.65	693.75	565.60	855.72	727.63
11		594.64	597.61	457.66	764.95	625.55
12	652.39	502.63	492.28		665.77	514.21
13	550.90	388.57	380.53	215.04	559.98	394.82
14	450.43	280.83	253.44	81.63	440.49	267.47
15	341.08	153.28			329.64	134.34
16	223.81	27.48	40977.39	40785.36	177.97	38986.83
17	99.09	34892.94	816.78*		26.84	848.79
18	34966.92	750.84		451.00	38882.81	670.21
19	827.64*	601.61				492.69

TABLE 10.1 (contd)

Wavenumbers for the (E-X) Bands of CuH

	4-3		5-0		5-1	
J	R(J)	P(J)	R(J)	P(J)	R(J)	P(J)
20	681.50	445.32				323.00
21	526.93	282.42				
22	365.63	113.42				
23	198.43	33936.12				
24	23.65	752.67				
25		563.64				
26		367.91				

TABLE 10.1 (cont'd)

Wavenumbers for the (E-X) Bands of CuH

	5-2		6-0		6-1	
J	R(J)	P(J)	R(J)	P(J)	R(J)	P(J)
0						
1						
2	38476.34	38445.00				
3		413.59				
4	429.88	373.85				
5	394.35	325.99	42609.58		40750.88	
6	350.30	269.95	562.92		707.15	
7	298.12	205.56	504.77	42407.70	652.56	40555.17
8	237.65	132.88	436.46	329.92	588.22	481.82
9	168.61	51.84	358.61	241.52	514.73	397.92
10	91.54	37963.05	270.69	142.99	432.20	304.49
11	5.97	866.01	172.90	34.45	340.59	202.11
12	37912.63	760.84	66.99	41917.31	240.19	90.58
13	813.65	647.94	41951.38	790.85	131.68	39970.29
14	700.58	527.79	862.94	655.22	13.45	841.90
15		401.78	693.75	510.11	39887.35	705.04
16	453.44	262.08	551.11	357.25	753.40	559.99*
17	310.48		393.57	196.12	606.36	406.47
18		36962.69	240.60	026.36	459.98	245.86
19			61.31	40843.67	290.43	72.58*
20				661.93	130.25	38900.51
21			40697.36	455.97		704.94
22						519.67

TABLE 10.1 (contd)

Wavenumbers for the (E-X) Bands of CuH

	6-2		7-0		7-1	
J	R(J)	P(J)	R(J)	P(J)	R(J)	P(J)
0						
1					41440.81	
2			43293.70	43260.98*	429.11	41395.57*
3			271.74	229.49	408.48	365.22*
4			239.35*	185.00	378.02	322.93*
5	38966.16		197.38	131.23	339.81*	272.10
6	925.56	38839.78	146.80	66.97*	290.94	212.05
7	874.51	777.24	86.59	42996.04	233.99	143.87
8	812.36*	707.88	19.84	914.37	171.17	65.73
9	745.11	628.35	42937.77	823.54	94.02	40979.92
10	667.62	539.91	862.62	726.26	24.82*	887.34
11	581.39	442.81	747.47	614.64	40913.67	781.47*
12	486.97	337.33				
13	384.75*	223.82	518.04	364.70	697.36	543.86
14	273.76	102.16	393.16		579.71	410.27
15	155.14	37972.58	258.50	77.27	452.57	271.15
16	29.06	835.23	114.47	41924.16	316.63	126.14
17	37890.21	690.24	41962.11	761.12	172.37	39972.09
18	753.03	538.39	800.23	589.53	19.53	809.13
19	592.52	374.14	630.20	408.48*	39859.19	638.35
20	442.32	212.46		220.69		459.98
21		26.80	264.99	24.82		273.95
22						
23				40608.55		

TABLE 10.1 (contd)

Wavenumbers for the (E-X) Bands of CuH

	7-2		8-0		8-1	
J	R(J)	P(J)	R(J)	P(J)	R(J)	P(J)
0						
1						
2						
3			842.21		41977.90	
4			809.96*	43756.51	947.17	
5			767.44*	701.93	907.16	41842.25
6			715.01*	637.50	859.19*	781.65
7			652.73	563.78	800.41	712.04
8			581.45	481.42	733.49	633.36
9			500.89	389.75	656.76	546.00
10			410.98	288.38	572.30	449.63
11	38154.81		311.56	177,88	478.24	344.14
12			202.75	57.71	375.57	230.33
13	950.58	38797.39	82.64	42928.92	261.51	106.05
14	839.78	670.21	42958.12	791.28	143.87	977.39
15	720.27		816.18	642.48	9.36	
16	592.20		674.58	489.06	876.22	691.07
17			515.16	318.50	725.87	528.98
18			353.78	149.40	573.01	369.33
19			181.49		410.27	

TABLE 10.1 (contd)

Wavenumbers for the (E-X) Bands of CuH

	9-0	
J	R(J)	P(J)
0		
1		
2		
3		
4	44333.62	
5	290.77	
6	237.39	44162.39
7	212.11	88.89
8	140.94	5.88
9	60.59	43948.47
10	43969.03	847.49
11	868.57	736.08
12	758.61	614.83
13	637.50	484.38
14	508.21	345.55
15	370.27	197.38
16	223.21	39.44
17	66.97	42873.29
18	42902.29	698.43
19	726.26	515.16
20		322.92
21		120.41

TABLE 10.1 (contd)

Wavenumbers for the (E-X) Bands of CuD

	4-2		5-2		6-2	
J	R(J)	P(J)	R(J)	P(J)	R(J)	P(J)
0						
1			38827.37*			
2		38374.33*	819.68*			
3		367.74*	810.38	38790.11*	39228.18*	
4	38378.85	347.01	796.12*	765.27	221.24*	
			782.55*		191.87*	
5	359.65	324.75	777.54	741.60	203.66*	
					184.39*	
6	336.62	294.55	754.85	712.11*	180.46*	39137.82*
				698.64*	134.08*	108.30*
7	309.42	260.88	727.30	678.64	155.22*	104.85*
					117.20*	85.43
8	276.68	223.14	695.38	640.90	108.30	66.63*
						20.09*
9	240.26	180.41	659.50	598.64	82.98	26.33*
						38958.48*
10	200.44	133.26	618.94	552.05	26.33*	964.60
					50.87*	
11	154.40	82.45*	573.74	500.96	38978.48	924.18
		80.53*				
12	102.56	26.99	524.15	445.08	935.96	877.54*
						852.05*

TABLE 10.1 (contd)

Wavenumbers for the (E-X) Bands of CuD

	4-2		5-2		6-2	
J	R(J)	P(J)	R(J)	P(J)	R(J)	P(J)
13		37966.19	470.65	385.36	884.40	790.11
14			412.66	321.69*	827.37	732.81
15			349.90	253.35*	765.27	666.78
16			283.32	180.43*	698.72	595.36
17			212.31	102.56*	628.17	518.58
18			139.37	22.60	552.05	437.78
19					472.90	352.51
20					388.46	263.04
21					300.67	169.06
22					212.16	70.81
23						37969.93

TABLE 10.1 (contd)

Wavenumbers for the (E-X) Bands of CuD

6-0

J	R(J)	P(J)
5	40851.81	
6		407949.36
10	684.67	
11	607.87*	
12	561.42	503.14

6-1

J	R(J)	P(J)
14		40021.98
15	40051.10	39953.21
16		878.80
17	39908.08*	
18		715.01

7-0

J	R(J)	P(J)
5	41266.99	
7	209.90	41162.84*

7-1

J	R(J)	P(J)
3	40957.88	
4		40913.52
5	923.287	
6	898.02	856.93
7	868.87	821.35
8	835.35	
9	797.04	

7-2

J	R(J)	P(J)
1		
2	39660.85*	
3	650.96	
4	636.05*	39607.25
5	617.37	582.36
6	594.01	
7	566.53	518.72
8	534.26	480.36
9	497.45	437.43
10	456.59	390.32
11	412.03	338.97
12	362.71	
13		223.35
14		159.76
15	191.87*	90.07

7-3

J	R(J)	P(J)
5	38349.90	38315.86*
6	327.60	285.31
7	300.67	253.23
8	270.38	216.36
9	235.23	175.26
10	196.06	130.01
11	153.38	80.53

TABLE 10.1 (contd)

Wavenumbers for the (E-X) Bands of CuD

	7-3 (contd)			8-0	
J	R(J)	P(J)	J	R(J)	P(J)
12	105.76	26.99	14	41276.60	41186.65
13	50.89*	37969.93	16		33.41

TABLE 10.1 (contd)

Wavenumbers for the (E-X) Bands of CuD

	8-1		8-2		8-3	
J	R(J)	P(J)	R(J)	P(J)	R(J)	P(J)
1						
2						
3						
4						
5	41336.89*					
6	312.60					
7	283.57	41236.31				
8	249.49	196.24	40947.64			
9	211.11	151.03	911.34		40649.00	40589.54*
10	168.02	102.26	869.91	40804.01		
11	120.29	48.54		752.15	565.74	493.97
12	68.13	40990.22	774.16	696.21	518.58	440.83
13	11.29	927.16	719.47	636.05*	465.72	380.99
14	40949.94	859.72	660.85	570.87	409.81*	319.80
15	883.94	787.84	597.88	502.16*	349.90*	253.35
16	813.63		530.10*	428.67	285.31*	
17			459.94	351.15	216.36	108.73
18						29.44
19				185.07		

TABLE 10.1 (contd)

Wavenumbers for the (E-X) Bands of CuD

9-0

J	R(J)	P(J)
14	43686.20	43596.23
15	617.43	522.02
16	542.92*	442.05*

9-1

J	R(J)	P(J)
3	41794.49*	
4		41749.36*
5	754.88	
6	720.07*	
	730.77*	
7	697.84	653.42
8	665.36	603.10*
		613.88*
9		
10	577.92	518.38
11	529.54	458.12
12	477.88	399.95
13	421.35	336.89
14	359.64	269.53
15	293.45	198.34
16	222.38	121.85
17	151.03	40.81
18		40955.09
19		868.87

9-2

J	R(J)	P(J)
14	40070.44	39980.34
15	6.63	911.34
16	39938.50	838.37
17	869.91	
18		677.71
19	715.01	594.01*
20		
21		413.72

9-3

J	R(J)	P(J)
12	38927.78	
13		
14		
15		
16	693.23	
17	628.17	38518.47
18	552.47	438.17
19		359.65
20	390.86	270.38
21		
22		95.04

TABLE 10.1 (contd)

Wavenumbers for the (E-X) Bands of CuD

10-0

J	R(J)	P(J)
16	42951.16	42851.70
17		
18	786.01	898.71
19	697.50*	
20	603.76	483.01
21		380.01
22		271.77

10-1

J	R(J)	P(J)
1	42223.69	
2	217.13	
3	202.07*	42184.05*
		186.65*
4	184.05*	162.84
	186.65*	
5	162.84*	
6	136.78	100.17*
7		61.01
8	84.34*	20.70
9	33.41*	41975.95*
10	41989.77*	936.84*
	990.51*	925.90*
11	941.55	871.71
12	888.53	812.36

10-1 (contd)

J	R(J)	P(J)
13	830.31	749.36
14	769.46*	680.72
15	700.78	607.87
16	630.45	529.54*
		531.05*
17	551.03	448.16
18	471.62	363.15
19	386.85	269.53*
20	297.21	175.45
21	203.24	76.17
22	104.70	40972.23
23	2.18	864.18
24	40895.19	

11-0

J	R(J)	P(J)
20	43004.59	42884.91
21	42906.90	780.95
22	802.45	672.77
23	694.75	559.20
24	582.22	442.05
25	465.46*	319.80
26		193.61*

TABLE 10.1 (contd)

Wavenumbers for the (E-X) Bands of CuD

11-1

J	R(J)	P(J)
1		
2	42617.43	
3	613.46*	
4	588.89*	562.56
5		543.31*
6		503.17*
	543.31*	
7	522.02*	
8		426.99*
9	438.97	389.78
10		
11	346.67*	276.60
12	292.31	
13	233.88	152.54*
14	171.37	84.34
15		11.18
16	32.25	41934.17
17	41955.38	41851.81
18	874.56	764.86
19	788.56	673.77
20	697.84	577.92
21	603.10	477.88
22	503.54	373.09
23	399.95	264.45

11-1 (contd)

J	R(J)	P(J)
24	291.63*	151.03
25	153.03	33.27
26	66.96	40911.30*
27	40949.94	

12-1

J	R(J)	P(J)
4	42992.18	
5	42975.99	
6	955.38	42906.90
7	919.04	874.15
8	887.28	838.66
9	862.51	786.01*
10	786.01	740.15
11		700.25
12	691.57	608.29
13	633.30	
14		483,01
15	503.17	410.70
16	430.38	331.60
17	353.35	250.56
18	271.77	162.84
19		71.93
20	42094.09	42975.95
21	41998.95	874.56

TABLE 10.1 (contd)

Wavenumbers for the (E-X) Bands of CuD

	12-1 (contd)			12-2	
J	R(J)	P(J)	J	R(J)	P(J)
22	898.94	769.46	14	40070.44	39980.34
23	794.49	660.04	15	6.63	911.34
24	684.87	545.82	16	39938.50	838.37
25	572.61	427.95	17	869.91*	
26	453.79	304.53	18	333.57	677.71
27	331.88	177.87	19		594.04
28	205.52	46.79	20		502.16
29	76.17*				
	75.13*				

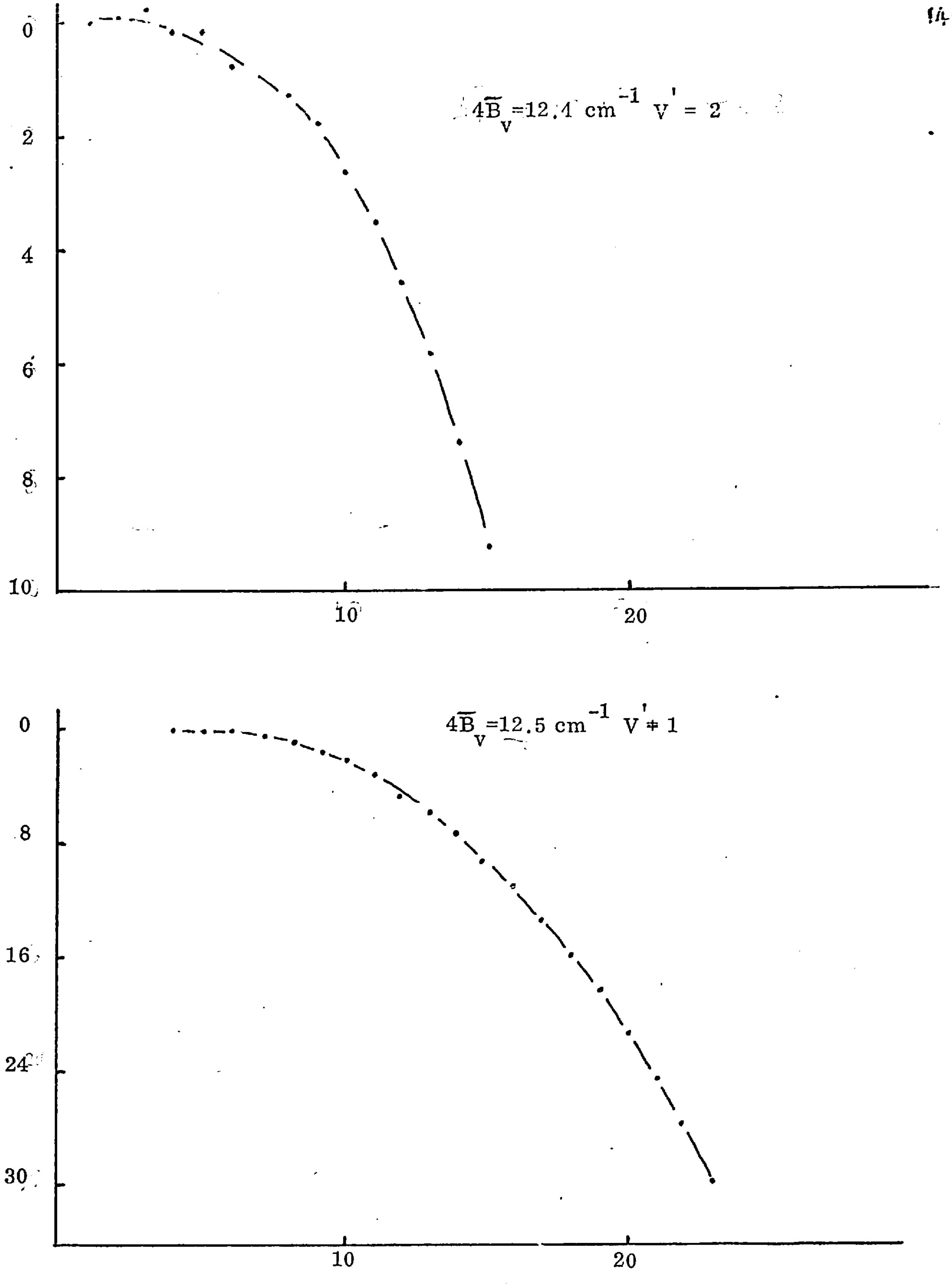

GRAPHS OF $\Delta_2 F - 4B_v(J+\frac{1}{2})$ v J

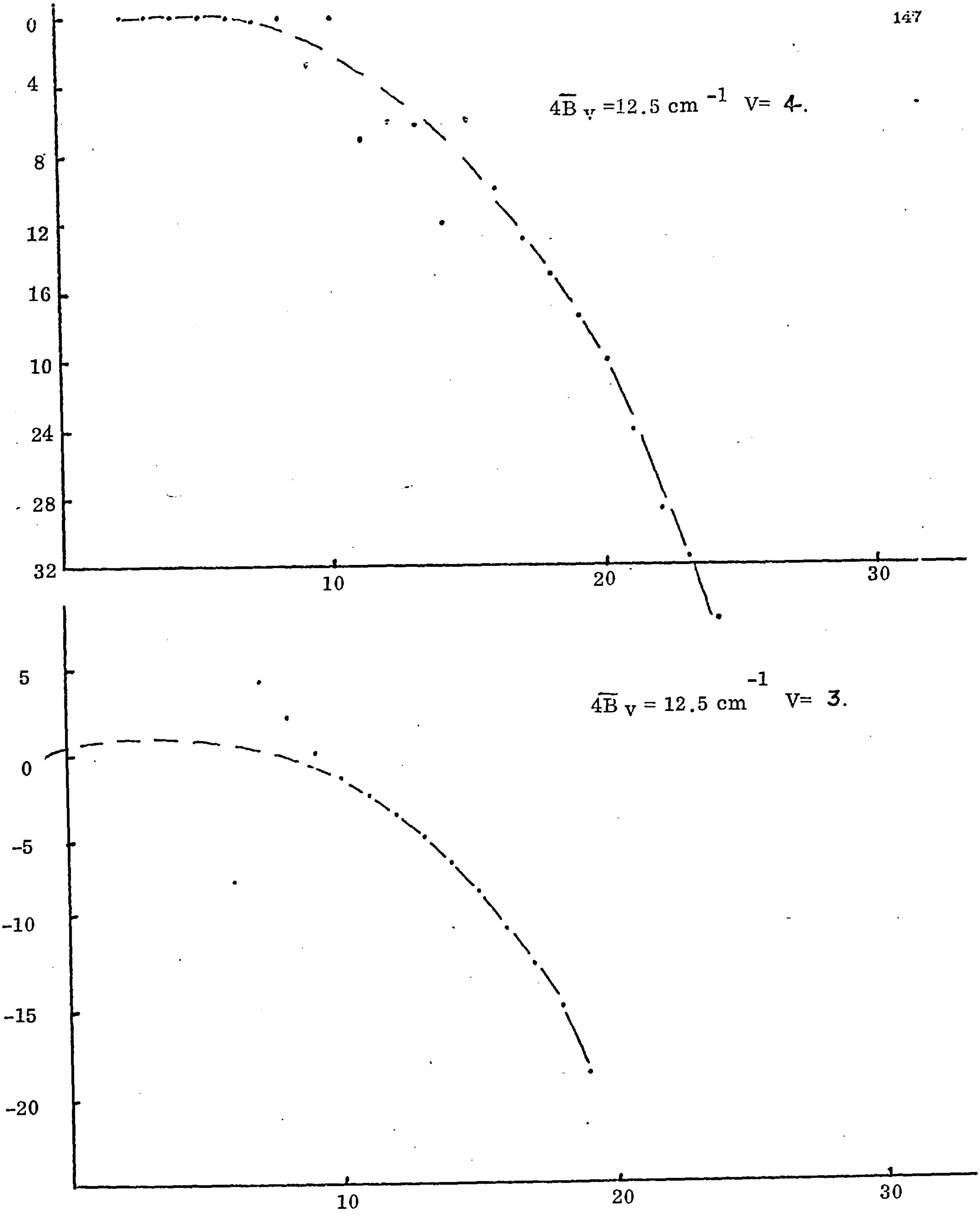

GRAPHS OF $\Delta_2F - 4B_v(J+\frac{1}{2})$ v J

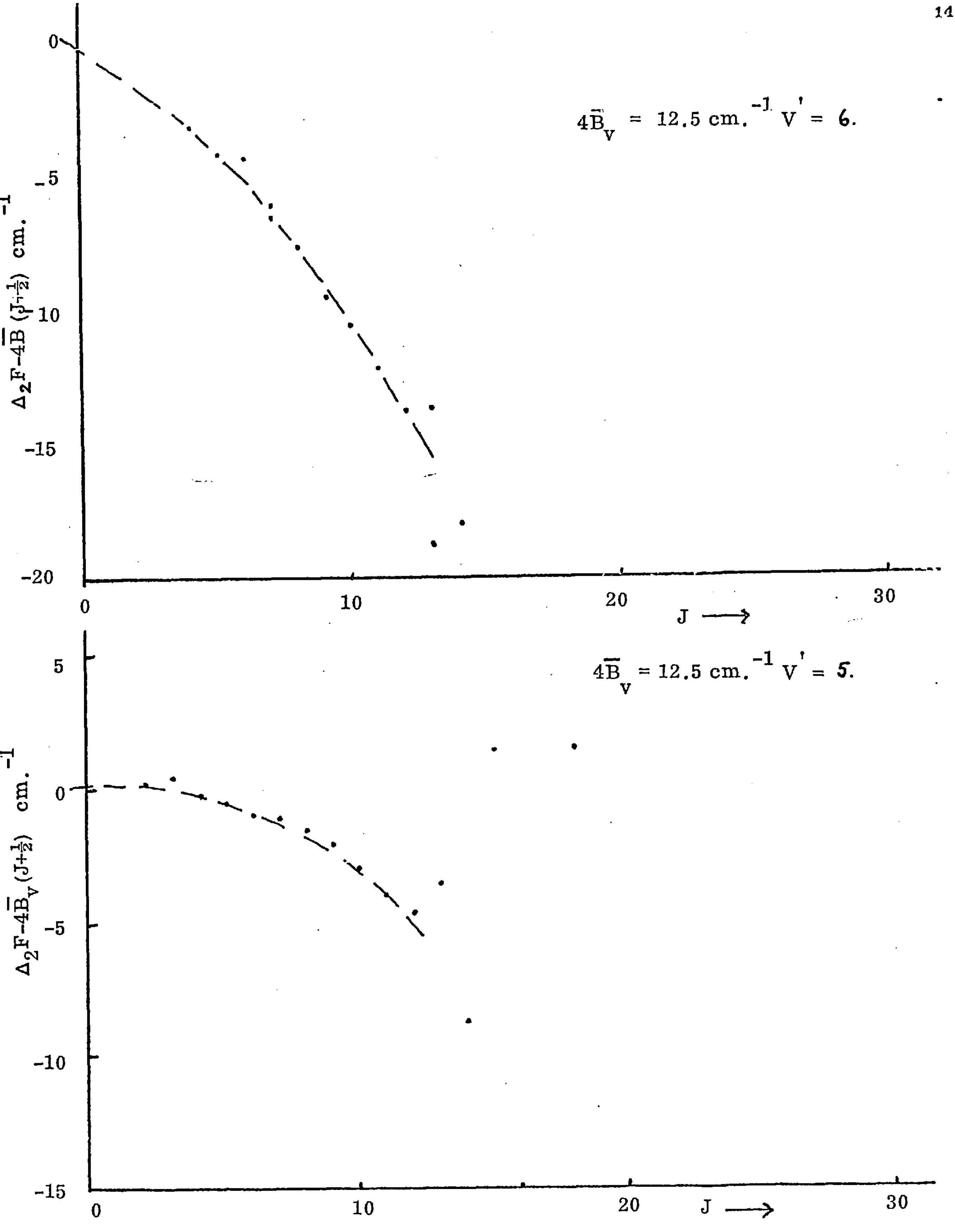

GRAPHS OF $\Delta_2 F - 4\bar{B}_V(J+\frac{1}{2})$ v J

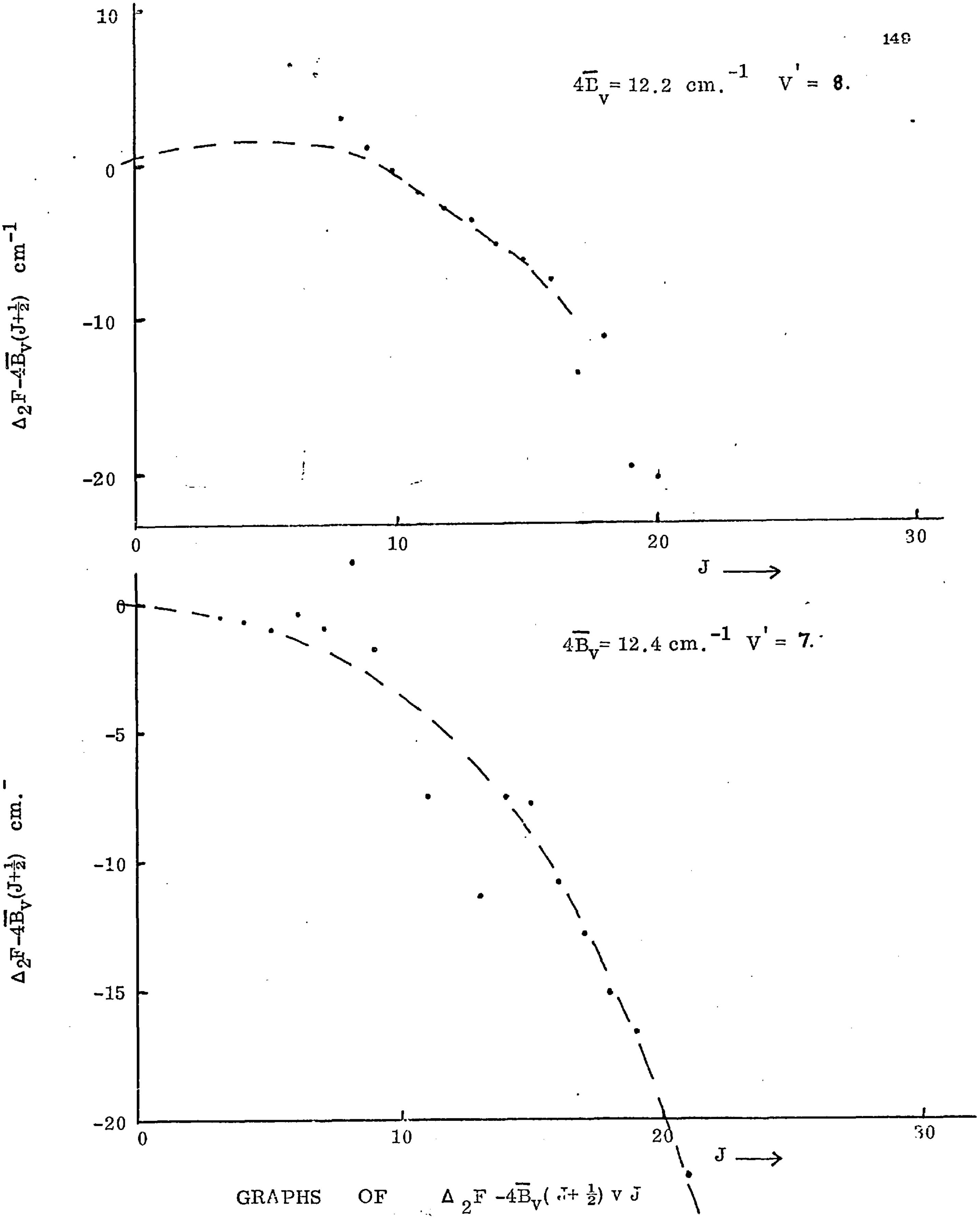

GRAPHS OF $\Delta_2F - 4\overline{B}_v(J+\frac{1}{2})$ v J

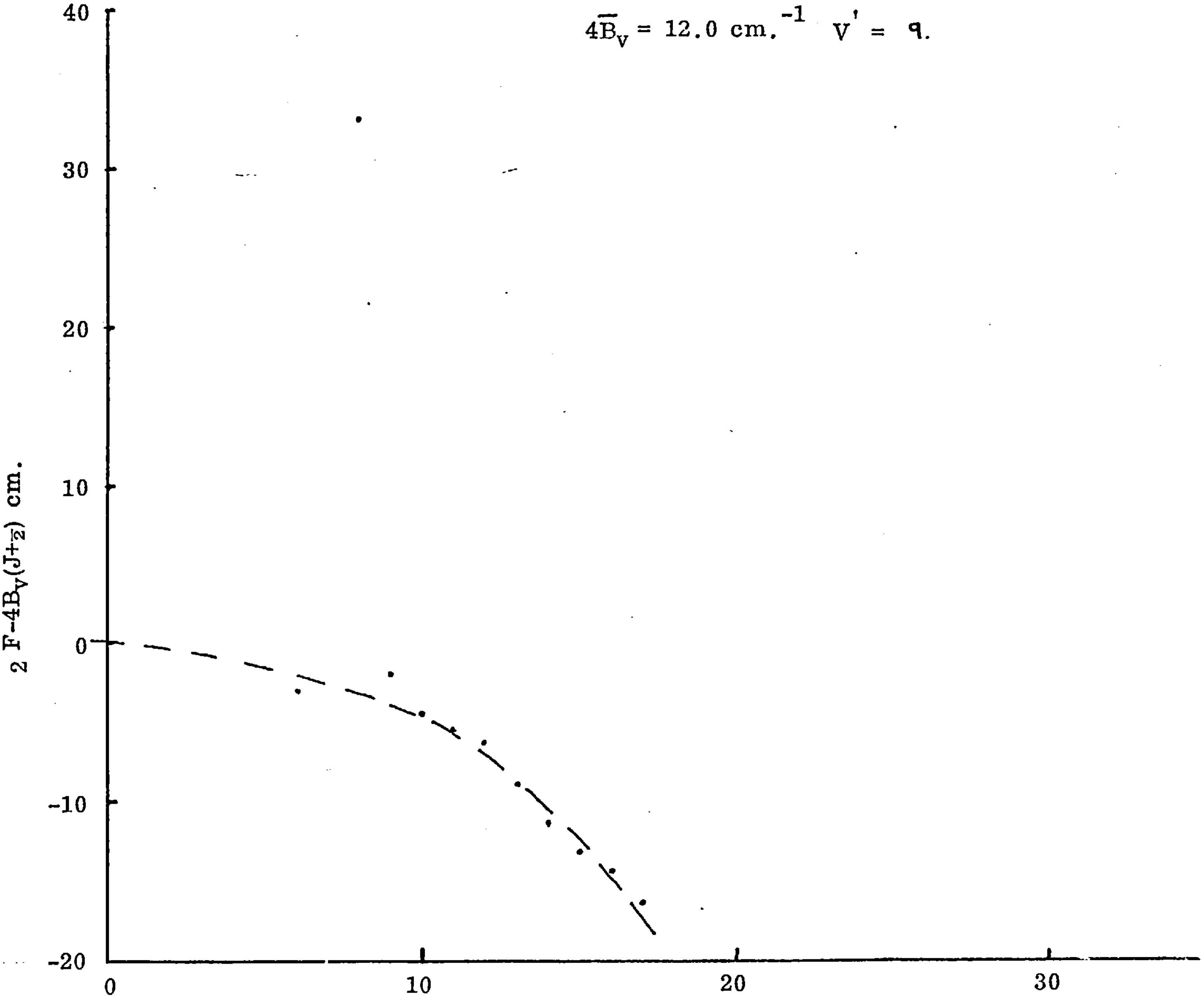

GRAPH OF $\Delta_2 F - 4\overline{B}_V\ (J + \frac{1}{2})$ v J.

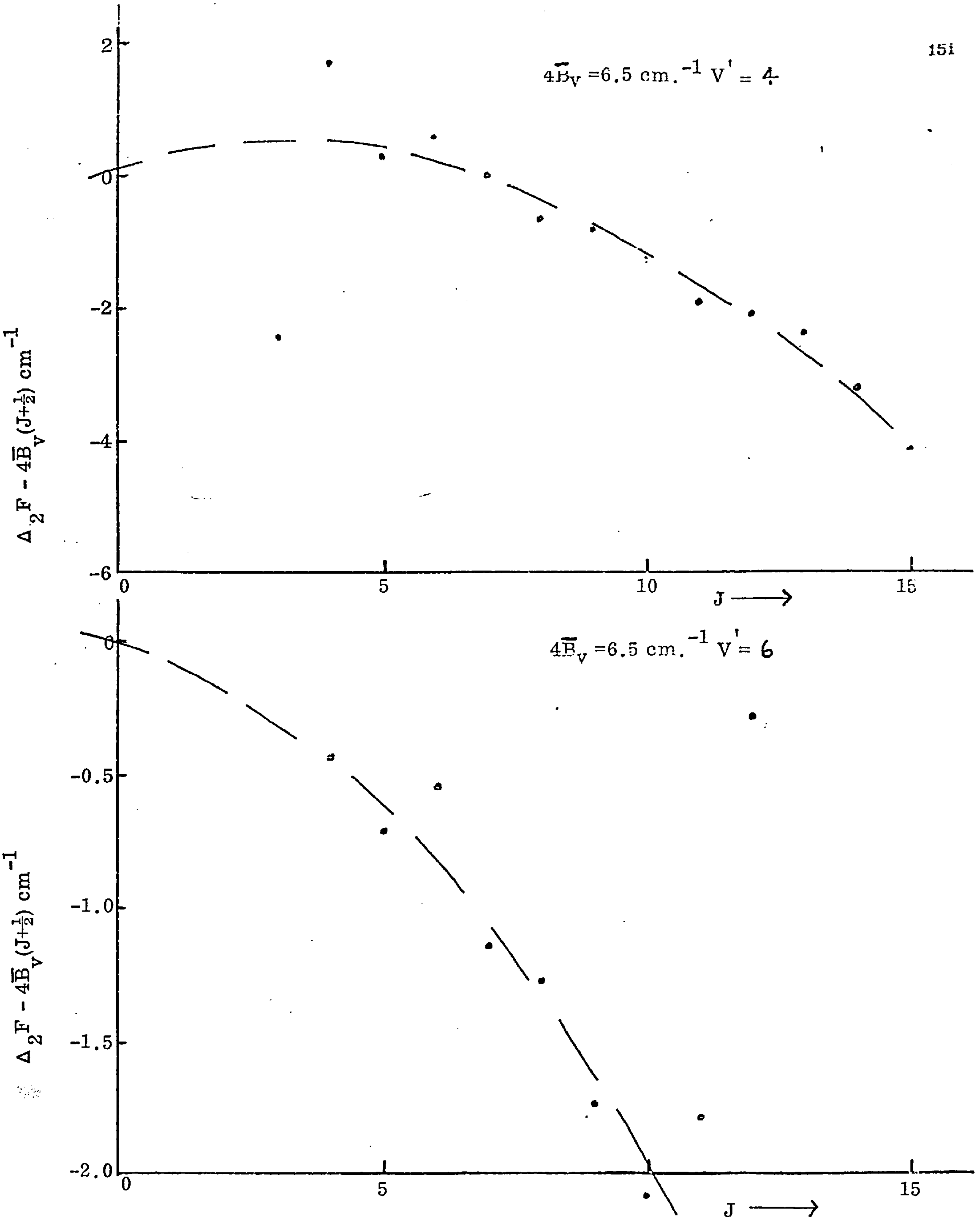

GRAPHS OF $\Delta_2 F - 4\overline{B}_V(J + \frac{1}{2})$ v J

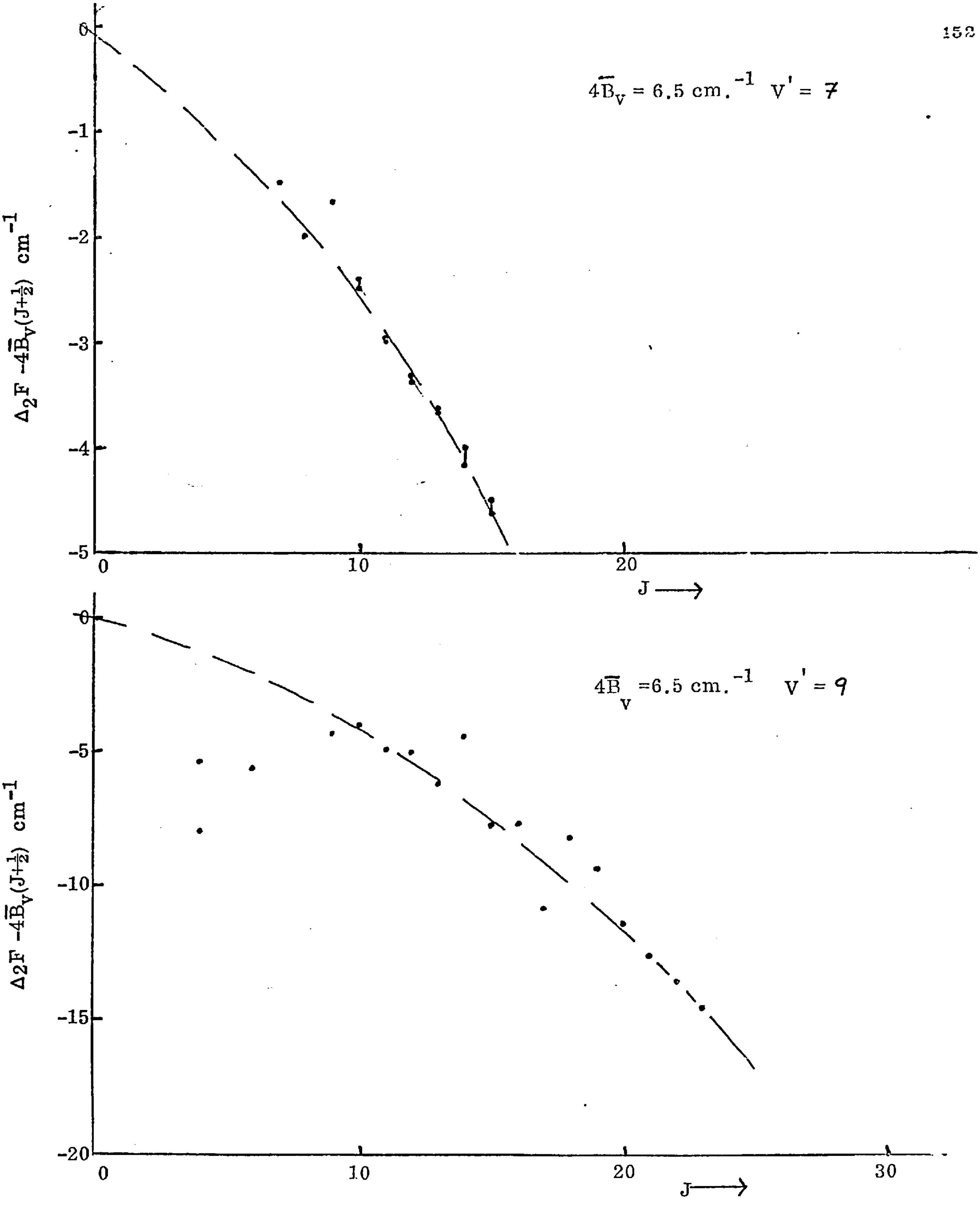

GRAPHS OF $\Delta_2 F - 4B_V(J+\frac{1}{2})$ v J

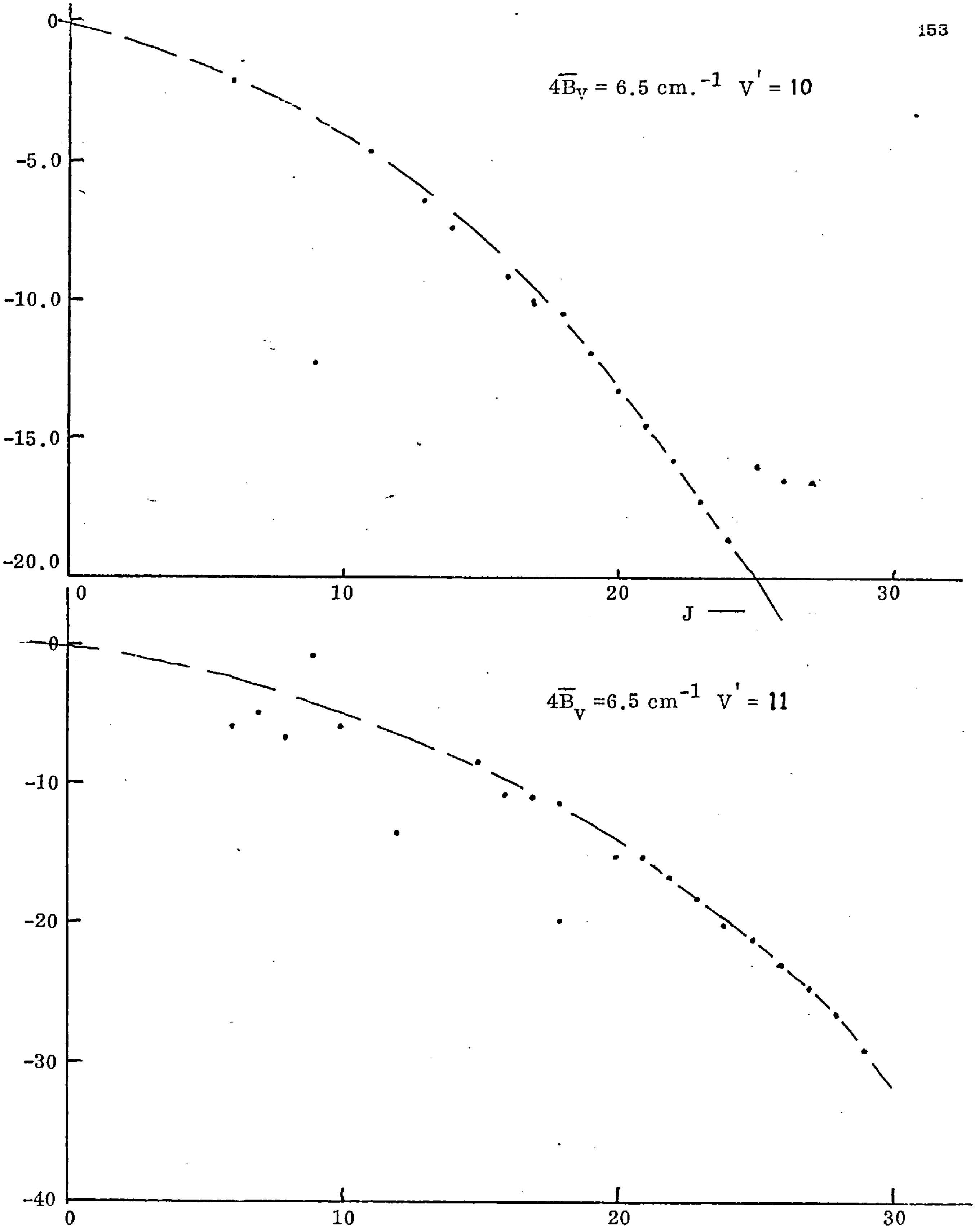

GRAPHS OF $\Delta_2 F - 4\overline{B}_V (J + \frac{1}{2})$ v J

TABLE 10.2

Energy Levels for the E State in CuH

J	V_o $F'_v(J\ 1)$	J	V_o $F'_v(J\ 1)$	J	V_o $F'_v(J\ 1)$
	v' 1		v' 2		v' 3
2					
3			40413.589		
4	39844.763		440.103		
5	875.497		471,467		41065.948
6	912.454		508.973		
7	954.896		552.616		41139.886
8	40004.395		601.975		191.556
9	59.612		657.937		248.194
10	121.835		720.802		310.105
11	186.889		787.157		378.073
12	260.867		861.317		451.540
13	337.605		938.903		530.620
14	422.207		41024.400		614.481
15	509.898		113.055		705.968
16			209.371		801.068
17	705.019				901.897
18	809.415		415.283		42008.094
19	917.422		524.263		117.264
20	41032.793		640.737		232.800
21			758.093		352.901
22			885.319		

TABLE 10.2

Energy Levels for the E State in CuH

J	V'_o (J 1)	J	V'_o (J 1)	J	V'_o (J 1)
	v' 4		v' 5		v' 6
2	41575.278		42159.663		
3	594.243		178.476		
4	619.387		203.335		
5	650.663		234.512		
6	688.195		271.639		42843.595
7	732.076		314.966		890.342
8	781.977		364.606		940.937
9	838.260		419.931		996.628
10	898.501		481.029		43057.700
11	969.469		547.973		124.519
12	42035.046		620.892		196.433
13	119.630		699.703		274.122
14			786.086		357.796
15	289.071		872.699		445.656
16	384.990		981.938		539.650
17	485.492		43963.911		639.336
18	590.656		160.023		739.536
19	701.804		276.756		853.582
20	817.483				957.614
21	938.094				

TABLE 10.2

Energy Levels for the E State in CuH

J	V_o $F'_v(J\ 1)$	J	V_o $F'_v(J\ 1)$	J	V_o $F'_v(J\ 1)$
	v 7		v 8		v 9
2					
3	43340.588				
4	365.418		43935.011		
5	395.454		964.687		44489.715
6	431.389		44000.049		524.784
7	474.209		42.482		564.799
8	522.709		88.809		648.228
9	579.986		142.117		701.089
10	637.082		199.765		759.897
11			264.557		822.651
12	770.283		334.180		891.379
13			409.497		965.444
14	923.527		488.42		45042.990
15	44011.766		576.67		126.819
16	104.724		662.05		216.489
17	202.261		762.45		311.002
18	305.583		858.84		410.436
19	412.979		966.57		515.043
20	525.866		077.16		621.934
21					
22	766.030				

TABLE 10.2

Energy Levels for the E State in CuD

J	V_o $F'_v(J\ 1)$	V_o $F'_v(J\ 1)$	V_o $F'_v(J\ 1)$
	v' 6	v' 5	v' 4
4	41928.32	41510.52	41093.34
5	951.81	526.69	109.42
6	972.25	546.13	128.24
7	994.69	569.08	150.85
8	42022.58	594.66	176.78
9	36.36	623.44	204.74
10	79.20	655.72	236.48
11	122.76* 98.22*	690.83	272.33
12	133.46	728.72	309.38
13	181.42	769.61	348.02
14	227.73	813.98	
15	275.89	861.18	
16	326.33	910.96	
17	379.47	964.07	
18	435.83	42019.97	
19	493.83	81.05	
20	555.76		
21	619.42		
22	686.83		
23	760.07		

TABLE 10.2

Energy Levels for the E State in CuD

J	V_o $F'_v(J\ 1)$	V_o $F'_v(J\ 1)$	V_o $F'_v(J\ 1)$
	v' 9	v' 8	v' 7
1			
2			
3	43187.49*		42351.095
4			366.62
5	217.99	42800.00	385.96
6	229.87	822.40	408.24
7	240.57		
7	262.07	847.80	433.89
8	291.72	875.85	462.32
9		907.28	493.67
10	351.56	941.66	528.48
11	388.27	979.02	567.01
12	429.31	43019.56	608.17
13	473.00	62.94	648.19
14	519.04	109.34	
15	568.05	158.54	
16	619.59	210.84	
17	678.24	267.60	
18	733.67		
19	797.87		
20	854.43		

TABLE 10.2

Energy Levels for the E State in CuD

J	V_o $F'_v(J\ 1)$ V' 12	V_o $F'_v(J\ 1)$ V' 11	V_o $F'_v(J\ 1)$ V' 10
1			
2		43987.02	43586.70*
3		6.46*	595.07
4	44416.33	13.04*	608.20*
			610.80*
5	439.10		625.95
6	465.18	53.11*	646.58
7	483.27	86.25	
8	513.64		710.70
9	558.68	135.14	729.58
10	559.65		764.15
11		205.40	800.28
12	643.00	243.74	839.96
13	684.95	285,53	882.46
14	728.81	330.77	928.86
15	777.77		975.38
16	827.59	429.46	44027.66
17	880.56	482.59	78.24
18	936.26	539.05	136.11
19		597.67	195.96
20	45054.90	658.65	258.02

TABLE 10.2 (contd)

Energy Levels for the E State in CuD

J	V_o $F'_v(J\ 1)$	V_o $F'_v(J\ 1)$	V_o $F'_v(J\ 1)$
	V' 12	V' 11	V' 10
21	118.65	722.81	322.95
22	184.60	789.20	390.36
23	253.12	858.58	460.81
24	323.40	930.16	533.72
25	397.91	45008.33	
26	472.73	85.90	
27	550.94	169.00	
28	631.50		

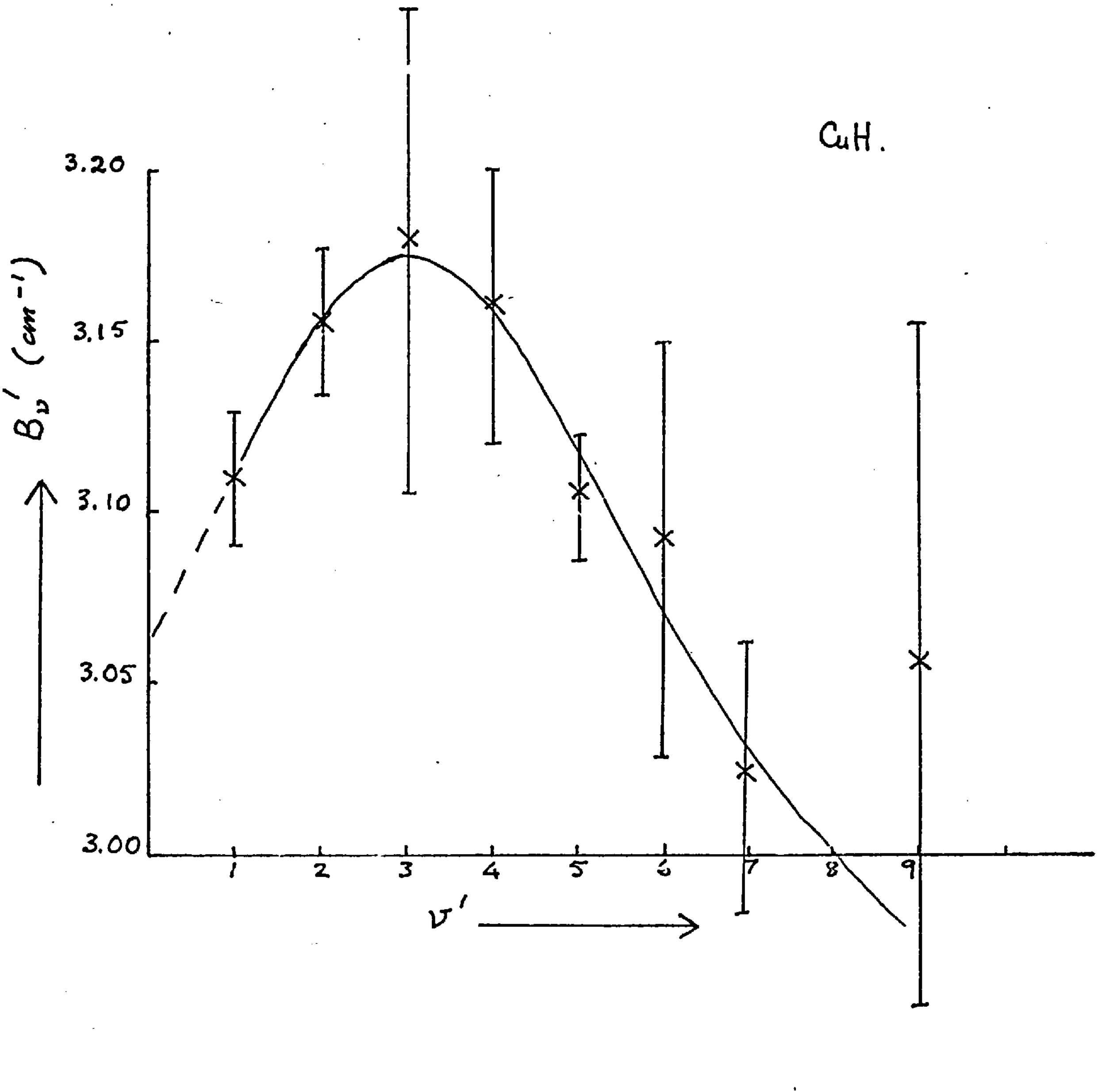

FIGURE 10,2

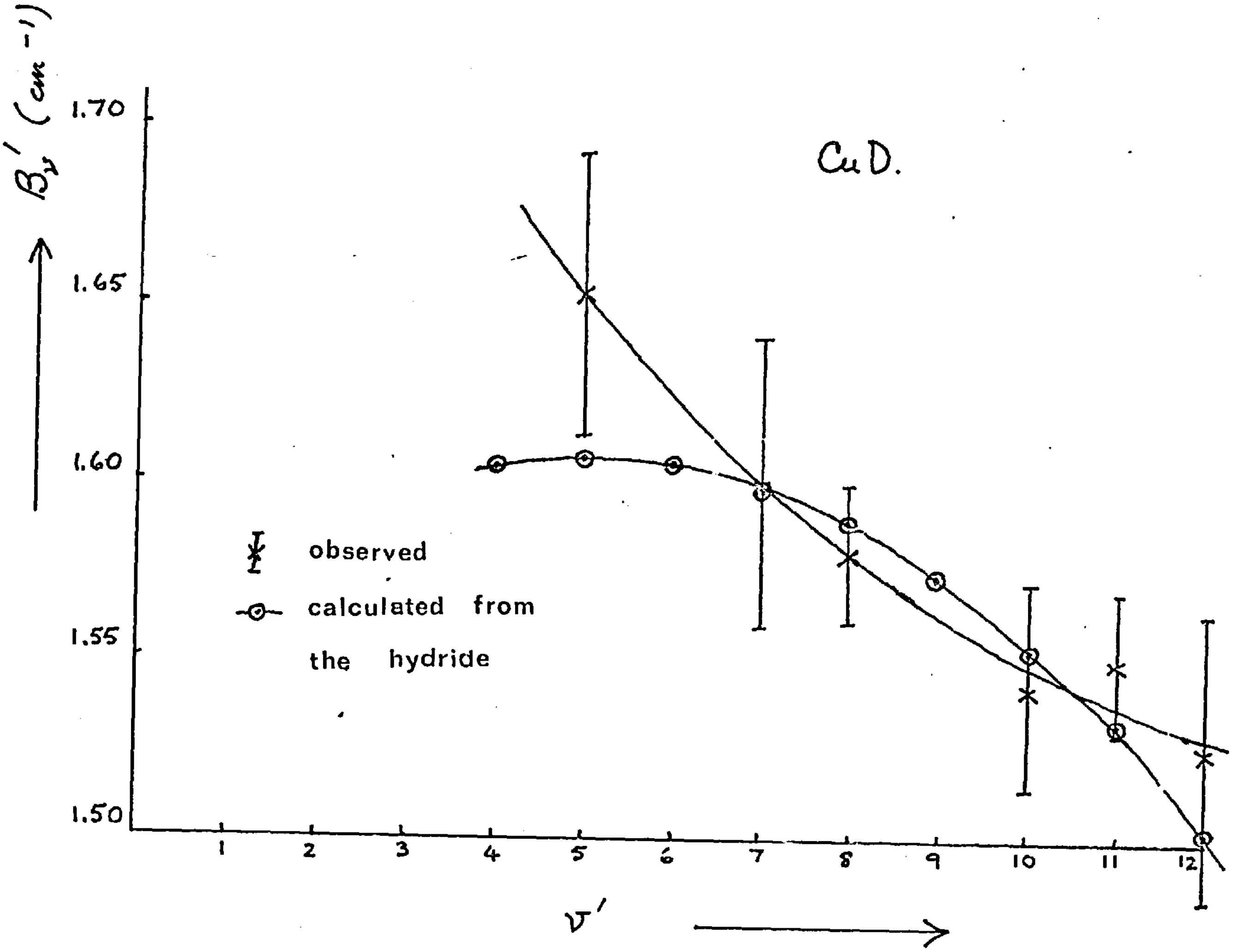
B_v' (cm^{-1})
1.70
1.65
1.60
1.55
1.50
CuD.
observed
calculated from the hydride
1
2
3
4
5
6
7
8
9
10
11
12
v'

FIGURE 10,3

TABLE 10.4.1

Constants for the E State Bands of CuH and CuD

CuH

V'		B'_v		D'_v	H'_v
1		3.109	0.02	3.42	5.6
2		3.156	0.02	3.84	7.9
3		3.176	0.07	4.07	8.4
4		3.160	0.04	3.69	4.95
5		3.106	0.02	0.96	-8.3 *10
6	**	3.091	0.06	3.32	12.0
7		3.026	0.04	2.74	4.0
18	†				
19	**	3.057	0.04	8.09	8.8 *10
				$*10^{-4}$	$*10^{-7}$

** Strongly perturbed band.

† Perturbations too strong to give meaningful value to B'_v.

CuD

V'		B'_v		D'_v	H'_v
4	†				
5		1.652	0.04	3.13	39.6
6	†				
7		1.600	0.04	-3.15	-150.0
8		1.580	0.02	0.763	5.7
9	†				
10		1.542	0.03	0.862	2.3
11		1.550	0.02	1.21	3.4
12		1.524	0.04	0.396	0.39
		$*10^{0}$		$*10^{-4}$	$*10^{-7}$

TABLE 10.4.2

Constants for the E State Bands of CuH and CuD

CuH

v'	v_o	B'_v	D'_v	$\Delta_2 G$
1	39782.64 (.2)	3.102	3.20	
2	40376.50	3.161	4.51	593.86
3	40965.57	3.171	3.69	589.07
4	41556.56 (.5)	3.151	4.36	590.99
5	42141.33	3.141	2.10	584.77
6	42719.03 (-.62)	3.126	4.44	577.70
7	43305.67	3.021	2.99	586.64
8	43875.60	2.983	2.85	569.93
9	44440.9	2.923	2.61	565.3

CuD

v'	v_o	B'_v	D'_v	$\Delta_2 G$
4	41061.61	1.569	2.08	416.21
5	41477.82	1,632	1.46	416.21
6	41886.70	1.659	1.60	408.88
7	42318.05	1.594	.38	431.35
8	42734.00	1.569	.94	415.95
9	43146.27	1.556	.17	412.27
10	43557.93	1.581	1.65	411.66
11	43968.06	1.533	.84	410.13
12	44371.03	1.517	.81	402.97

Numbers in brackets are the difference between the quadratic and cubic derivations of v_o, where the cubic was significantly better than the quadratic.

CHAPTER 11

ISOTOPE EFFECTS

11.1 The Vibrational Numbering

The ratio of the natural isotopes of copper Cu_{63} and Cu_{65} is approximately 1 : 2. This effect was first used to identify the carrier of the band system, Plate (9.1), then as an aid to picking out the branches. This isotope splitting appears to be regular through all the perturbations. Graph 11.1 shows the measured splitting for two adjacent bands with the same lower state. These bands were chosen because the lines near the origin were well resolved and free of the perturbation and they were in the longer wavelength region where the wavenumber difference is largest. Using the formula given by Hertzberg(23):

$$\Delta v_{65,63} = (p-1)(w_e'(v'+\tfrac{1}{2})-w_e''(v''+\tfrac{1}{2}))-(p^2-1)(w_e'x_e'(v'+\tfrac{1}{2})^2 - w_e''x_e''(v''+\tfrac{1}{2})^2)$$

where Δv is the extrapolated splitting at zero rotation. The term $w_e'x_e'$ can be set to zero since it represents a small and inaccurate correction. This then gives $v' = 2$ and 3 for the two upper state bands to the nearest integers. Replacing these numbers in the formula gives:

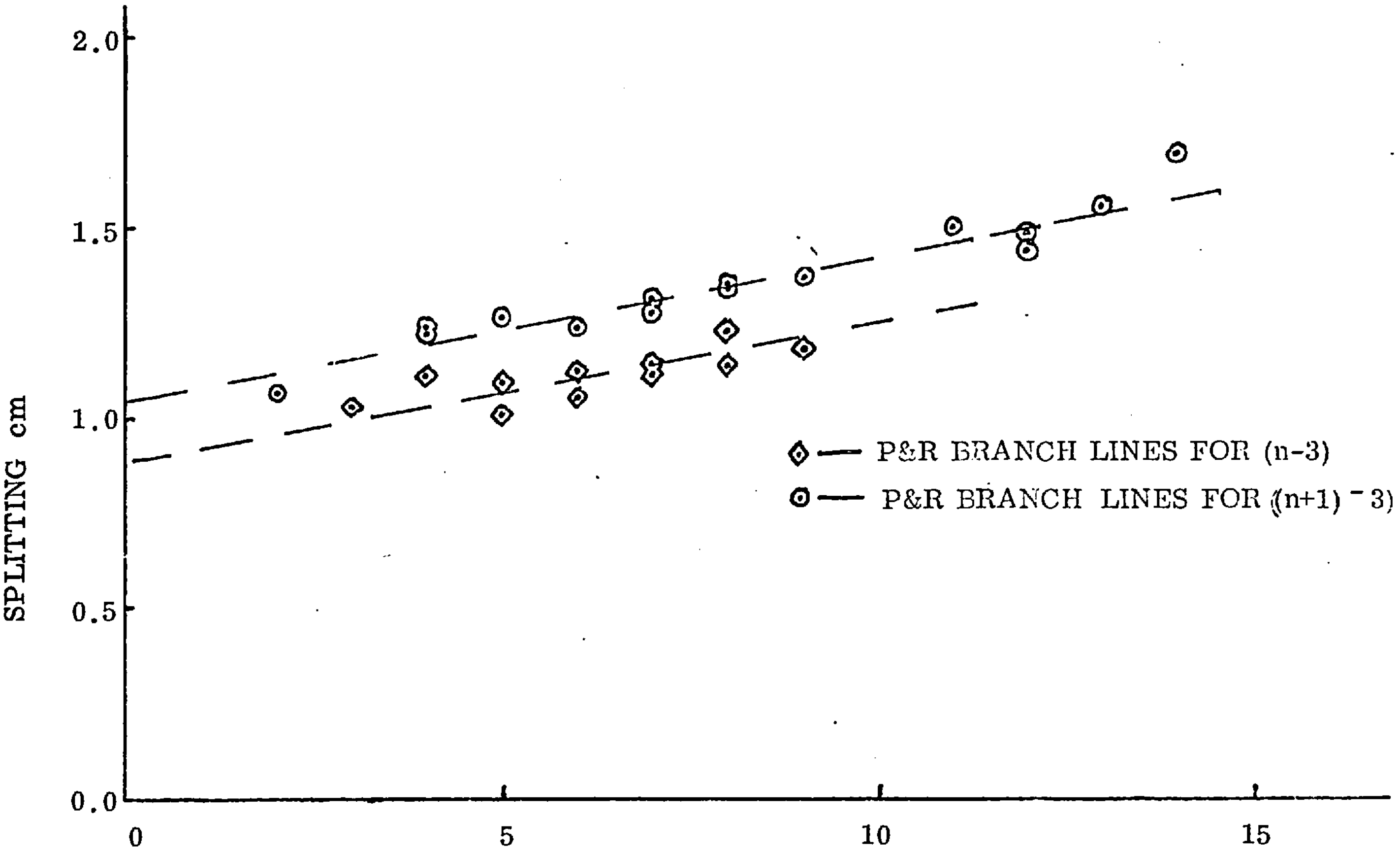

GRAPH OF $Cu_{63}H$, $Cu_{65}H$ ISOTOPE SPLITTING.

FIGURE 11,1

$$\left.\begin{array}{ll} \Delta v_2 \text{ observed} = 1.03 \pm 0.1 & \text{calculated} = 1.056 \\ \Delta v_3 \text{ observed} = 0.90 \pm 0.1 & \text{calculated} = 0.917 \end{array}\right) \text{cm}^{-1}$$

The value of p used was .99976 and the values of w_e'' and $w_e''x_e''$ were taken from ref 36. The numbering would now agree with the first choice of ref 1 and can now be tested in the deuteride system. Table 11.1 gives a series of deviations of the origins of the deuteride bands assuming that the first observed state is v' = 2, as indicated by the isotope splitting and for v' = 1; the values of the upper state constants of this analysis and that of ref 1 are included. Clearly the numbering with the first observed hydride state being v' = 1 gives a much better fit with the deuteride origins than using the best fit derived from the Cu_{63}, Cu_{65} isotope effect. The first deuteride band observed is then v' = 4. The tables have been given in detail so that any doubt about the numbering of the bands due to the large difference between the derived constants in this analysis and that of ref 1 can be shown to lead to only a small difference in the predicted deuteride origins; also the small differences between the second and third lists show that there is no advantage in using a three term formula to fit the hydride origins with regard to their fit with the deuteride bands. The use of

TABLE 11.1

$v' * = 2$

$w'_e = 604.9 \quad pw^{r}_e = 431.2$

$w'_e x'_e = 1.65 \quad p^2 w'_e x''_e = .838$

v_{07}	41739.98
v_{08}	42161.7
v_{09}	42573.8
v_{010}	42988.3

$v' = 2$

$w'^{/}_e = 574 \quad pw'_e = 409$

$w'_e x'_e = -3.6 \quad p^2 w'_e x'_e = -1.83$

$w'_e y'_e = -.27 \quad p^3 w'_e y'_e = -.098$

v_{05}	40900.9
v_{06}	41321.3
v_{07}	41741.5
v_{08}	42161.1
v_{09}	42579.4
v_{010}	42995.7

$v' = 1$

$w'_e = 601.6 \quad pw'_e = 428.8$

$w'_e x'_e = 1.65 \quad p^2 w'_e x'_e = .838$

v_{04}	41069.4
v_{05}	41489.8
v_{06}	41908.6
v_{07}	42325.6
v_{08}	42744.9
v_{09}	43154.7
v_{010}	43566.8

$v' = 1$

$w'_e = 580/ \sim 413.4$

$w'_e x'_e = -2.7 \sim -1.37$

$w'_e y'_e = -.27 \sim -.098$

v_{04}	41068.7
v_{05}	41487.4
v_{06}	41906.8
v_{07}	42325.0
v_{08}	42741.5
v_{09}	43155.8
v_{010}	43567.3

TABLE 11.1 (contd)

$v' = 1$

$w'_e = 591.4 \sim 421.5$

$w'_e x'_e = -.696 \sim -.354$

$w'_e y'_e = -.157 \sim -.057$

		Observed deuteride origins
v= 4	41067.3	41061.6
5	41488.1	41477.8
6	41907.6	41886.7
7	42325.7	42318.1
8	42738.9	42734.0
9	43156.0	43146.3
10	43567.5	43557.9
		43968.1

* v' is the assumed number for the first observed state.

≠ These are the values given by ref 1.

the three term formula is desirable since then the comparison of these bands with the comparable bands in the group 1a hydrides is more complete. However, the predicted $\Delta_2G(1-2)$ extrapolated from ref 1 is much smaller than the observed $\Delta_2G(1-2)$ and the constants derived here are outside the errors given by ref 1. Both the three and two term formula are given but the data is insufficient to determine which is to be preferred.

Whichever set of constants is used, there is a systematic deviation between the observed and predicted values of the deuteride origins of approximately 8 cm^{-1}. Without the $v' = 0$ band the derived constants are too inaccurate to assume other than that this is due to inaccuracy in these constants. The direction of the discrepancy indicates that the Δ_2G value for the bands $v' = 0$ and 1 will be higher than that predicted from the three term formula, which favours the use of a positive $w_e'x_e'$ to describe the system. This would fit in more easily with the group 1 hydrides where the maximum in the Δ_2G values occurs at a higher v' value than the maximum in the B_v' values..

11.2 The Isotope Effect in the 2200 Å Band

To follow up the possibility that there was a true discrepancy between the v_e values for the hydride and deuteride, an analysis of the deuteride

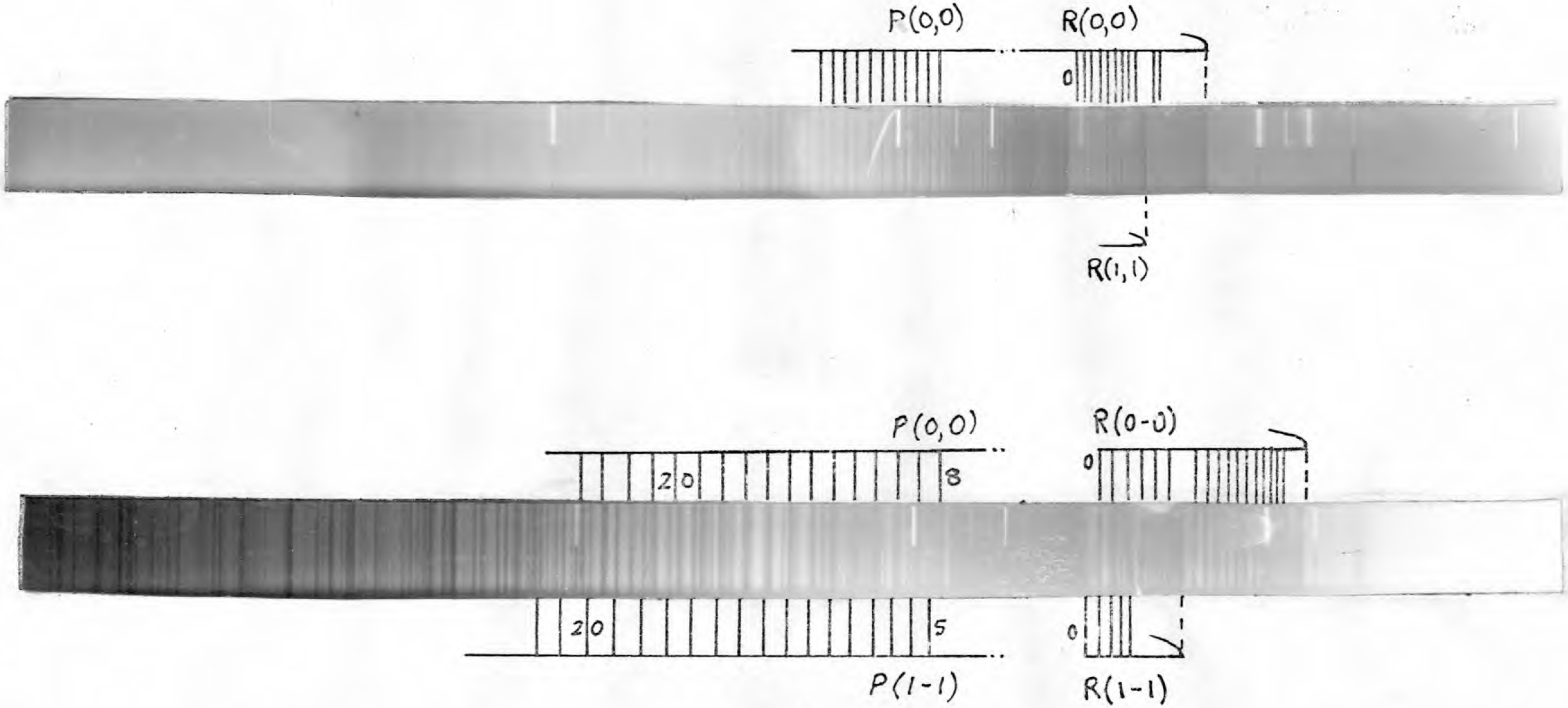

The spectra of CuH and CuD near 2200 Å.

PLATE 11.1

band at 2200 Å was made in order to check the v_e difference for this system. This also provides a check on the numbering of this band system. A table of the measured wavenumbers (11.2) and the second differences is given. The derived v_e is the same for the hydride and deuteride within the experimental accuracy, the derived constants are

$$v_{oo} = 44648.2 \qquad B'_v = 3.886 \qquad D'_v = 1.362 - 4$$

The numbering agrees with ref$^{(33)}$and there was no trace of any other bands except the (1,1). Both the hydride and deuteride are broadened rapidly when the ambient pressure is raised though the levels are distant from the dissociation limit. The absence of the (1,0) and (0,1) bands is due to the almost identical shapes of this potential and the ground state which by the Franck Condon principle, leads to a negligible transition probability off the diagonal sequence. Plate (11.1) shows the 2200 Å hydride and deuteride bands showing the striking difference between the isotope effect on this compact system compared with the (E-X) system.

11.3 Detailed Analysis of the Hydride, Deuteride Isotope Effect

To check the accuracy of the individual levels in the deuteride, which do not in general have the cross correlation from several lower states to

TABLE 11.2

Wavenumbers for the (D-X) Bands of CuD

	(0-0) R(J)	P(J)	$_2F'(J)$
	44656.35		
1	663.19		
2	670.71		
3	678.46	44623.70*	
4	684.48		
5	692.31*		
6	697.65	597.24	100.41
7	704.13	587.95	117.18
8	710.22	579.02	131.20
9	716.05	568.68	147.37
10	720.72*	558.89	161.83*
11	726.63	549.15	177.48
12	731.59		
13	736.44		
14	740.99	519.76	221.23
15	745.22	508.38	236.84
16	749.24	496.95	252.29
17	752.93	486.48	266.45
18	756.16	475.42	280.74
19	759.57	464.11	295.46
20	762.64	453.14	309.50
21	765.52	441.00	324.52
22		430.04	

* Line uncertain

the same upper state, a table of the predicted energy levels was produced. v_e was derived by obtaining the best fit to the observed v_o's of the deuteride. A table of the constants derived for the deuteride (11.3) shows that B_v' max is higher than in the hydride and the maximum is flatter. The derived constants are in fair agreement with the experimentally observed values and the table of the derived wavenumbers was used to pick out the perturbations marked in the Gero Schmid plot, and by deriving the wavenumbers of the P and R branches was used to check the assignment of doubtful levels. Since the perturbation occurs as a triplet of a known form, it is possible to assign perturbed members even where there is no confirming transitions with a fairly high degree of confidence.

From the detailed examination of the derived and experimental energy levels in the deuteride two major discrepancies are apparent; the fit becomes consistently poor for high J values, and there is a consistent but non-predictable difference in a band. The first observation adds weight to the point raised earlier that an extra term is necessary to fit the energy levels in a band. The deuteride bands are longer than observed in the hydride but an extra term can still be absorbed in B_v and D_v since there is an insufficient length of unperturbed band to obtain a significant value for

TABLE 11.3

Predicted Constants for the E-X Bands of CuD

	v_o	B'_v	D'_v
4	41059.02	1.604	1.37
5	41479.82	1.606	1.37
6	41889.32	1.604	1.35
7	42317.42	1.597	1.33
8	42730.62	1.586	1.29
9	43147.72	1.573	1.23
10	43559.22	1.553	1.17
11	43967.80	1.530	1.09
12	44373.15	1.503	0.999

H_v. Only in the first three members of the hydride are there sufficient levels to produce reasonably accurate values for H_v.

The appearance of a consistent difference between the observed and predicted v_o values which persists throughout each band is less easily explained. It may be due to a vibrational perturbation, and there is some justification for this assumption since the Δ_2G values in the hydride are also slightly disordered even where the origin is free from the perturbation of the $^3\Pi$ state. However there is no simple resonance like pattern to the displacements in either the hydride or deuteride.

11.4 Isotope Effect in the Perturber

The analysis of the $^3\Pi$ state was not continued to produce a least squares fit to the observed perturbation maxima, since the accuracy of the data would give no significant difference compared with the results of Ringström (ref 1). However, the perturbation maxima which were estimated and are shown in the Gero Schmid plots, figures (11.4), (11.5), deviate quite significantly from those used by ref 1 to derive the constants for the $^3\Pi$, even for those cases where the perturbation formula given in Herzberg - $dE = \frac{1}{2}(\text{sq rt}(4\ W_{12}{}^2 + d^2) - d)$ - could be used to derive the position of the maximum (a form of linear interpolation between the most perturbed adjacent levels was used otherwise). A simple linear fit of the perturbation maxima shows good agreement with Ringström's data, but naturally does not yield any information regarding the curvature of the second observed state reported by Ringström(1). The limited accuracy of the data allows the use of a simplified form of the term value equations of the $^3\Pi$ given by Herzberg(23)

$$T_3 = v_o + B_v(J(J+1) + \sqrt{(Z_1)}) \qquad Z_1 = \Lambda\ Y(Y+1) + 4J(J+1)$$

$$T_2 = v_o + B_v(J(J+1)) \qquad Y = A/B_v$$

$$T_1 = v_o + B_v\ (J(J+1) - \sqrt{(Z_1)})$$

For this case $\Lambda = 1$ and Y will be taken as 15 (ref 1) and for the change from hydride to deuteride Y is constant. Also B_e is approximately equal to B_v and it is assumed that $v' = 0$ is the first observed state and that it dissociates to the ^2P state in copper. Then $\Delta G(0,1) = w_e - 2w_ex_e = 1760\ cm^{-1}$. If it is assumed that the $^3\Pi$ state is regular then using the formula $D_e = {}^{we}/_{4w_ex_e}$ for the dissociation energy gives w_e and w_ex_e. This gives $w_e = 1904$ and $w_ex_e = 72$ and now the position of the perturber in the deuteride can be checked.

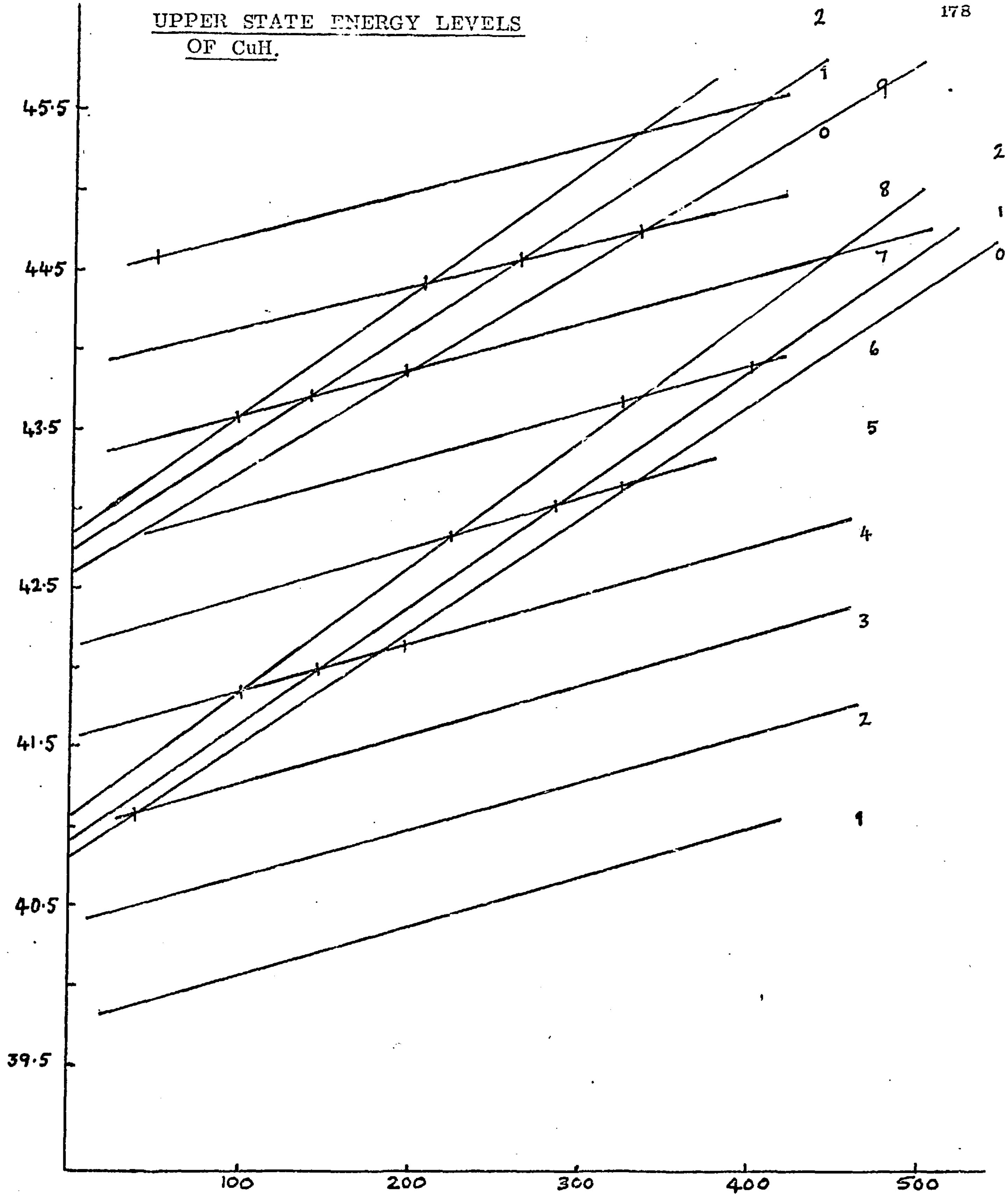
UPPER STATE ENERGY LEVELS OF CuH.

GERO - SCHMID PLOT FOR CuH

FIGURE 11,1

UPPER STATE ENERGY LEVELS OF CuD.

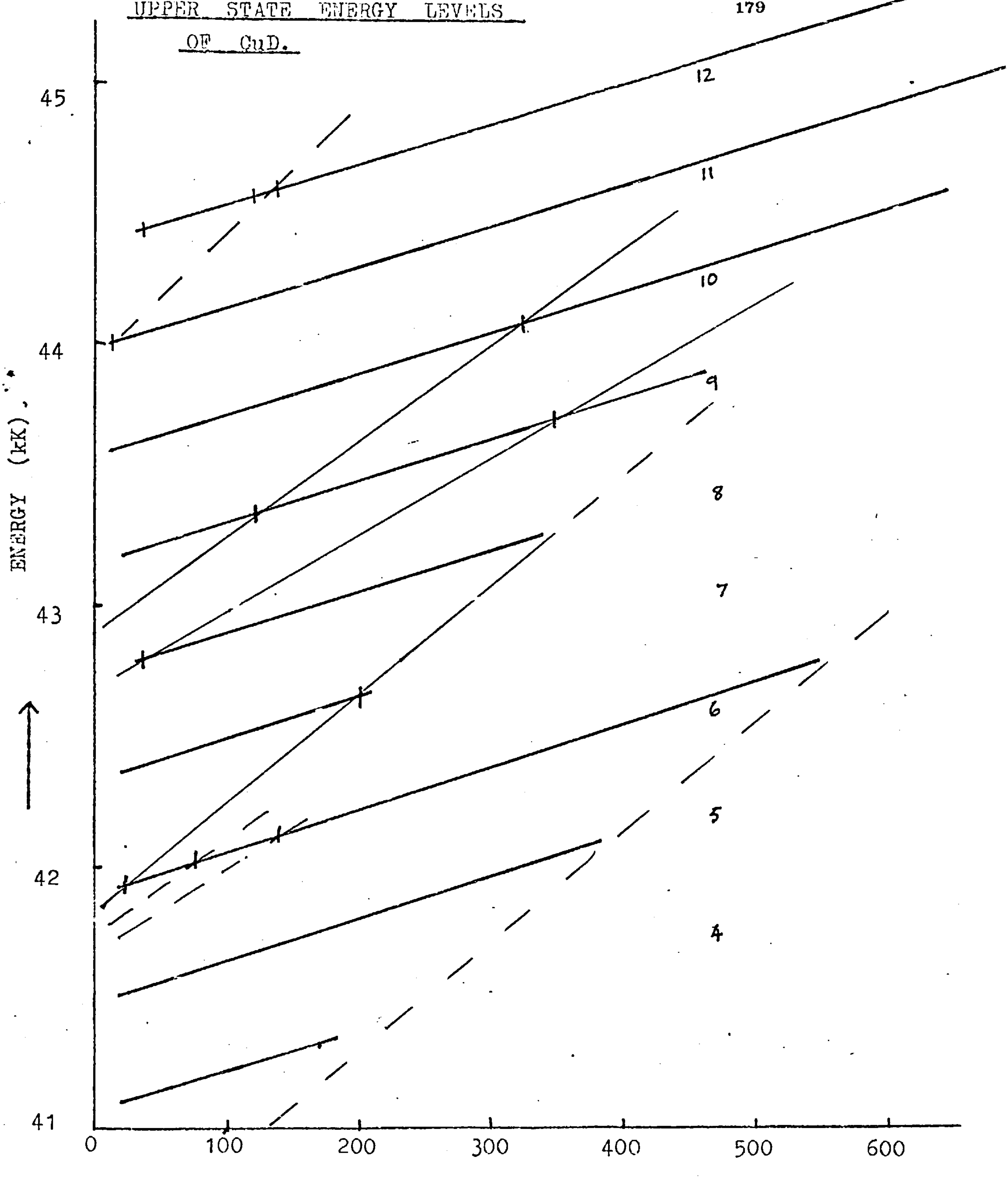

GERO SCHMID PLOT FOR CuD.

FIGURE 11,4

It does not matter significantly to which of the ^2P components the $^3\Pi$ dissociates since the value for w_e if the upper state is assumed is 1900 and $w_e x_e$ is 70. A list of the origins on this assumption and the possibility that v' = 1 is the first observed perturber state is given below. If v' = 1 is assumed to be the first state then w_e = 2048 (2040) and $w_e x_e$ = 72 (70).

Origins of the $^3\Pi_2$ State in the Deuteride

v'	v' = 0 first perturber	v' = 1 first perturber
0	40925	39004
1	42208	40394
2	43417	41700
3	44552	42940
4	45600	44100
5		45190

Clearly the fit assuming v' = 1 is the first observed perturber gives the best agreement with the deuteride. In fact it gives an excellent fit considering the crude way in which the origins were derived. However, this also is a weakness in the derivation and one cannot exclude the small possibility that the first observed state is the v' = 0 state of the $^3\Pi$. This leaves the problem of why the v' = 0 state of $^3\Pi$ did not perturb the $E\,^1\Sigma$ state, the v' = 1 and 2 series of the $^1\Sigma$ state would certainly intersect the $^3\Pi$ but there is no observable displacement of the series. A possible explanation may be that the $^1\Sigma$ state contains less of another perturbing state in the v' = 1 and 2 levels and will hence not be able to be perturbed by the $^3\Pi$ whose perturbation is strictly breaking the triplet-singlet rule for perturbation. It must also be added here that the accuracy of the position of the perturber in the deuteride is very much less accurately determined than in the hydride.

CHAPTER 12

THE ELECTRONIC STATE

12.1 Assignment of the states

Table (12.1) and figure (12.1) show the levels observed in this analysis and the Cu I levels, and the Franck-Condon parabola. The $E^1\Sigma$ state is probably formed by the "intersection" of the $^1\Sigma$ state dissociating to the ^2P state of Cu I and the ionic state formed by the $(3d^{10})\,^1S_0$ and H^- $(2s^2)\,^1S_0$ which will form a $^1\Sigma$ state. If the $^3\Pi$ perturber state is also assigned to the ^2P state then there remains only a $^3\Sigma$ state that can be formed from the configuration of CuH $(3d^{10}4s4p)$. Since much of the region analysed contained no residual unidentifed lines one may reasonably assume that there are no line transitions due to $^3\Pi - X^1\Sigma$ in the region analysed.

The configuration assigned to the two Σ states is $(3d^{10})s\sigma p\sigma$ and to the Π states $(3d^{10})s\sigma p\pi$. The $s\sigma$ and $p\sigma$ orbitals have a large overlap and strong bonding for the $^1\Sigma$ and the reverse in the $^3\Sigma$, the spins forming bonding and antibonding pairs. For the $s\sigma$ and $p\pi$ orbitals the overlap of the states is normally smaller and the spin pairing less important. Then the $^3\Pi$ can be more stable than the $^1\Pi$. The normal order of the states is $^1\Sigma$, $^3\Pi$, $^1\Pi$, $^3\Sigma$ but in this case the $^1\Sigma$ has been effectively perturbed upwards above the $^3\Pi$. If

TABLE 12.1

Relative Intensities* of the Observed CuH Bands

v"	0	1	2	3	4	5
v'						
0						
1			3	5	12	
2		VW	12	7	16	20
3	VW	40	60	24	4	
4	VW	40	60	12		
5	60	60	24			
6	160	200	32			
7	100	100	VW			
8	160	60				
9	100					

* Visual estimates from the strongest members in a band with an approximate correction for temperature and pressure.

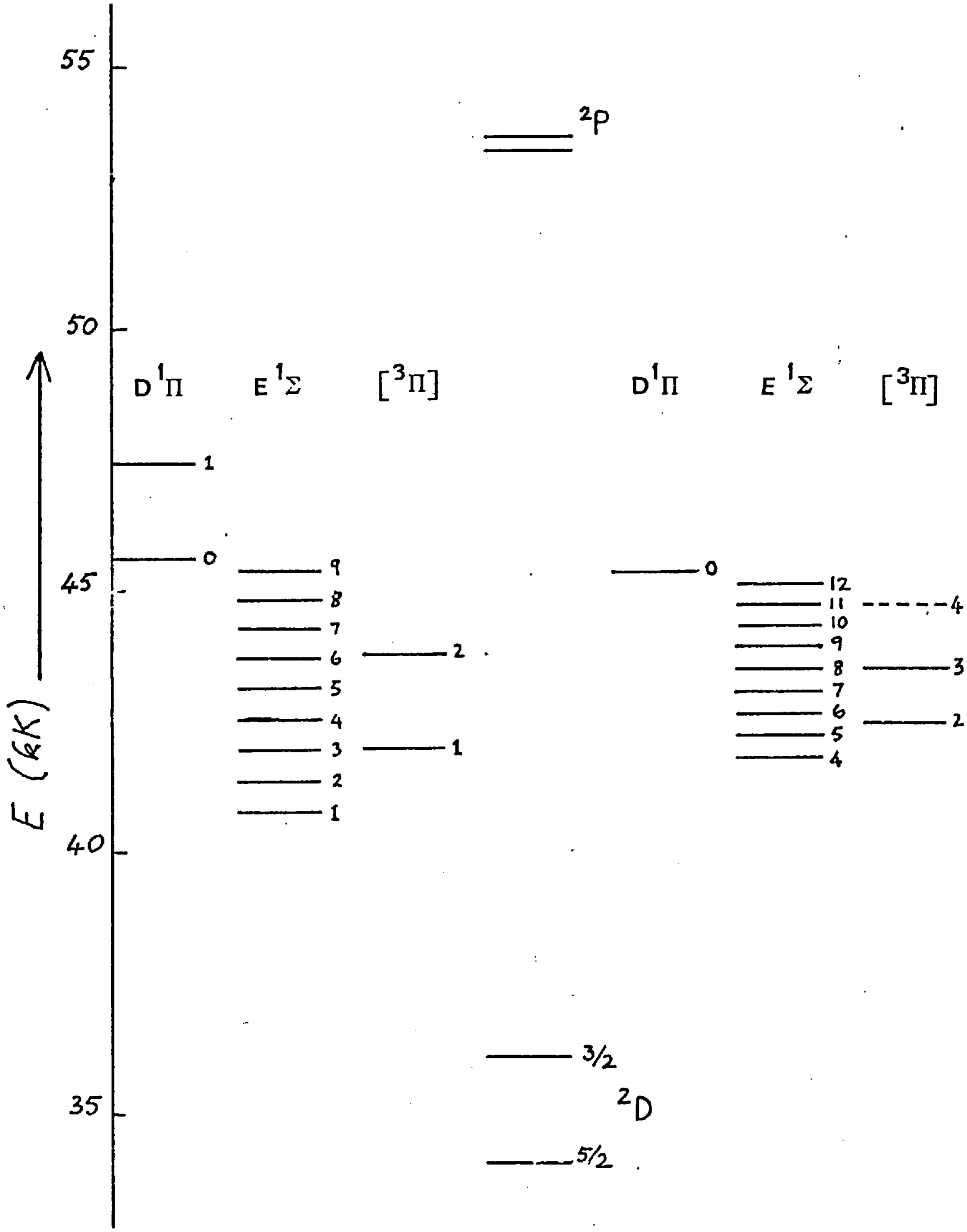
55
50
45
40
35
E (kK)
²P
D ¹Π
E ¹Σ
[³Π]
D¹Π
E ¹Σ
[³Π]
1
0
9
8
7
6
5
4
3
2
1
2
1
0
12
11
10
9
8
7
6
5
4
4
3
2
3/2
²D
5/2

FIGURE 12, 1

the $^3\Sigma$ state is disposed of by assuming that it is either unstable or only marginally stable then there remains no suitable state that can be associated with a vibrational perturbation of the $^1\Sigma$ state. There is insufficient data on this perturbation to try and associate it with a more highly excited state of CuH, though the results do show that the $^3\Pi$ perturber cannot account for all the disturbances in the v'_0s for either CuH or CuD.

None of the results presented here would conflict with the assignment of the states given by Ringström, the changes in the numbering of the $^1\Sigma$ and $^3\Pi$ states however does indicate that the order of the four states dissociating to the ^2P term is $^3\Pi$, $^1\Sigma$, $^1\Pi$, $^3\Sigma$, the last state is assumed to be dissociating.

12.2 The E State in the 1a and 1b Group Hydrides

Though a considerable amount of data is available for comparison of the 1a group hydrides(37), (26), the resultant molecular states are not very similar due to the changing position of the ^2D and ^2P terms in the metal atom, and then in AuH the large splitting in the ^2D. The corresponding $C\,^1\Sigma$ state in AuH appears to be formed as a normal atomic state whereas in CuH it appears to be formed by an "intersection" with the ionic state, and hence would be more similar to the group Ia hydrides. If this interpretation is correct then the $A^1\Sigma^+$ state of CuH would be comparable to the ground state of the group Ia hydride and the $E^1\Sigma^+$ to the first excited state. The $A^1\Sigma^+$ state of CuH is perturbed in its highest observed vibrational level and one would expect that the higher vibrational levels would also be perturbed if the state is a combination of the ionic and atomic states. An intersection with the $X^1\Sigma^+$ state can be excluded since $^{(\text{Herzberg})}$I(Cu) - E(H) = 6.98 eV (56,700 cm^{-1}) and this places the ionic state 6.98 eV above the ground state. Then the point of intersection of the ionic state with the asymptote of the ground state occurs at less than 1.5 r_e(of the ground state) so that one would not expect the $X^1\Sigma^+$ state to be partially ionic. The $A^1\Sigma^+$ state, however, is 12000 cm^{-1} higher and now the point of intersection would be at 2.5 Å, that is between 1.5 and 2 r_e which Herzberg describes as a transitional region, and in this case would appear to account for the behaviour of the $E^1\Sigma$ and the $A^1\Sigma$ states.

In AuH however the ionization potential is higher and the corresponding AO^+ state is only 9000 cm^{-1} above the ground state this makes the point of intersection above the criterion given by Herzberg so that one would rather expect that the effect of the ionic state would only occur for the $C^1\Sigma^+$.

The comparison with the group 1b hydrides leads one to expect a maximum in B_v', a maximum in $\Delta_2 G'$ above the maximum in B_v', and an inner parabola in the Fortrat diagram. Of these only the first point is observed with certainty. Observation of the inner parabola was very unlikely since unlike the group 1a hydrides the observed transition is between the upper state formed by the intersection and the ground state which is completely free from the mixed states. The formation of the wide intensity parabola is just becoming apparent in the table (12.1) and there was at least one extra fairly strong band going to a high v" value in the plate near 3200 Å which could not be extracted from a high density of background lines due to either the $E^1\Sigma - X^1\Sigma$, or states dissociating to the ^2D in Cu $-X^1\Sigma$. The single observed transition to v" = 5 shows that there is no apparent anomaly in this state as expected since this state is not involved with the ionic state.

12.3 Summary

The $E^1\Sigma^+$ state was analysed for CuH and CuD. The numbering of the state and that of its main perturber $a^3\Pi$ were determined. The analysis of the hydride was probably concurrent with Ringström's work and this latter work was used extensively to check the analysis given here and to obtain the least squares fit to the $^3\Pi$ perturber term value equations. The analysis of the one extra hydride band v' = 1 clearly shows the maximum in the B'_v values and significantly alters the electronic constants for the $E^1\Sigma^+$ state. The work on CuD is much less complete than for the hydride due to the complete overlapping of the band lines above the highest band analysed, and to two diffuse absorption regions in the more open part of the spectrum which have not been identified.

The spectrum of CuH was always free from the Cu_2 bands reported by Ringström and it may be that Cu_2 bands are beginning to appear at the lower temperatures used for CuD.

A brief analysis of the (0-0) CuD band of the $D^1\Pi$ state verifies the numbering in this state and shows that there can only be a small difference in v_e with the change from CuH to CuD. The rapid broadening of this state with increasing ambient pressure was observed though the lines had been shown to be sharp when produced at "zero" pressure in the flash pyrolysis apparatus, and the levels are remote from the dissociation limit. (45)

This investigation and that of Ringström still leave several important features of this state to be determined, the most apparent being to observe the v' = 0 level. In the investigations of the group 1 hydrides the electronic constants were invariably altered as lower states were analysed so that one can expect similar changes if the v' = 0 level is observed. The difficulty however is that to observe this state one would require in absorption, to go to very high temperatures and try to pick out bands remote from the high intensity parabola in a region containing a large number of strong bands, or in emission attain some population in this very excited state without exciting too many nearby states. A method of selective excitation would appear to be the only reasonable solution. Similarly to complete the analysis of the deuteride, which is effectively about 8 times denser than the hydride, some selective excitation would be necessary. Neither the hydride nor the deuteride has been analysed to a high enough v' value to be assured that the potential curve has become like a normal atomic state dissociating to the ^2P level, further analysis in absorption however would require moving very close to the vacuum region.

REFERENCES

1 U Ringstrcm Can J Phys 46,2291 1968.

2 T E Nevin Proc Roy Irish Acad 48,1 1942
" 50,123 1945

3 B Kleman and U Uhler Can J Phys 37,537 1959

4 W Garton Inaugural Lecture Imperial College 1963

5 L Nelson and N Kuebler Proc Xth Coll Spectro Int no36 1962.

6 G Porter Proc Roy Soc (London) A200,284 1950.

7 L Nelson and N Kuebler J Chen Phys 37,47 1962.

8 " " Spectrochim Acta 19,781 1963.

9 A Bass, N Kuebler and L Nelson J Chem Phys 40,3121 1964.

10 A Rajaratnam Unpublished work at Imperial College.

11 A Lyman Science 64,89 1926.

12 J Wheaton Appl Optics 3,1247 1964.

13 L Nelson and J Lundberg J Phys Chem 63,433 1959.

14 L Holland Vacuum Deposition of Thin Films Chapman & Hall 1956.

15 R Pearse and A Gaydon The Identification of Molecular Spectra III ed 1965.

16 J Anketel PhD thesis (London) 1967.

17 N Kuebler and L Nelson J Opt Soc Am 51,12,1411 1961.

18 M Chun and K Rose J App Phys (USA) 41,2,614 1970.

19 R Measures PhD thesis (London) 1964.

20 Handbook of Physics and Chemistry 45th ed The Chemical Rubber Co.
1964-65.

21 J Roberts and A Miller Heat and Thermodynamics Vth ed 1960.

22 J Jeans The Dynamical Theory of Gases IV ed 1925.

23 G Herzberg Molecular Spectra Vol 1 , The Spectra of Diatomic Molecules

24 R Learner PhD thesis (London) 1961.

25 S Penner Quantitative Molecular Spectroscopy and Gas Emissivities 1959.

26 U Ringstrom Arkiv f Fys 27,17 1964.

27 H Griem Plasma Spectroscopy 1964.

28 R Breene The Shift and Shape of Spectral Lines 1961.

29 C Allen Astrophysical Quantities II ed 1963.

30 R Frerichs Z f Phys 20,170 1923.

31 E Bengtsson Z f Phys 20,229 1923
" and E Hulthen Trans Faraday Soc 25,751 1929.

32 E Hulthen and R Zumstein Phys Rev 28,13 1926.

33 B Grundstrom Z f Phys 98,128 1935.

34 A Heimer and T Heimer Z f Phys 84,222 1933
T Heimer Z f Phys 95,321 1935.

35 M Jeppesen Phys Rev 50,445 1936.

36 U Ringstrom Arkiv f Fys 32,12 1966.

37 R Learner Proc Roy Soc A 269,327 1962.

38 K Codling PhDthesis (london) 1960.

39 J Samson Techniques of Vacuum Ultraviolet Spectroscopy 1967.

40 R Learner Unpublished work at Imperial College.

41 H CrosswhiteSpectrum of Iron I. John Hopkins Spectroscopic Report no 13 1958.

42 G Harrison MIT Wavelength Tables 1939
& M Wilson (Cu I standards).

43 M Wilson Ph D thesis (London) 1964 & S Budd.

44 N Aslund Arkiv f Fys 30,377 1965.

45 S O'Conner J Phys B ser2 2,541 1969.